國 立 交 通 大 學

材料科學與工程研究所

博 士 論 文

碳基介電薄膜的製備與其應用在 ULSI 連線技術之特性評估

Thin Film Preparation and Characterization of Carbon-based Dielectrics for ULSI Interconnect Technology

研究生：李延煒

指導教授：陳家富博士

中 華 民 國 九 十 三 年 六 月

碳基介電薄膜的製備與其應用在 ULSI 連線技術之特性評估

Thin Film Preparation and Characterization of Carbon-based Dielectrics for ULSI Interconnect Technology

研 究 生：李 延 煒　　　　指 導 教 授 ： 陳 家 富 博 士

Student : Yan-Way Li　　　　**Advisor : Dr. Chia-Fu Chen**

國立交通大學

材料科學與工程研究所

博 士 論 文

A DESSERTATION

SUBMITTED TO INSTITUTE OF MATERIALS SCIENCE AND ENGINEERING

COLLEGE OF ENGINEERING

IN PARTIAL FULFILLMENT OF THE REQUIREMENTS

FOR THE DEGREE OF DOCTOR PHILOSOPHY

IN

MATERIALS SCIENCE AND ENGINEERING

SEPTEMBER 2002

HSINCHU, TAIWAN, REPUBLIC OF CHINA

碳基介電薄膜的製備與其應用在 ULSI 連線技術之特性評估

研 究 生：李延煒　　　　　　　　　　　指導教授：陳家富博士

國立交通大學 材料科學與工程研究所 博士班

中 文 摘 要

本實驗嘗試以無柵極離子束沉積法(gridless ion beam deposition，GIBD)及電漿輔助化學氣相沉積法(plasma-enhanced chemical vapor deposition，PECVD)分別製作非晶質碳及碳化矽薄膜，並且探討其漏電流及介電常數等特性及其應用在銅製程中蝕刻阻止層的可能性評估。

首先利用 GIBD 法在常溫下以乙炔(C_2H_2)及氬氣(Ar)混合氣體沉積非晶質碳膜，並加以退火及氫電漿處理來改變薄膜特性。經拉曼分析結果顯示，I_D/I_G 強度比及 D 特徵峰波數(wavenumber)皆隨著乙炔流量的增加而減小，乙炔流量增加至 60 sccm 時有類鑽石(diamond-like)化的最佳條件，因此我們利用此條件所形成的 DLC 膜再分別作真空退火及氫電漿處理，探討其對 DLC 膜之特性影響，結果顯示 DLC 膜隨著退火溫度增加，I_D/I_G 強度比逐漸地增大，同時薄膜密度也由 3.44 g/cm^3 減小到 2.89 g/cm^3，而退火溫度從 200℃至 300℃時漏電流密度會逐漸的增大，推測此現象可能是因退火時造成薄膜中的碳逐漸石墨化所致。另外經氫電漿處理後的 DLC 膜則隨著處理時間的增加而漏電流逐漸減小，經氫電漿處理 6 分鐘後的漏電流密度為 3×10^{-7} A/cm^2 (在 1

MV/cm 的電場下)，明顯低於未經處理之 DLC 膜(1×10^{-4} A/cm^2)，介電值為 3.4 也明顯低於未經氫電漿處理的 DLC 膜介電值(3.83)。

其次，利用 PECVD 法來沉積碳化矽薄膜時，以矽烷(SiH_4)及甲烷(CH_4)之混合氣體作為反應氣體源，基材溫度保持在 250℃下沉積含氫非晶質碳化矽(a-SiC:H)薄膜。並分別以薄膜測厚儀及汞探針電性量測系統量測薄膜的厚度及介電常數，結果顯示，隨著甲烷流量的增加，薄膜的沈積速率、折射率及介電常數皆明顯的減小。以 5%的矽烷濃度最佳條件下所形成的碳化矽(C/Si:68/25)膜的折射率為 1.76、介電常數為 3.6、漏電流 1.79×10^{-8} A/cm^2 (在 1MV/cm 的電場下)為最小及沉積速率為 1.32 Å/s。再將此碳化矽薄膜分別施以氫(H_2)及氨(NH_3)電漿表面處理，結果經氨電漿表面處理後的薄膜除了表面粗糙度較氫電漿處理的表面粗糙度大外，薄膜表面會形成氮化層，致使薄膜漏電流密度明顯的降低，而經氫電漿表面處理後的薄膜表面碳含量皆隨著處理時間的增加而減少的同時漏電流密度亦有降低的趨勢。

Thin Film Preparation and Characterization of Carbon-based Dielectrics for ULSI Interconnect Technology

Student : Yan-Way Li Advisor : Dr. Chia-Fu Chen

Institute of Materials Science and Engineering

National Chiao Tung University

ABSTRACT

The purpose of this work is research the dielectric properties of a-C and a-SiC:H films, deposited respectively by using gridless ion beam deposition (GIBD) and plasma-enhanced chemical vapour deposition (PECVD), to evaluate the possibility for using in the etching-stop layer of copper interconnect technology. Amorphous hydrogenated carbon (a-C:H) films were deposited from gas mixtures of acetylene (C_2H_2) and argon (Ar) in a GIBD system supplied with dc power. Vacuum annealing and hydrogen plasma treatment were performed on the a-C:H films and their effects on the physical and electrical characteristics of the films were investigated. The structure and properties of the film were investigated as functions of the C_2H_2 flow rate, using Raman spectroscopy. The Raman spectra revealed that the Raman I_D/I_G ratio and D peak position decreases with C_2H_2 flow rate, indicating more diamond-like character of the films. Otherwise, the annealed a-C:H films exhibited that the Raman I_D/I_G ratio increases with annealing temperature, but the film density decreases simultaneously, indicating more graphite-like character for the annealed films as the annealing temperature was increased. The dielectric constant of the annealed a-C:H films was reduced from 3.8 to 2.9, but the leakage current density was obviously increased while the annealing temperature

was increased from 200℃ to 300℃. However, the leakage current density and dielectric constant of the hydrogen-plasma-treated a-C:H films were clearly lower than those of the as-deposited a-C:H films.

Amorphous SiC:H films were deposited from a mixture of silane and methane gases, using PECVD. Reducing the ratio of the silane flow rate decreased the deposition rate of the a-SiC:H films, decreasing the refractive index and dielectric constant, but increasing the optical band gap and the hydrophobicity of the surface. It has a minimum refractive index (1.76), dielectric constant (3.6), leakage current density (1.79×10^{-8} A/cm^2 at the electric field of 1MV/cm) and deposition rate (1.32 Å/s) for the concentration of silane, which is 5% in the mixture gas. XPS data indicate that the carbon concentration of the a-SiC:H films declined as the methane flow rate increased, but the silicon concentration increased. Carbon-rich films were treated with hydrogen and ammonia plasma for various periods, but were then converted into films with higher silicon content. Increasing the ammonia or hydrogen plasma treatment duration roughened the surface, even though the original film had a smooth surface, with a roughness of 0.231 nm. Ammonia plasma treated film has larger roughness (1.741 nm) than that of by using hydrogen plasma treated films (0.829 nm). The ammonia ionization species reacted with Si to promote the formation of silicon nitride. Accordingly, the leakage current density of a-SiC:H films declined as the ammonia plasma treatment time decreased, but the dielectric constant slightly increased. As expected, the leakage current density and the dielectric constant of a-SiC:H films declined as the hydrogen plasma treatment period increased.

致　謝

首先，我要向我的指導教授陳家富博士，致上誠摯的謝意與最高的敬意。六年來在陳老師的教導下學習了許多專業領域的知識，在學習的過程中難免遭遇挫敗，老師總能在我思考混沌時給予即時的協助與鼓勵；在生活上從老師的身教與言教中學習到處事待人的生活哲學，更豐富了我生命的寬度與廣度，由衷地感謝陳老師數年來的指導與照顧。感謝和喬科技(股)公司的張志高博士等研究群，非常熱情地提供實驗所需的過濾式電弧沉積設備與技術指導，感謝您們的幫忙與指教。此外，感謝在台灣積體電路(股)公司工作期間，承蒙王英朗博士的指導，使我能參與半導體製程的 CVD 鍍膜工作，真是個難得的機會。另外亦感謝明道管理學院的汪大永校長，感謝您在我碩士階段的教導，奠定我在真空鍍膜領域的基楚與興趣。

感謝"新素材與薄膜實驗室"所有努力的夥伴，感謝大家的協助與勉勵，尤其是曾欲仁、徐耀斌及林琨程學長與歐耿良在學業與生活上的討論與協助。同時也感謝毫微米實驗室的潘扶民博士的論文指導與修改，以及孫旭昌與蔡國強工程師等研究群在 PECVD 設備與分析儀器上的技術協助。

最後要深深感謝我的父母與研究所時的女朋友現在的老婆，沒有先母當年對我修讀博士學位堅持，就沒有今天取得博士學位的我，感謝您！我的母親。更感謝老婆在這六年的時光中鼓勵我、支持我，讓我在每遇挫折時仍能持續學習與堅持。

僅以此論文感謝在我生命中出現的您們，及許許多多的朋友與貴人，因為您們我才能堅持不退縮，在此致上我最深深的感謝。

TABLE OF CONTENTS

Abstract (in Chinese) ii

Abstract (in English) iv

Acknowledgements vi

Table of contents vii

List of figures ix

List of tables xii

Chapter 1 Introduction 1

1.1 Motivation of this study 1

1.2 Thesis outline 9

Chapter 2 Paper review and Fundamental Theories 11

2.1 Plasma-Enhanced Deposition of Film 11

2.1.1 Plasma Fundanmental 11

2.1.2 Plasma-Enhanced Chemical Vapor Deposition 13

2.2 Cu Metallization and Low-K Dielectrics 16

2.2.1 RC time delay 16

2.2.2 The needs of Cu metallization 18

2.2.3 The needs of low-K dielectrics 19

2.2.4 The needs of Cu Diffusion Barriers 23

Chapter 3 Effect of Post-treatment on Electrical Properties of Amorphous Hydrogenated Carbon Films Deposited by Gridless Ion Beam Deposition 32

3.1 Introduction 32

3.2 Experimental 34

3.3 Results and discussion 36

3.4 Conclusions 44

Chapter 4 Effects of Ammonia Plasma and Hydrogen Plasma Treatment on the Electrical Properties of PECVD Amorphous Hydrogenated Silicon Carbide Films 55

4.1 Introduction 55

4.2 Experimental 57

4.3 Results and discussion 60

4.3.1 Characteristics of the PECVD a-$Si_mC_n:H_y$ films 60

4.3.2 Effects of ammonia plasma and hydrogen plasma treatment on the a-$Si_{0.28}C_{0.65}$:H_y films 66
4.4 Conclusions 72

Chapter 5 Conclusions and future work 98

References 102

Publication lists 114

LIST OF FIGURES

Fig. 2.1 Plasma chemistry of the hydrogen molecule as the impinging electron energy in increased. 26

Fig. 2.2 Schematic representation of the plasma-enhanced CVD reaction process. 27

Fig. 2.3 Calculated delays for Al/SiO_2 and Cu/Low-K interconnect systems. 28

Fig. 2.4 Integration of Cu and low-K dielectrics into a dual damascene architecture. 29

Fig. 3.1 Metal-insulator-semiconductor (MIS) structure. 46

Fig. 3.2 The fitted curves of Raman spectra of the a-C:H films. 47

Fig. 3.3 Graphs of (a) Raman I_D/I_G ratio, and (b) D-peak position of a-C:H films as a function of C_2H_2 gas flow rate. 48

Fig. 3.4 Raman spectra of the a-C:H films with different annealing temperatures, (a) 100℃, (b) 200℃, (c) 300℃, and (d) 400℃. 49

Fig. 3.5 Graphs of (a) Raman I_D/I_G ratio and (b) D-peak position of a-C:H films with various annealing temperatures in vacuum. 50

Fig. 3.6 Density of a-C:H films for various vacuum annealing temperatures. 51

Fig. 3.7 J-E curves of a-C:H films with different vacuum annealing temperatures. 52

Fig. 3.8 (a) Dielectric constant (K) of a-C:H films with different vacuum annealing temperatures, and (b) Dielectric constant of a-C:H films with different hydrogen plasma treatment periods. 53

Fig. 3.9 J-E curves of a-C:H films with different hydrogen plasma treatment. 54

Fig. 4.1 Schematic diagram of the PECVD system. 74

Fig. 4.2 Deposition rate of a-$Si_mC_n:H_y$ films as a function of x value [x = SiH_4/(SiH_4)+(CH_4)]. 75

Fig. 4.3 Optical energy gap (Eg), and refraction index (n) of a-$Si_mC_n:H_y$ films as a function of x value [x = SiH_4/(SiH_4)+(CH_4)]. 76

Fig. 4.4 Dielectric constant (K) of a-$Si_mC_n:H_y$ films as a function of x value [x = SiH_4/(SiH_4)+(CH_4)]. 77

Fig. 4.5 IR spectra of the a-$Si_mC_n:H_y$ films of different methane flow rates. 78

Fig. 4.6 ESCA spectra of the near surface region of a-$Si_mC_n:H_y$ films with various methane flow rate, (a) 35 sccm, (b) 50 sccm, (c) 70 sccm, and (d) 100 sccm. 79

Fig. 4.7 The composition of the near-surface region of the a-$Si_mC_n:H_y$ films with various methane flow rate, analyzed by ESCA. 80

Fig. 4.8 The water contact angle and the dispersive component of the free energy of the a-$Si_mC_n:H_y$ films as a function of methane flow rate. 81

Fig. 4.9 The surface roughness of a-$Si_mC_n:H_y$ films with various films thickness, (a) 10 nm, (b) 50 nm, (c) 100 nm, and (d) 150 nm. 82

Fig. 4.9(e) The surface roughness of a-$Si_mC_n:H_y$ films with various films thickness. 83

Fig. 4.10 Dielectric constant (K) of a-$Si_mC_n:H_y$ films with various films thickness. 84

Fig. 4.11 AFM images of a-$Si_{0.28}C_{0.65}:H_y$ films with varies

ammonia plasma treatment periods, (a) 0 min, (b) 5 min, and (c) 20 min, and (d) AFM roughness of a-SiC:H films with various plasma treating periods. 85

Fig. 4.12 AFM images of hydrogen plasma treated a-SiC:H films with varies hydrogen plasma treatment periods, (a) 5 min, (b) 15 min, and (c) 20 min. 86

Fig. 4.12 (d) Roughness of plasma treated a-SiC:H films with varies hydrogen plasma treatment periods. 87

Fig. 4.13 XPS spectra of Si 2p binding peaks for the a-$Si_{0.28}C_{0.65}:H_y$ films with various ammonia plasma treatment periods. 88

Fig. 4.14 The content of a-$Si_{0.28}C_{0.65}:H_y$ films with different ammonia plasma treatment period. 89

Fig. 4.15 FTIR absorption spectra of a-SiC:H films for various hydrogen plasma treatment periods. 90

Fig. 4.16 The outmost layer content of a-SiC:H films with various hydrogen plasma treatment periods. 91

Fig. 4.17 J-E characteristics of a-$Si_{0.28}C_{0.65}:H_y$ films before and after ammonia plasma treatment and a-SimNn:Hy films, (a) a-SimNn:Hy, (b) a-$Si_{0.28}C_{0.65}:H_y$, and with various plasma treating periods, (c)5 min, (d)10 min, (e)15 min, and (f) 20 min. 92

Fig. 4.18 J-E characteristics of a-SiC:H films before and after hydrogen plasma treatment and a-SiN:H films, (a) a-SiN:H, (b) a-SiC:H, and for various plasma treatment periods, (c) 5 min, (d) 10 min, (e) 15 min, and (f) 20 min. 93

Fig. 4.19 Dielectric constant (K) of a-$Si_{0.28}C_{0.65}:H_y$ films with various ammonia plasma treating periods. 94

LIST OF TABLES

Table 2.1(a) Dielectric constant of several materials. **30**

Table 2.1(b) Some recent promising low-K materials. **31**

Table 4.1 Deposition parameters, hydrogen/ammonia plasma treatment parameters, and characteristics of the a-SiC:H films. **95**

Table 4.2 Frequencies of IR peaks and assignments. **96**

Table 4.3 The dielectric constant (K) of a-SiC:H films for various plasma treatment periods. **97**

Chapter 1

Introduction

1.1 Motivation of this study

Carbon-based materials generally have a high hardness, a low friction coefficient, a large refractive index, a wide band gap, a high breakdown electric field, and extremely high thermal conductivity. Therefore, such materials have considerable potential for use wear-resisting, electronic and optoelectronic applications. Our laboratory has achieved much in the field of fabricating and applying diamond and amorphous carbon (a-C) films.[1-4] Carbon-based thin films have recently attracted much attention due to carbon's unique range of bonding configurations sp^1, sp^2 and sp^3 and its ability to exhibit a wide variety of properties, from those of graphite to diamond. Among these materials, hydrogen-free tetrahedral a-C films have attracted special interest due to their many sp^3 bonded carbon atoms, more than those of other a-C coatings, which lead to many powerful properties, such as extreme hardness, optical transparency, good electrical insulation and biocompatibility.[5-7] Our previous studies [5,6] have demonstrated that a-C films could be deposited by physical vapor deposition (PVD), and they are characterized by extreme hardness and good electrical insulation.

The wide range of applications of silicon carbide (SiC) thin films in optoelectronics (such as light-emitting diodes, color displays, and other devices) and high-temperature electronic devices (such as hetero-junction bipolar transistors, photovoltaic cells, and others) has attracted a lot of scientific interest. Besides, their chemical inertness, transparency over a broad range of wavelengths and hardness allow SiC thin films to be used in heat-sinks, optical filters, antireflection hard coatings, X-ray masks and corrosion-resistant materials. Furthermore, SiC films can also be used as a thin buffer layer in the growth of diamond films on silicon.[8] Silicon carbide films deposited by various methods and on different substrates have therefore been the subject of extensive research during the last few years.[9-15]

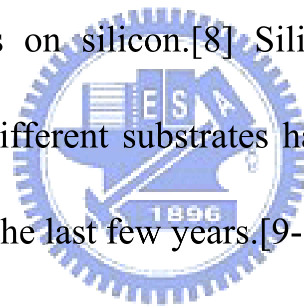

The physical and chemical properties of the films depend primarily on the deposition technique used. Traditional PVD processes, such as magnetron sputtering, which is used on a broad scale in wear tool coatings, fail to make smooth and continuous layers in the manufacturing of ultra-thin films.[16] The most success has been achieved using ionized PVD. The flux of sputtered or evaporated neutral atoms experiences in-flight ionization and subsequent acceleration in an electrical field, straight toward the surface of the wafer. Ion beam deposition and vacuum arc deposition may be candidate plasma sources

for ionized PVD because the self-ionization in the process generates the plasma required for directional deposition much more effectively.[17] The use of the bias voltage is to produce an additional ion bombardment at the substrate without influencing the other process parameters. The consequences of the ion bombardment effect are an increase in film density, inhibition of a columnar film growth, an improvement in adhesion, an increase of residual stress, and a change in the micro-hardness. McKenzie [18] suggested that filtered arc deposition should be a useful method of accessing high-compressive-stress regimes because of its narrow and controllable energy distribution and high flux rates. Newer developments, such as the vacuum arc-based deposition of a-C films, are becoming increasingly important. Much interest has been shown in the use of tetrahedral a-C films, deposited by filtered arc deposition, in the fabrication of electronic devices.[19-23] Recent developments have shown that effective plasma filtering techniques, using curved magnetic ducts to separate the plasma from the particles, can effectively suppress the deposition of droplets on the substrates at a reasonable deposition rate.[24,25] Unfortunately, the macro-particle filter reduces the deposition area and greatly complicates the use of the vacuum arc method for coating substrates. So far, the method has not been considered for semiconductor manufacturing since the deposition area and the

emission of microscopic liquid metal droplets from the plasma source remain outstanding issues. Besides, gridless ion beam deposition is a combination of ion implantation and physical vapor deposition (PVD), in which energetic ion bombardment is used to synthesize high-quality film materials. In this technique, the deposition is energetic; restated, the carbon species arrives with an energy significantly greater than that represented by the substrate temperature. The resultant films are dense, transparent, insulating, amorphous and display a high degree of sp^3 character.[26] Therefore, one of the aims of this work is to prepare a-C:H films deposited by the GIBD system and then to perform vacuum annealing treatment and hydrogen plasma treatment to investigate the influence of the treatments on electrical properties of the films.

Chemical vapor deposition (CVD) techniques for growing carbon films have been developed in recent years,[27,28] opening up a wide field of applications of carbon films. Chemical vapor deposition offers excellent uniformity and additional degrees of flexibility; depending on the temperature of the sample, the gas dynamics and the surface composition of the substrate. The resulting films are characterized by highly aspect ratio. Among the reasons for growing films using CVD methods is the capacity to produce a wide range of films and metal coatings, and semiconductors in either a crystalline or

amorphous form, with high purity and desirable characteristics. Krishna [29] demonstrated that hydrogenated amorphous carbon (a-C:H) thin films deposited by radio-frequency plasma-enhanced CVD (PECVD), exhibit a lowest defect density. Since carbon-based films are relatively new materials, the electrical properties of semiconductive carbon-based films have received extensive attestation. Carbon-based films can be synthesized in a low-pressure and low-temperature CVD process and are widely expected to be adopted for sub-100 nm IC technology.

The manufacturing of the interconnect system in an integrated circuit represents one of the key processes in the semiconductor industry. Current technology integrates up to seven levels of high-density wiring for leading-edge logic chip applications, such as microprocessors. The decreasing feature size and the increasing complexity of the global wiring introduce signal delays, related to the increasing resistance of the longer metal lines, and the capacitance between them. The wiring and the gate RC delays have become equally important in limiting the maximum speed of the integrated circuit. Accordingly, we have seen a dramatic acceleration of research and development on low-K dielectric materials and copper metallization, to further reduce wiring RC delays. [30] Copper is now replacing aluminum as the main conducting material for all types

of integrated circuits in sub-180 nm technology nodes. Copper has a significantly lower electrical resistivity than aluminum (ρ_{Cu} = 1.7 $\mu\Omega$, ρ_{Al} = 2.65 $\mu\Omega$) and is much more resistant to electromigration, a common problem that affects the reliability of aluminum metal lines.[31] In metallization process, dielectric films, made of inorganic material, include amorphous fluorinated carbon (a-C:F), fluorosilicate glass (FSG), dielectric SiO_2 and SiN deposited by PECVD. The films, a-C:F,[32,33], FSG,[34,35] and fluorine-doped siliconoxide (SiOF),[36,37] have recently received considerable attention as potential inter-metal dielectric materials of low permittivity (K). The incorporation of fluorine, which has a high electronegativity (4.1) and reduces the polarizability of the overall network, typically reduces the refractive index and dielectric constant of the thin films.[37,38] At high temperatures, however, the diffusion of fluorine is enhanced and can interfere with the surrounding layers. The fluorine in the fluorinated dielectric layer can diffuses to accumulate at the interface.[39] The fluorine content at the interface greatly enhances Cu-Si intermixing, since fluorine atoms in the interface create silicon dangling bonds and weakly positively charged silicon atoms.[40,41] Therefore, Cu atoms may significantly penetrate into the fluorinated dielectric during heating. A diffusion barrier must be used to prevent copper atoms from diffusing into the fluorinated

dielectric. Silicon nitride (SiN) films exhibit good barrier response to copper diffusion, etching selectivity to oxides, high dielectric, mechanical and chemical stability and electrically insulating characteristics. They are essential for the semiconductor industry to surround silicon integrated circuits, and as diffusion barriers against H_2O and metal ions,[42] as passivation films, [43] as gate and capacitor dielectrics.[44] However, silicon nitride suffers from a high dielectric constant of ~ 7.2.[45] This high dielectric value increases the overall inter-layer dielectric (ILD) time delay. Consequently, silicon nitride must be substituted for a barrier material with a lower dielectric constant.

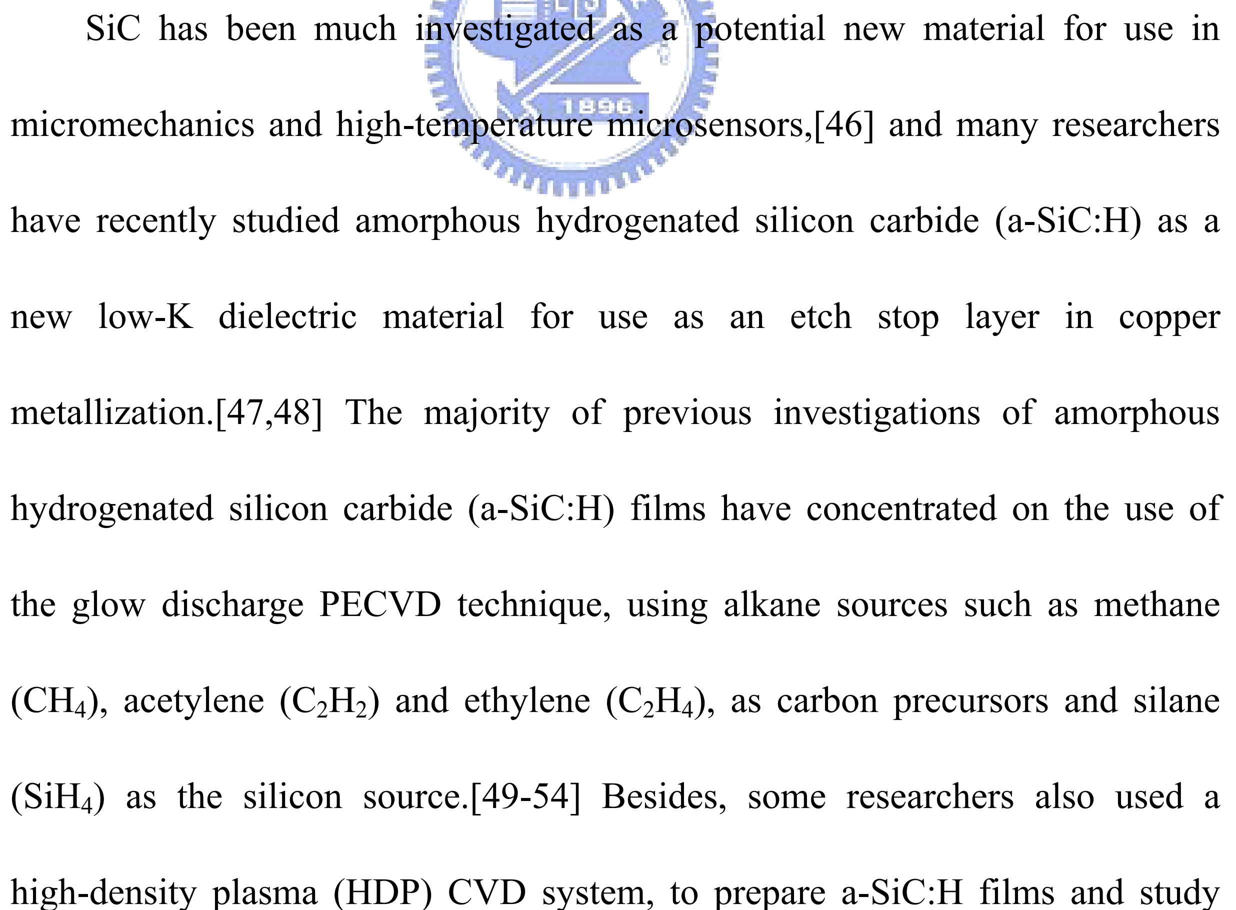

SiC has been much investigated as a potential new material for use in micromechanics and high-temperature microsensors,[46] and many researchers have recently studied amorphous hydrogenated silicon carbide (a-SiC:H) as a new low-K dielectric material for use as an etch stop layer in copper metallization.[47,48] The majority of previous investigations of amorphous hydrogenated silicon carbide (a-SiC:H) films have concentrated on the use of the glow discharge PECVD technique, using alkane sources such as methane (CH_4), acetylene (C_2H_2) and ethylene (C_2H_4), as carbon precursors and silane (SiH_4) as the silicon source.[49-54] Besides, some researchers also used a high-density plasma (HDP) CVD system, to prepare a-SiC:H films and study

their characteristics.[48] However, the electrical properties of low-temperature deposited carbon-based films have rarely been investigated despite the fact that numerous studies of details of the electrical properties of carbon-based films have been conducted. The current leakage characteristics of conventional SiC involve its conduction through silicon. Si has an electronic polarizability 20 times that of carbon. Consequently, substituting the less polarizable carbon atoms for silicon in SiC should yield a lower dielectric constant than that of SiC. Nevertheless, these low-k materials, that contain Si-H groups, easily react with moisture to increase their leakage current and dielectric constant. The films has limited applicability at present. The hydrogen content is well known to increase with the amount of carbon,[55,56] and hydrogen plays a role in passivating the dangling bonds in the films. Dangling bonds can then easily react with moisture to form -OH bonds during the exposure of the dielectric films to the atmosphere, increasing the dielectric constant and the leakage current of the films. Consequently, hydrogen plasma treatment can be used for providing hydrogen atoms to passivate the surface and reduce the density of dangling bonds. The leakage current of hydrogen silsesquioxane (HSQ) decreases as the hydrogen and ammonia plasma treatment duration is increased.[57] Ammonia gas is commonly use as the depositing source of a-SiN films in PECVD and the

ammonia plasma generates various ionized species such as NH^{++}, N_2^+ and H.[58] Liu et al. described how the passivation layer, following ammonia plasma treatment, effectively reduced the moisture uptake and the lengths of the diffusion paths of copper penetration through HSQ.[59]

This work prepares a carbon-based thin film with a lower dielectric constant than the silicon nitride film, which greatly impedes Cu diffusion and has a high chemical stability. The interaction of the copper electrode with the dielectrics was examined by making electrical measurements, using metal-insulator- semiconductor (MIS) structures.

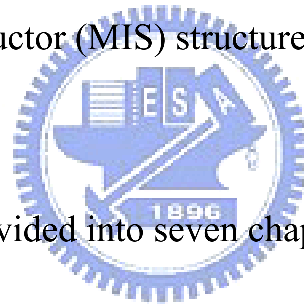

1.2 Outline of Thesis

This dissertation is divided into seven chapters.

Chapter 1 introduces the general background to, and motivation for the growth of carbon-based films by PVD and CVD, and their applications in Cu metallization.

Chapter 2 describes the reactive mechanism and the deposition behavior associated with the plasma-enhanced deposition of films. The introduction of Cu metallization for applications in multilevel interconnect architecture also described.

Chapter 3 describes the use of a mixture of argon and acetylene gases to

deposit amorphous hydrogenated carbon (a-C:H) films. The effects of annealing and hydrogen plasma treatment on the electrical properties and the structure of a-C:H films are discussed.

Chapter 4 describes the characteristics of PECVD carbon-rich a-SiC:H films and the effects of deposition parameters on the films' electrical properties. The effects of hydrogen and ammonia plasma treatment on the electrical and the surface properties of carbon-rich a-SiC:H films are also discussed.

Chapter 5 summarizes all experimental results and provides suggestions for future work.

Chapter 2

Paper review and Fundamental Theories

2.1 Plasma-Enhanced Deposition of Film

2.1.1 Plasma Fundanmental

The use of plasma provides many advantages. For instance, energetic charged particle collisions can produce meta-stable species (such as redicals), new reaction paths and control of film microstructure and mechanical properties can be enhanced through ion bombardment, and directionality in film deposition and etching can be achieved through the acceleration of charged species in a directional potential gradient.

We consider the fundamentals of plasma chemistry by focusing on the interactions between electrons, ions, and neutrals in a discharge. Let us begin with a definition:

The plasma is a quasi-neutral gas of charged and neutral particles, which exhibits collective behavior.

Any body of gas typically contains three species: neutral atoms or molecules, ions, and electrons. Their relative concentrations (i.e., the degree of ionization) are considerably different in plasma. From the relative inefficiency of energy transfer through elastic collisions between electrons and ions or

neutrals, the inelastic processes were important for the coupling of an external power supply to sustain the plasma. The energetic of the inelastic processes depend to a great extent on the energy levels intrinsic to the gas species.

Five fundamental inelastic processes account for the majority of chemical processes occurring in plasma: (a) ionization, (b) excitation, (c) relaxation, (d) dissociation, and (e) recombination. Many other processes that occur in discharges are species dependent. All five fundamental processes can be found in the plasma of hydrogen as the energy input to the plasma is gradually increased. To illustrate the fundamental inelastic processes, following the plasma chemistry of hydrogen in a hypothetical situation where all electrons have equal energies and this energy can be gradually increased.[1]

At low energies, electron-H_2 collisions are elastic and electrons suffer only momentum changes as shown in Fig. 2.1. The H-H bond strength is approximately 4.5 eV so we would expect atomic hydrogen to be formed when the electron energy is increased to this level. However, the cross section for this process is small and the mechanism requires the hydrogen molecule to be raised to an excited state. This excitation occurs at an energy of about 9 eV. Above this energy, electron impact results in the dissociation of the molecule to form two hydrogen atoms with each of them having a significant kinetic energy. The

ionization potential for H_2 molecules to form positive hydrogen ions is 15.4 eV. At this energy, significant formation of singly ionized hydrogen molecules is seen. As the energy of electrons is increased further, an excited state for the positive hydrogen ion is reached, resulting in the formation of an H/H^+ pair. The hydrogen atoms produced have their own excited states, which can be achieved through collisions with other atoms, ions, or electrons. In a typical glow discharge the electron energy distribution is Maxwellian, so all these processes can occur concurrently in the discharge.

2.1.2 Plasma-Enhanced Chemical Vapor Deposition

The rapidly rising applications of plasma-CVD technology have led to considerable in research on the area of basic reaction mechanism. Techniques that permit deposition of films with thickness less than 1 μm have been developed. PECVD can produce thin film of a thickness below 0.1 μm with an excellent integrity and uniformity.

Reaction mechanisms involved in the film formation in plasma-enhanced CVD are not yet well understood, due to the complexities of the reaction system, i.e., (1) the cold plasma is not in thermal equilibrium, (2) gases used in the process are sometimes poly-atomic molecules, and (3) lack of basic data such as reaction cross sections. Furthermore, gas phase reactions in the plasma and

surface reactions on the substrate may all contribute to the film formation process. Figure 2.2 shows the reaction process in the film formation schematically. Gas molecules are excited, ionized or dissociated in the plasma mainly by electron impact. Thus excited molecules, atoms, radicals, molecular and/or atomic ions are produced and travel through the sheath layer to reach the substrate surface. The flow of reaction gases and the configuration of the electrodes and the substrate holder all affect the spatial distribution of the particle density. Particles reaching the substrate surface migrate and find adsorption sites on the surface. Finally, the surface species react with each other, resulting in the film formation. Dissociation of molecules during adsorption may also occur. The surface bombardment by ions accelerated in the sheath affects surface reactions and film properties.

In typical CVD processes, films are formed purely through thermo-chemical reactions at the substrate surface. The reaction proceeds under a nearly thermodynamic equilibrium condition. On the other hand, plasma-enhanced CVD is a film formation process that causes excited species to react with each other. This makes it possible to deposit films at lower substrate temperatures than a thermal CVD process, in which a high substrate temperature is necessary to overcome the activation energy. In order to produce the cold

plasma, low pressure is of course required. Plasma-enhanced CVD is, however, a film formation process that includes which includes chemical reactions. Therefore, high densities of active species are required in order to get higher deposition rates. The pressure ranges in plasma-enhanced CVD lies between 0.1 and 10 Torr. Mean-free paths of gas particles at this pressure range are as short as several hundred micrometers. Most electron energies are probably in the range 0.5-10 eV and the plasma density is 10^{9}-10^{12} cm^{-3}. The degree of ionization is less than 10^{-5}. The population of free radicals is much greater than those of ions, and some radicals have much longer lifetimes. Many reactions occur among excited molecules and among ions and molecules in the plasma and the sheath layer, which complicates the film deposition mechanism further.

When the flow rate of reaction gas per unit electric power used for maintaining the plasma is relatively small, the deposition rate of the film is limited by the effective flow rate of the reaction gas. When the gas flow rate is high, the deposition rate is limited by externally supplied electric power. Although the deposition rate also changes with the substrate temperature, the dependence of the deposition rate on the activation energy is often very obvious. Occasionally, the experimental activation energy may even take a negative value when deposition rates are plotted directly against the inverse of the substrate

temperature.

Even though plasma reaction mechanisms are still not well understood, PECVD applications to film formation has moved forward rapidly because of the technological demand from industries. In principle, compounds which contain elements comprising the desired film and have a higher vapor pressure can be selected as the source gas, and any film can be deposited by plasma-enhanced CVD. Hydrides and halogenides have been widely used. Organometallic compounds can also be used as source gases. Many detailed studies have been done to correlate the deposition conditions with film properties of a-Si, Si-N and Si-O. These have already been applied to semiconductor and electronic industries for mass production.

2.2 Cu Metallization and Low-K Dielectrics

2.2.1 RC time delay

Interconnect parasitic capacitance begins to dominate the overall signal delay for integrated circuits of sub-100 nm technology, as shown in Fig. 2.3[2], and it adversely affects the packing density, reliability, and manufacturing cost of integrated circuits (ICs). Unlike transistor scaling, where performance can be improved with reduced gate length, scaled interconnects suffer from severely increased RC time delay due to higher wire resistance (R) of narrower metal

leads and higher intra/inter-level capacitance (C) between more tightly spaced interconnects. Moreover, reduced interconnect cross-sectional area also results in higher conduction current density, which exacerbates the issue of electromigration.[3] Therefore, the interconnection delay must be reduced by using new materials to alleviate the problem of achieving high performance ultra-large-scale integrated (ULSI) circuits without compromising the requirements of driving speed, crosstalk interference, and dynamic power dissipation imposed by the small feature sizes.[4]

In the high frequency (~ GHz) region, the interconnect delay within ULSI circuits is directly related to the RC time delay constant, as expressed by the following eq.:

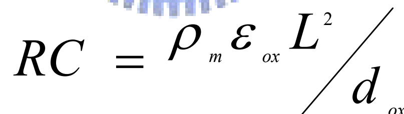

$$RC = \rho_m \varepsilon_{ox} L^2 / d_{ox}$$

where ρ_m: sheet resistance of the interconnect

ε_{ox}: dielectric constant of the inter-metal dielectric (IMD)

L: length of the interconnect

d_{ox}: thickness of the IMD

From the above equation, the RC time delay can be reduced by reducing the length of the interconnect, increasing the thickness of the IMDs, and utilizing a low resistivity interconnect as well as a low dielectric constant

(low-K) IMD. Nevertheless, a longer interconnect is inevitable since both larger chip size and multilevel metallization are needed to meet the requirements of the increased functional complexity and packing density of the integrated circuits. Moreover, increasing the thickness of the IMDs would raise the concerns of planarization and via-filling. Therefore, using interconnects with a low resistivity and IMDs with low dielectric constant becomes a feasible approach for reducing the back-end RC time delay.[5-6]

2.2.2 The needs of Cu metallization

Most recently, Cu has been extensively used to substitute for the conventional Al and its alloys in deep sub-quarter-micron multilevel interconnect applications for the following reasons.[7-17]

1. Cu has a lower electrical resistivity than Al and its alloys (1.7 μΩ-cm compared to 3.0 μΩ-cm), and exhibits an excellent resistance to electro/stress-migration and hillock formation.
2. Cu can be conformally deposited into high aspect ration vias and contact holes using electrochemically deposited (ECD) as well as chemical vapor deposited (CVD) techniques, both of which inherently render much better step coverage than the currently used physical vapor deposition (PVD) methods.

3. Cu can be selectively chemical vapor deposited at fairly low substrate temperatures, thus is technically compatible with most low-K dielectrics.
4. Cu has a better thermal conductivity, higher melting point, and lower reactivity with most of the diffusion barrier materials than Al and its alloys.

Before extensive applications of Cu metallization in the Si-based ULSI circuits become feasible, however, there are many reliability issues remained to be solved. Cu is known to have a poor adhesion to most promising IMDs, and readily drifts through SiO_2 at temperatures as low as 250℃ under accelerated electric field .[18-25] Moreover, Cu diffuses fast in Si and introduces deep-level traps; it also forms Cu silicides at low temperatures (200℃).[15, 25-28] Thus, the use of diffusion barriers between Cu and its underlying layers is necessary to foster adhesion and avoid Cu out-diffusion through SiO_2 and/or mewly developed low-K IMDs.[29-31]

2.2.3 The needs of low-K dielectrics

With Cu successfully integrated with SiO_2 in advanced sub-0.25 μm circuits for improved interconnect conductivity and reliability,[32] the process integration of Cu with low-K dielectrics can further improve IC performance by reducing the interconnect parasitic capacitance. Moreover, Cu/low-K designs in 0.13 μm technology node require only six metal levels to maintain a constant

RC, compared to 12 levels in the Al/SiO_2 system.[33] More interconnect levels need more process steps, and each additional step reduces final production yield. Although Cu interconnects offer the promise of 30% faster operation speed with fewer metal levels and a lower cost of production, achieving high yields for chips with Cu interconnects remains a serious challenge, making low-K the key enabler for high performance.[34] Using low-K materials as IMDs not only ameliorates the problem of parasitic capacitance, which is dominated by the interline capacitance component in long parallel lines,[35] but also reduces the crosstalk interference between adjacent metal lines and the dynamic power consumption. Furthermore, it has been demonstrated that incorporating low-K dielectrics into multilevel interconnect is of much benefit to cost saving, as opposed to using the standard process.[36] Consequently, both performance improvement and cost saving can be achieved by using low-K materials as the IMDs.

In order to integrate new low-K dielectrics into conventional manufacturing process and to minimize the risks and costs of integration, various low-K dielectrics developed for as IMD purpose must meet stringent requirements for their electrical, physical, and chemical properties, a number of the most importance of which are listed as follows.[2,37]

1. Low dielectric constant for frequencies up to 1 GHz. (The dielectric constant of the standard plasma silicon oxide is 4.2 and values lower than this are desirable.)
2. High breakdown field strength (>2 MV/cm) and low leakage current density. (The effective resistivity should be greater than 10^{15} Ω-cm.)
3. Low mechanical stress (preferably compressive to weak tensile with magnitude <30 MPa.) and good adhesion to other dielectrics (oxides/nitrides) and metals (such as Ta, TaN, TiN and Cu.)
4. High thermal stability (Tg>400℃, stable up to 425℃ for short periods) and high thermal conductivity.
5. No moisture absorption or permeability to moisture.
6. No trapped charges and no sodium impurities.
7. Good thickness uniformity, step coverage, and gap filling capability, even for future 300-mm wafers.
8. Capability of being dry etched.

So far, each low-K candidate under evaluation exhibits its own attractive material properties, but no single material satisfies all the listed requirements. For example, thermal stability is one of the major concerns for the practical use of low-K dielectrics. Due to continuous high-temperature thermal cycles in the

back-end fabrication process, such as CVD-W deposition, post etching annealing, baking and curing of spin-on low-K films, and final deposition of oxides/nitrides passivation layers, it is suggested that low-K materials are preferably capable of withstanding the thermal treatment at 450℃ for at least two hours. This criterion disqualifies many prospective low-K materials for the IMD applications.[38]

Low-K (K<3.0) dielectrics are currently being extensively developed on both organic (carbon-based) and inorganic (SiO_2-based) materials using both spin-on deposition (SOD) and chemical vapor deposition (CVD) techniques. Although spin-on is the most widely used method, low-K films grown by CVD are receiving widespread attention for potential back-end-of-line (BEOL) applications. Table 2.1(a) and Table 2.1(b) summarizes the dielectric constant of some materials and recent promising low-K materials for interconnect applications.[39] Three facts about the low-K material can be addressed. First, due to the fluorine-induced corrosion to metal lines, some of the low-K organic fluorinated polymers have been phased out. Second, fluorinated silicate glass (FSG) deposited either by plasma-enhanced CVD (PECVD) or by high-density-plasma CVD (HDPCVD) processes has already been integrated into BEOL applications despite its relatively high dielectric constant. In addition

to the conventional SOD, the CVD silsesquioxanes with dielectric constants below 3.0, such as methylsilane (1MS)- and trimethylsilane (3MS)-doped organosilicate glasses (OSGs),[40-44] are presently available for process development, and are expected to find widespread use. Third, there are more and more organic and inorganic porous low-K materials with dielectric constants below 2.0 under evaluation. However, the integration challenges concerning the mechanical strength, electrical reliability, and process compatibility of the porous low-K materials may defer their applications in IC manufacturing.

2.2.4 The needs of Cu Diffusion Barriers

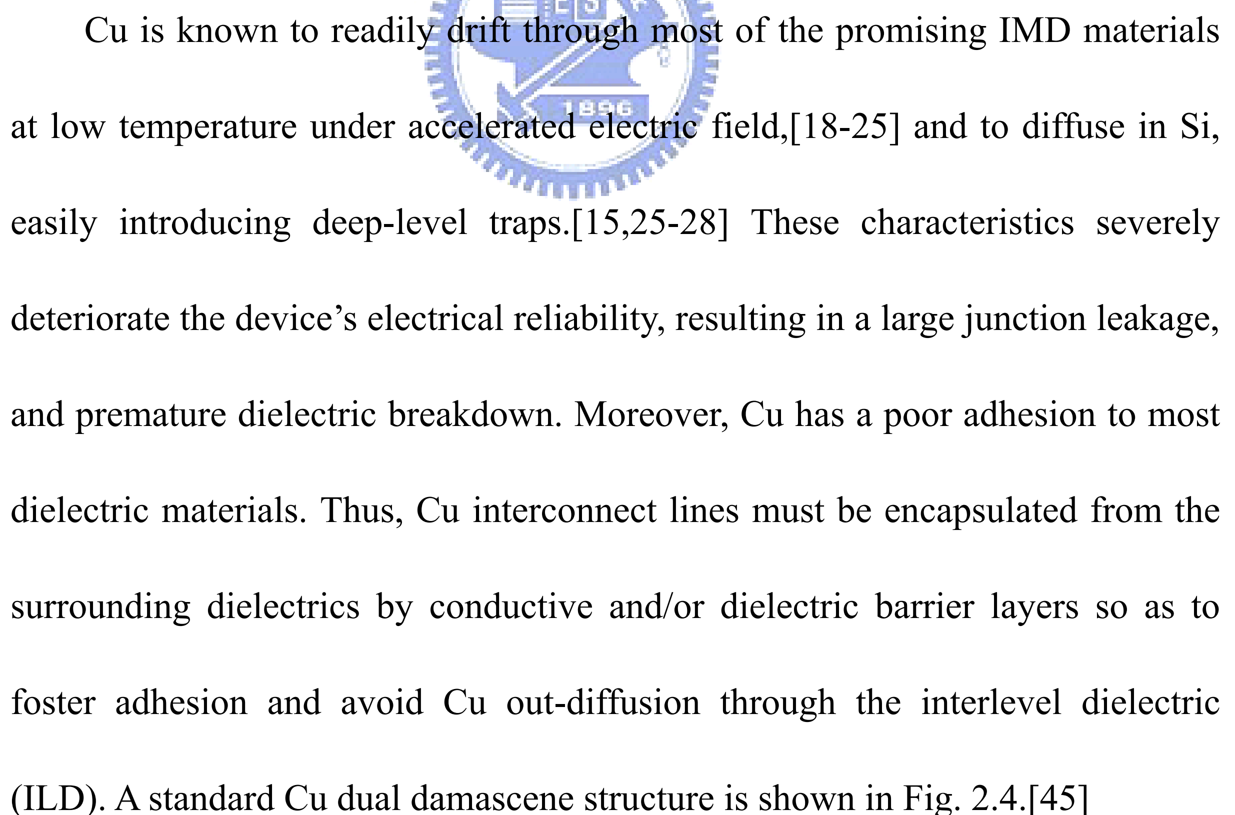

Cu is known to readily drift through most of the promising IMD materials at low temperature under accelerated electric field,[18-25] and to diffuse in Si, easily introducing deep-level traps.[15,25-28] These characteristics severely deteriorate the device's electrical reliability, resulting in a large junction leakage, and premature dielectric breakdown. Moreover, Cu has a poor adhesion to most dielectric materials. Thus, Cu interconnect lines must be encapsulated from the surrounding dielectrics by conductive and/or dielectric barrier layers so as to foster adhesion and avoid Cu out-diffusion through the interlevel dielectric (ILD). A standard Cu dual damascene structure is shown in Fig. 2.4.[45]

The prospective conductive and dielectric barriers for Cu interconnects

must be effective against Cu out-diffusion and must be thin enough because the typical conductive and dielectric barriers have a relatively high resistivity and a high dielectric constant, respectively. These barrier films should be well adhered to the Cu layer, easily removed during Cu chemical mechanical polishing (CMP), and not reactive with Cu. Refractory metals (such as Ti, W, Ta, Cr and Mo) and their silicides and nitrides have been regarded as potential candidates for conductive barriers because of their high thermal stability, high melting points, and good electrical conductivity.[14-19,30,46-49] Specifically, Ta and TaN films deposited by PVD or CVD are the most promising materials in serving as the primary conductive barrier layer. It is well known that Ta does not alloy with Cu and that TaN possesses a dense microstructure as well as a high melting point at 3087℃. There are a number of studies on the barrier capability of Ta-based barrier layers between Cu and Si substrate as well as Cu and SiO_2 dielectric. However, little work has been reported on the study of integrating the barrier layers with Cu and low-K dielectrics. As for the dielectric barriers, PECVD silicon nitride (SiN) has been the most favorable candidate because of its barrier capability against ionic impurities, moisture resistance, chemical inertness, and ease of integration. In addition to being used as a dielectric barrier against Cu diffusion, PECVD SiN has been used as an etching stop layer (ESL)

and a final capping/passivation layer in the Cu damascene structures. Nevertheless, since PECVD SiN has a high dielectric constant (K=7~9), new dielectric barriers with lower dielectric constants (such as PECVD silicon carbide) are generally used when Cu interconnects are further scaled down to the 0.13/0.10 μm nodes.[50,51]

In this thesis, we reported our study on the development of PECVD SiC:H film as the diffusion barrier for Cu interconnect technology. The barrier efficiency of thin deposited SiC:H layers in the Cu/dielectric/Si metal-insulator-semiconductor (MIS) capacitor structures is investigated using both electrical measurements and materials analyses. For comparison, the dielectric barrier capability of thin PECVD SiN films is also studied.

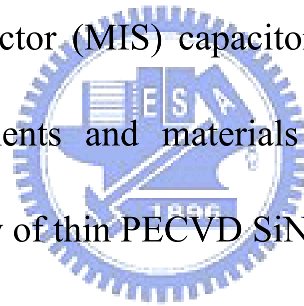

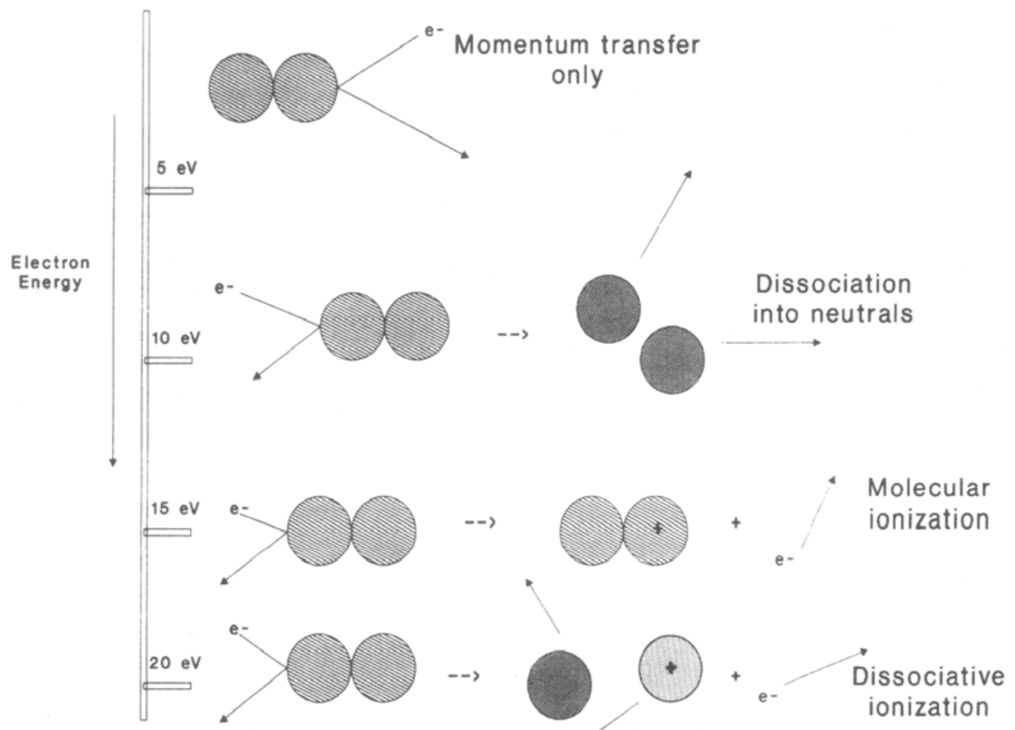

Fig. 2.1 Plasma chemistry of the hydrogen molecule as the impinging electron energy is increased.

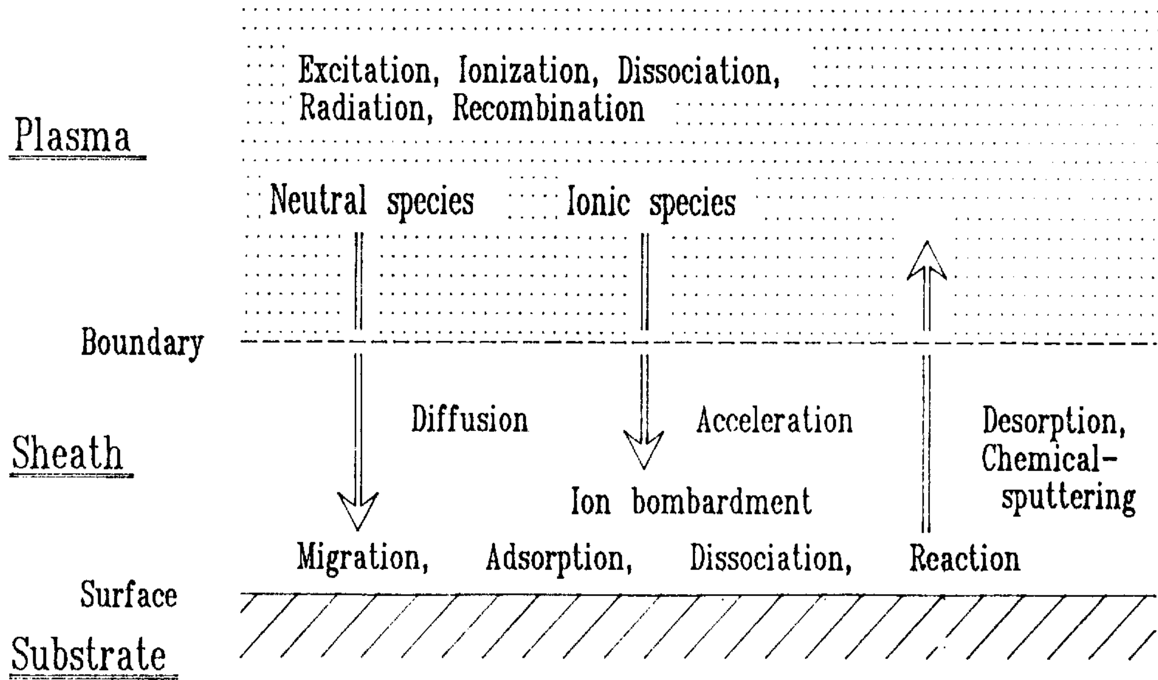

Fig. 2.2 Schematic representation of the plasma-enhanced CVD reaction process.

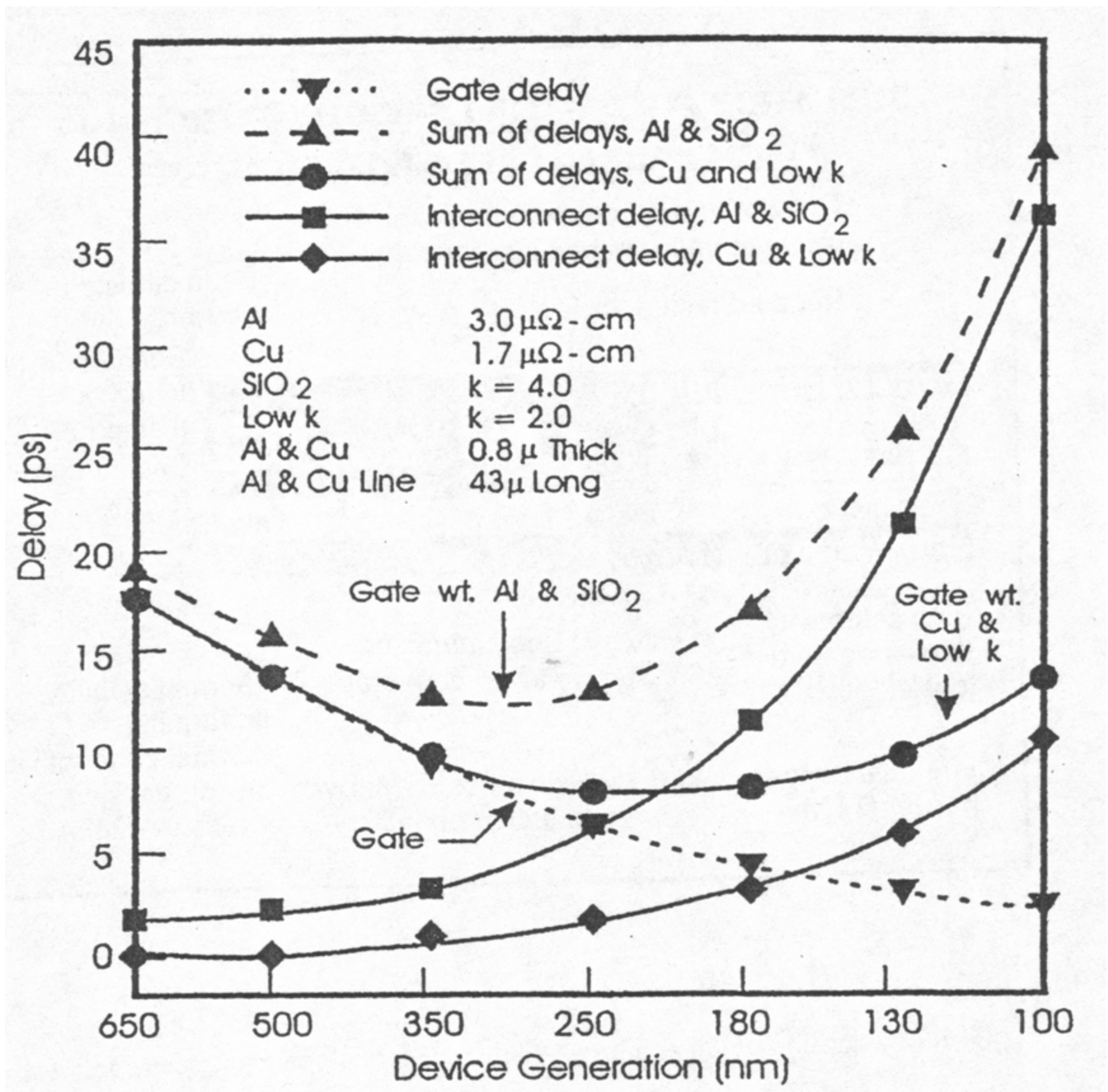

Fig. 2.3 Calculated delays for Al/SiO_2 and Cu/Low-K interconnect systems.

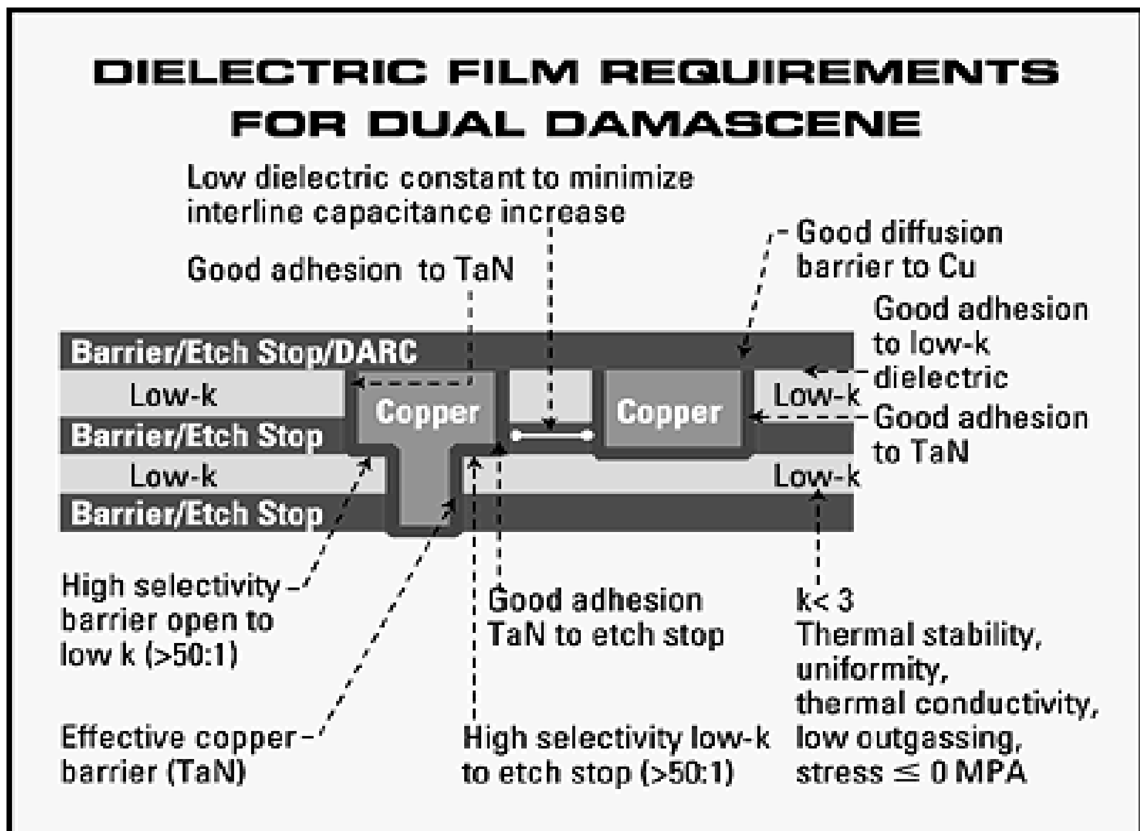

Fig. 2.4 Integration of Cu and low-K dielectrics into a dual damascene architecture.

Table 2.1(a) Dielectric constant of several materials.

Materials	Dielectric constant
Vacuum	1.00000
Air	1.006
Silicon wafer	11.7
SiC 6H (single crystal)	9.66
Acetone	27
Water	81
Metal	∞

Table 2.1(b) Some recent promising low-K materials.[39]

Low-K material	Dielectric constant	Product name	Deposition method	Supplier/source users
Fluorinated SiO_2	3.2-3.6	FSG	PECVD or HDP-CVD	AMAT, Novellus Mattson, TEL
Silsesquioxane	2.5-3.0	HOSP/LOSP FOX/HSQ Flowfill Black diamond 3MS 4MS	SOD SOD CVD CVD CVD CVD	AlliedSignal Dow Corning Trikon AMAT Dow Corning Schumacher/NVLS
Poly(arylene ether)	2.6-2.8	SiLK FLARE Velox	SOD SOD SOD	Dow Chemical AlliedSignal Schumacher
Polylene	2.2-2.9	Polylene-N Polylene-AF4	CVD CVD	PRI, TI, Mattson Novellus/TI
Fluoro-Polymer	1.9-2.0	PTFE	SOD	Gore
Fluorinated amorphous carbon	2.0-2.6	a-F:C/FLAC	CVD	Novellus, AMAT NEC, Sharp MIT, UT Arlington
Diamondlike carbon	2.4-2.8	DLC	CVD	IBM
Porous silica Mesoporous silica Porous Silsesquioxane Porous polyimide	1.2-2.3	Nanoglass - - Nanofoam -	SOD SOD SOD SOD SOD	AlliedSignal, TI SNL, PNNL IBM, Gatech IBM UCLA/CNXT
Air-bridge	1.0			

Chapter 3

Effect of Post-treatment on Electrical Properties of Amorphous Hydrogenated Carbon Films Deposited by Gridless Ion Beam Deposition

3.1 Introduction

Hydrogenated carbon films are produced primarily by hydrocarbon cracking. They exhibit 'diamond-like' properties, such as high hardness, high electrical resistivity, chemical inertness, and optical transparency.[1-3] The unique combination of these properties renders a-C:H films attractive for technological applications. In electronic applications, a-C:H can be used in place of silicon dioxide as an insulator, since its resistivity is very high. Recently, much attention has shifted towards the development of carbon-based films, deposited by plasma-enhanced chemical vapor deposition (PECVD) or high-density plasma CVD using hydrocarbon or hydrofluorocarbon precursors, to generate materials with low dielectric constants.[4-11] These unique properties in the a-C:H film may be attributed to the contained hydrogen atoms, which help to stabilize the tetrahedral bonds of carbon atoms. Increasing the proportion of tetrahedral bonds simultaneously promotes the dielectric properties of the a-C:H film.[12] Adjusting the deposition conditions, however,

was found to be able to yield a-C:H films with low dielectric constants, which make them extremely interesting for use as inter-metal dielectric layers in multiplayer metal integrated circuits.[13] Nevertheless, these films easily absorb moisture, increasing the dielectric constant and leakage current, since the dangling bonds can easily react with moisture to form -OH bonds. Choi et al.[14] suggested that in the annealing of films, the number of dangling bonds decreases as the annealing temperature increases. Hydrogen plasma treatment is also used for providing hydrogen ions with the ability to passivate the surface of the dielectric and reduce the number of dangling bonds.[15]

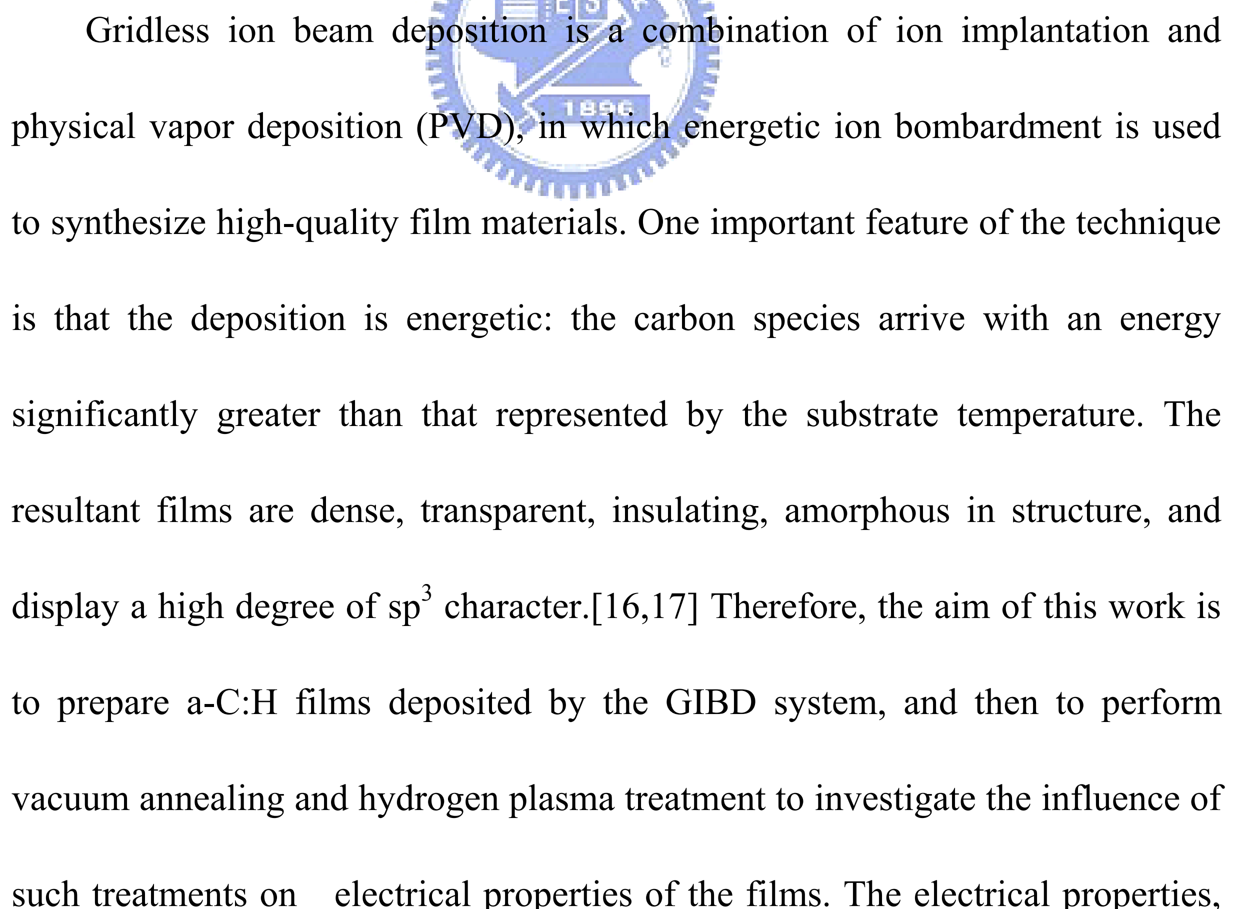

Gridless ion beam deposition is a combination of ion implantation and physical vapor deposition (PVD), in which energetic ion bombardment is used to synthesize high-quality film materials. One important feature of the technique is that the deposition is energetic: the carbon species arrive with an energy significantly greater than that represented by the substrate temperature. The resultant films are dense, transparent, insulating, amorphous in structure, and display a high degree of sp^3 character.[16,17] Therefore, the aim of this work is to prepare a-C:H films deposited by the GIBD system, and then to perform vacuum annealing and hydrogen plasma treatment to investigate the influence of such treatments on electrical properties of the films. The electrical properties,

such as the leakage current density and the dielectric constant, will be evaluated with a metal-insulator- semiconductor (MIS) structure.

3.2 Experimental

One-side-polished, p-type/boron-doped 4-inch silicon wafers with resistivity of 1~10 Ω-cm and (100) orientation were used as substrates. Before the deposition, wafers were cleaned by the RCA procedure, rinsed in de-ionized water, and then dried in a nitrogen ambient. The film thickness used here was typically 300 nm and the film was deposited by GIBD at about 80℃ which involved heating by ion bombardment. The deposition source had no grid and was named "end-Hall" type ion producer.[18] The ion source was located 25 cm from the sample holder and the ions arrived with normal incidence. No bias or extra heating or cooling system was applied to the substrate. Before the deposition, the samples were sputtered by 500 eV argon beam for 10 min. High-purity (99.995%) argon (Ar) and acetylene (C_2H_2) were monitored by mass flow controllers and introduced separately into the deposition system. The annealing treatment of a-C:H films was carried out in vacuum for 1 h at 100, 200, and 300℃ respectively. Otherwise, the pressure for the hydrogen plasma treatment of post-deposited a-C:H films was set by the PECVD system at 300 mTorr and the plasma treatment period was 1, 3, and 6 min, respectively. The

substrate temperature was maintained at 250℃, and the rf power was maintained 100 W and the hydrogen gas flow was fixed at 400 standard cubic centimeter per minute (sccm).

The refractive index and thickness of the a-C:H films were determined by the n&k Analyzer 1200. The film density was calculated from the geometrical thickness and the mass/cm^2, which determined by Rutherford backscattering spectrometry (RBS) of 2-MeV He$^+$ ions. Raman spectroscopy is probably the most common technique used for evaluation of carbon films because of its ability to distinguish between different forms of carbon. The microstructure and quality of the a-C:H films were determined by the Renishaw micro-Raman spectroscopy system 1000. Raman measurements were performed at 514.5 nm at 1 cm^{-1} resolution; integration times were 3 min at 50 mW Ar ion laser power. In order to investigate the dielectric properties of a-C:H films, a MIS capacitor was employed to carry out the electrical measurements, as shown in Fig. 3.1. Circular metal insulator silicon structures were fabricated by sputtering aluminum through a shadow mask onto the dielectric films. A 1-μm-thick copper film was sputtered on the wafer back surface for a good substrate contact. After copper film was deposited, the samples were annealed in a nitrogen ambient at 200℃ for 30 min. The leakage behavior was measured by

applying a staircase voltage ramp using an HP 4156B semiconductor parameter analyzer, for which the MIS capacitor was biased at accumulation polarity. Leakage current-voltage (I-V) measurements were performed to investigate the leakage properties. The high-frequency capacitance-voltage (C-V) measurements were performed at 1 MHz using a HP 4280A C-V meter. The dielectric constant was estimated from the capacitance in the accumulation region of the MIS sample and the film thickness.

3.3 Results and Discussion

Amorphous carbon generally is considered to include a mixture of sp^3 (diamond-like) and sp^2 (graphite) bonding structures, in which the bond angles are no longer the ideal values of 109°28' and 120°. Accordingly, the shape and peak positions of the corresponding Raman spectra may be different. The spectra can generally be deconvoluted into Gaussian or Lorentzian peaks at approximately 1550 cm^{-1} (G peak) and 1355 cm^{-1} (D peak), as shown in Fig. 3.2. Single-crystal graphite exhibits a Raman spectrum with a single line at 1580 cm^{-1}, while crystalline diamond gives a single sharp line at 1332 cm^{-1}. The literature generally splits these into a graphite or G peak at 1580 cm^{-1} for crystalline graphite or a band around 1450-1500 cm^{-1} for amorphous sp^2 and another band at around 1360 cm^{-1}, referred to as the D or disordered peak.

More diamond-like films have generally a lower G peak wavenumber and a lower D peak/G peak intensity ratio, I_D/I_G ratio, so these two parameters can be used to assess the quality of carbon films. The peak intensities in the Raman spectra were fitted to the sum of two Gaussian line shapes and plotted against the integrated intensity ratio, I_D/I_G. Figure 3.3 plots the graphs of (a) the Raman I_D/I_G ratio, and (b) the D peak position of a-C:H films as functions of the C_2H_2 gas flow rate. Increasing the C_2H_2 gas flow rate from 10 sccm to 60 sccm decreases the I_D/I_G intensity ratio from 0.734 to 0.691 and the D peak position from 1288.4 cm^{-1} to 1285.6 cm^{-1}. The graphs indicate that a higher C_2H_2 flow rate corresponds to a lower I_D/I_G ratio and D peak position. With increasing the C_2H_2 gas flow rate will be decreased the particle energy during growth because of the reduction of the mean free path. Zou et al. found that favors a more porous structure and brings a slow decrease of the density, a decrease of the hardness, and an increase of the hydrogen content, and of the bonding ratio sp^3/sp^2.[19] Hydrogen doping also greatly affects the structure of an a-C:H films. Raising the C_2H_2 gas flow rate decreases the I_D/I_G intensity ratio and shifts the Raman D peak downward, indicating an increase in the sp^3/sp^2 bond ratio of the a-C:H films.[20,21] According to the model for amorphous carbon proposed by Beeman,[24] the position of the peaks contain information

concerning bond-angle disorder and the bonding in the formed crystallites. The bond-angle disorder with a certain percentage of tetrahedral bonds will shift the D peak and G peak downward. Thus, the a-C:H film possesses diamond-like character as the C_2H_2 gas flow rate increases.

Figure 3.4 shows the Raman spectra of the a-C:H films with different annealing temperatures from 100℃ to 400℃. Figure 3.5 summaries the (a) Raman I_D/I_G ratio and (b) the D peak position of annealed a-C:H films from Fig. 3.4 as plots versus various annealing temperatures in a vacuum. Increasing the annealing temperature from 100℃ to 400℃ increases the I_D/I_G intensity ratio from 0.82 to 1.02, but the D peak position herein is unobvious trend. Furthermore, Figure 3.6 presents the variation of the mass density of the film with annealing temperature, as determined by RBS analysis. The figure indicates that the density decreases from 3.44 g/cm^3 to 2.89 g/cm^3 as the annealing temperature are increased. The mass density (ρ) should indicate the extent to which the films are graphite-like (ρ=2.25 g/cm^3) or diamond-like (ρ=3.51 g/cm^3). This implies that a-C:H film may contain a small percentage of tetrahedral bonds which are broken upon annealing. Therefore, verified whether the annealed a-C:H film has a progressive micro-structural rearrangement occurs during annealing process. The results are consistent with the model proposed by

Dillon et al.,[21] who predicted a progressive growth in number and/or size of graphitic domains for amorphous carbon films annealed at increasing temperature. Furthermore the intensity ratio I_D/I_G can be used to get a quantitative estimation of the sp^2 cluster size (L). A critical diameter at around 12 Å, which makes I_D/I_G be a maximum.[22] Below the critical diameter, the Raman measurement on graphite at a different degree of disorder suggested the functional relation

$$\mathbf{I_D/I_G \propto L} \qquad \textbf{(1)}$$

where L is the typical graphite cluster size. When the samples are annealed, the grain size increases, and the relation between relative intensity and grain size can be expressed as [23]

$$\mathbf{I_D/I_G \propto L^{-1}.} \qquad \textbf{(2)}$$

As shown in Fig. 3.4(a), the I_D/I_G intensity ratio increases with annealing temperature, obeying the rule of Eq. (1). The trend of I_D/I_G intensity ratio decreases with annealing temperature maybe brought by higher annealing temperature that inducing the grain size of sp^2 cluster is large enough. During annealing treatment, Friessnegg et al. found that a generation, in the meanwhile, of defects due to hydrogen effusion was observed.[31] Akkerman et al.[32] and Wild and Koidl [33] reported that the released hydrogen atoms and hydrocarbon

radicals produce hydrogen and hydrocarbon molecules in the bulk of the films during annealing; these molecules then diffuse through the carbon network out of the films. If this process also dominates the evolution of hydrogen in the films produced, then the slight increase in thickness is mainly due to the transformation of a diamond-like structure to a graphite-like structure.[34]

The addition of hydrogen to a growing carbon film, such that the generated C_2H_2 gas reacts with the plasma during film deposition, prevents the nucleation of the graphite phase and stabilizes the tetrahedral bonding, thereby enhancing the diamond-like characteristics of the film.[20,25,26] As the hydrogen content of the films increases, however, the dangling bonds still remains on the surface of the films. The dangling bonds can thus easily react with moisture to form -OH bonds and thus affect the electrical properties. Figure 3.7 plots the leakage current density (J) against applied electric field (E) for a-C:H films annealed at different temperatures. The a-C:H films annealed below 200℃ have a lower leakage current density than the others since the heating removes the absorbed moisture, promotes the movement of hydrogen and activates the electrical defects which compensated unintentional impurities[27] on the film. However, the a-C:H films annealed at 300℃ have a higher leakage current density than the as-deposited films. As previous

describes the effect of overheating on the a-C:H films rearranging their microstructure from a diamond-like one to a graphite-like one, which is a conductive component, thus increasing the leakage current density. The heating also changes the hydrogen distribution and/or content.[28]; transforms the films into graphite-like amorphous carbon films, causing the band-gap to diminish and the carefully nurtured semi-conducting properties to be lost.[29,30] Figure 3.8 shows the dielectric constant (K) of a-C:H films against vacuum annealing temperature and hydrogen plasma treatment period. Figure 3.8(a) shows that vacuum annealing treatment reduces the dielectric constant of the a-C:H films from 3.81 to 3.18 as the annealing temperature increases from 100℃ to 300℃. As previous describes the effusing effects of hydrogen [7] and moisture on a-C:H films as a result of annealing that leaves pores in the insulating film. The decrease of the dielectric constant can be explained as follows: the pores introduced in the film as a result of annealing causes reduction in mass density of the film, shows in Fig. 3.6. Thus, the changes in the character and number of network bonds in the films during annealing lead to an increase in the mean size of the micro-pores.[33] These pores reduce the dielectric constant, since the dielectric constant of air in a pore is close to that of a vacuum. It has a lowest dielectric constant at 3.18 while the a-C:H film

annealed at 300℃.

Hydrogen plasma also affects the electrical properties of the a-C:H films. The as-deposited a-C:H films were treated with hydrogen plasma to reduce their dielectric constant and leakage current, as shown in Fig. 3.8(b) and Fig. 3.9. The variation in the thickness of the films thus treated is hardly visible, but their surfaces become rougher and covered with more pinholes as the period of hydrogen plasma treatment is increased. Horn et al. suggested that under impact of H atoms the hybridization of carbon atoms at a C:H film surface change from sp^3 to sp^2 character in the temperature range 400 to 700 K.[35] The species of sp^2 character is preferentially etched by hydrogen plasma.[36] Thus, the rugged C:H film surface results from hydrogen plasma erosion. Besides, hydrogen ions create dangling bonds by displacement or chemical abstraction of bonded hydrogen in the film in forming hydrogen molecules, which leave the film. The second step concerns the relaxation of these dangling bonds. They can be saturated by free hydrogen atoms or by forming double bonds with neighboring carbon atoms. These processes were established by Horn et al.[35] Thus the surface of the a-C:H film is passivated during hydrogen plasma treatment and the dielectric constant is unobvious change as the plasma period increases. Figure 3.9 shows the leakage current density of

a-C:H films after hydrogen plasma treatment at 250℃ for 1 min, 3 min and 6 min. The leakage current decreases as the period of hydrogen plasma treatment increases. The sp^2 content on the surface is etched away during plasma treatment, and the hydrogen radicals help to passivate the surface with respect to air oxidation and annihilate surface dangling bonds. Consequently, the a-C:H films with lower leakage are obtained because the leakage source on the surface is eliminated by the hydrogen-containing plasma. Thus it has a lowest leakage current density of 3×10^{-7} A/cm^2 with an electric field at 1MV/cm after hydrogen plasma period by 6 minutes. However, the hydrogen plasma interacts with the a-C:H films only in the outermost layer of the film to a thickness of about 40 Å, which is dependent on the ion energy.[37,38] Thus, the hydrogen plasma did not affect the bulk of the a-C:H films. Accordingly, the dielectric constant was not obviously changed as the plasma treatment period increased, but the value was lower than that for the as-deposited films, as shown in Fig. 3.8(b).

The process requires a low-dielectric material or a dielectric material of reduced thickness to reduce the effective dielectric constant in a copper damascene structure. Post-treatment by either annealing or using hydrogen plasma facilitates the reduction of the dielectric constant and leakage current of

a-C:H films. However, after the films were annealed at an elevated temperature (≥ 300℃), their microstructures were converted from diamond-like to graphite-like and the film density had decreased. The overheated film possessed a higher leakage current density, due to the transition in the microstructure, since the insulation of the graphite-like structure is weaker than that of the diamond-like structure. Otherwise, the properties and the variation in the thickness of those hydrogen-plasma-treated films are hardly visible for a-C:H films, since hydrogen plasma treatment only improves the surface.

3.4 Conclusions

Highly sp^3-bonded a-C:H films were deposited using a GIBD system. The films possessed more diamond-like characteristics as the C_2H_2 flow rate was increased. After the films were annealed at an elevated temperature, their microstructures were changed from diamond-like to graphite-like, and the leakage current density increased. The mass density decreases from 3.44 g/cm^3 to 2.89 g/cm^3 as annealing temperature is increased, indicating that the annealed a-C:H film has more graphite-like character and thus a higher leakage current density than the as-deposited film, on the other hand, the dielectric constant decreases as the annealing temperature is increased. Hydrogen plasma treatment can significantly improve the electrical characteristics. The variation

of the surface properties of these plasma-treated a-C:H films is barely visible and their electrical properties are greatly enhanced, since hydrogen plasma treatment significantly passivates the surface.

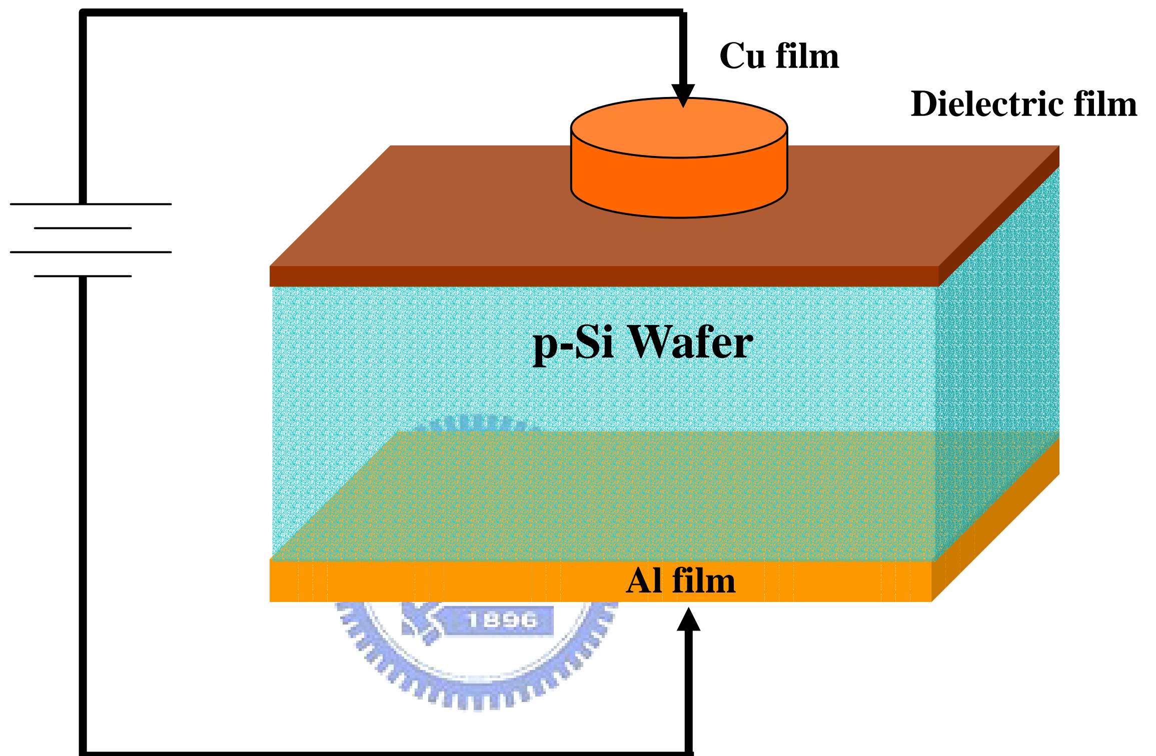

Fig. 3.1 Metal-insulator-semiconductor (MIS) structure.

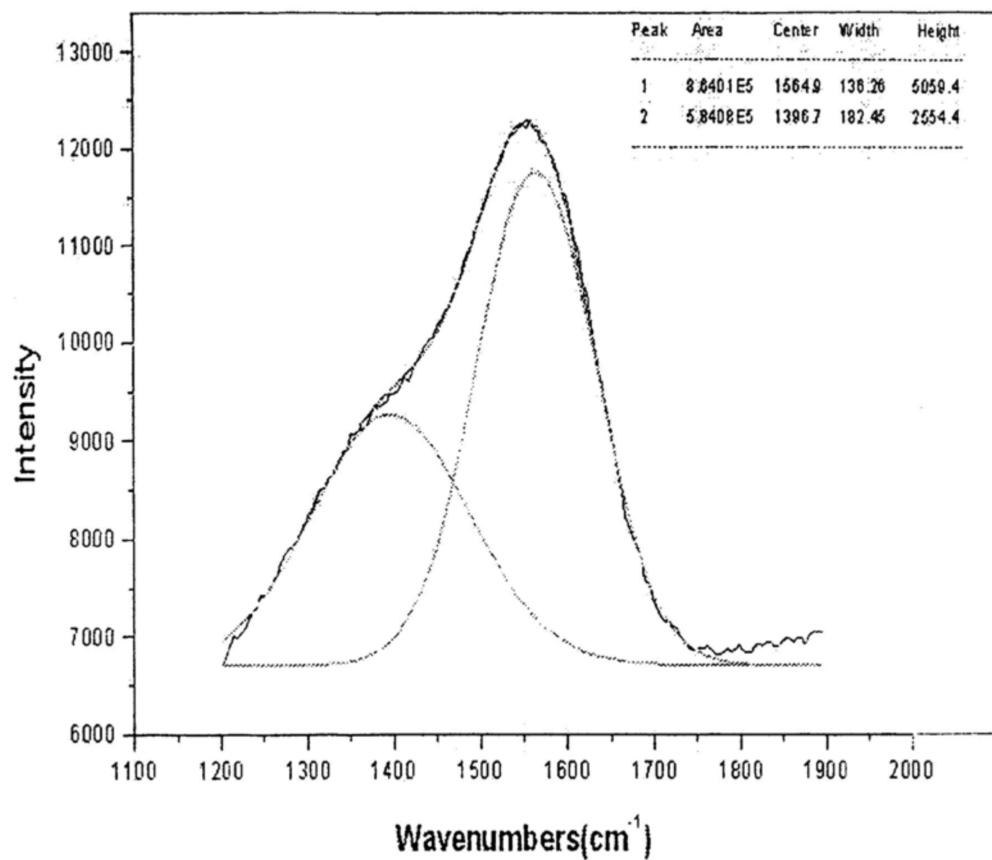

Fig. 3.2 The fitted curves of Raman spectra of the a-C:H films.

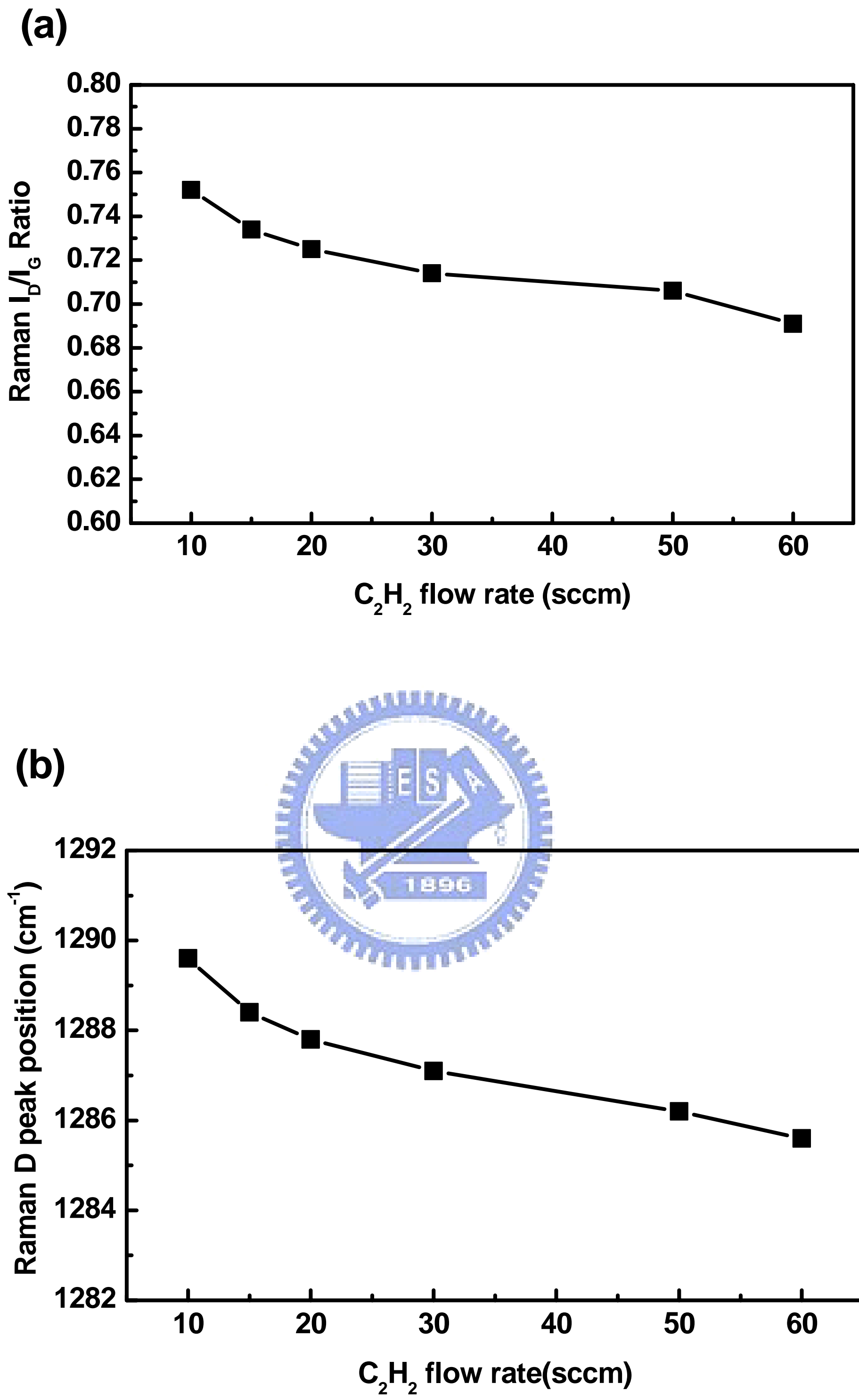

Fig. 3.3 Graphs of (a) Raman I_D/I_G ratio, and (b) D peak position of a-C:H films as functions of C_2H_2 gas flow rate.

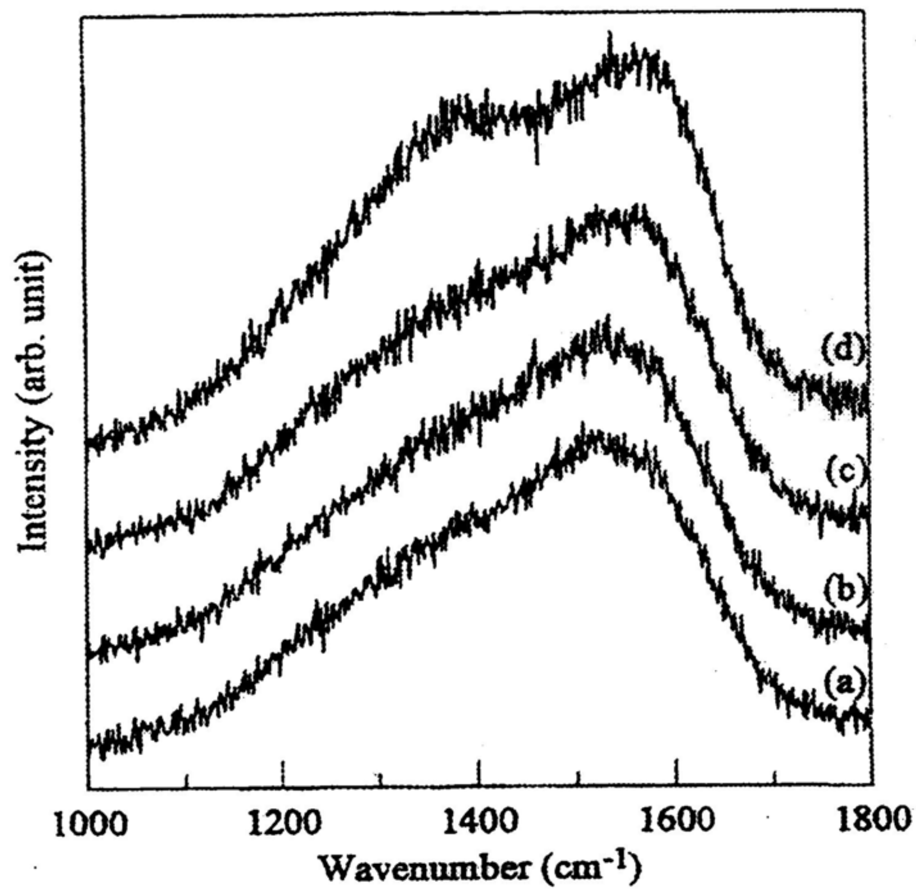

Fig. 3.4 Raman spectra of the a-C:H films with different annealing temperatures, (a) 100℃, (b) 200℃, (c) 300℃, and (d) 400℃.

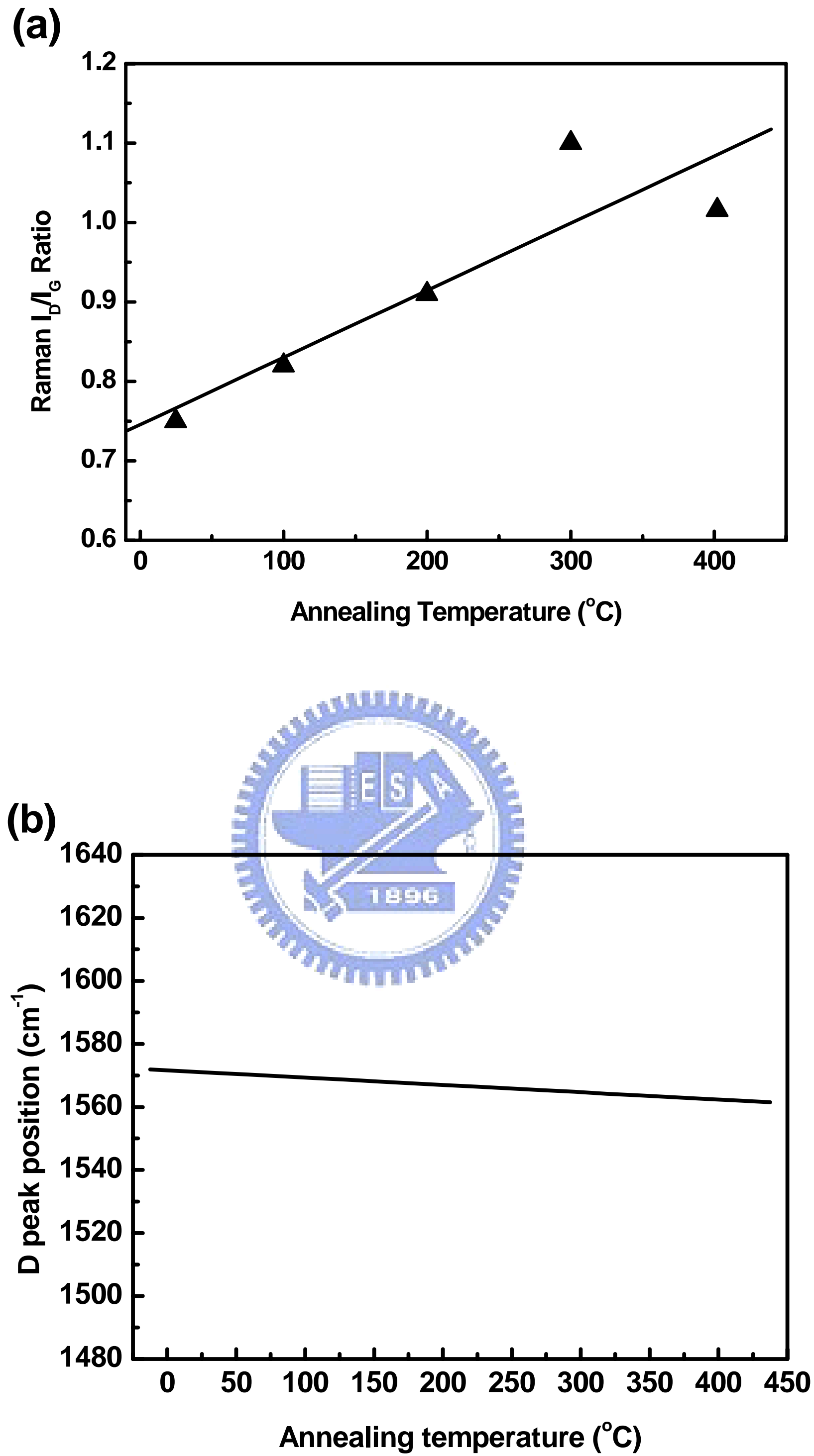

Fig. 3.5 Graphs of (a) Raman I_D/I_G ratio and (b) D-peak position of a-C:H films with various annealing temperatures in vacuum.

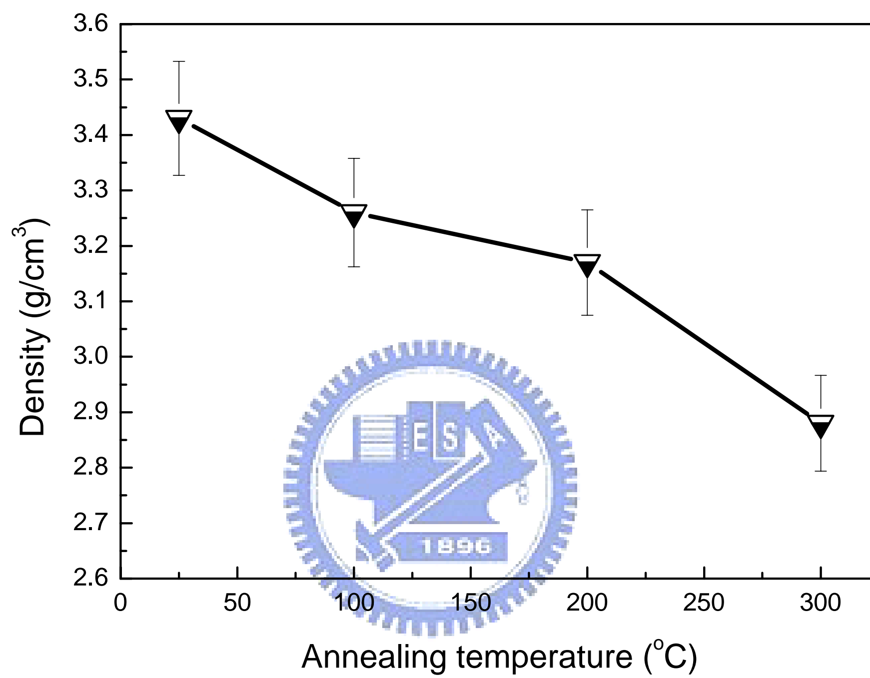

Fig. 3.6 Density of a-C:H films for various vacuum annealing temperatures.

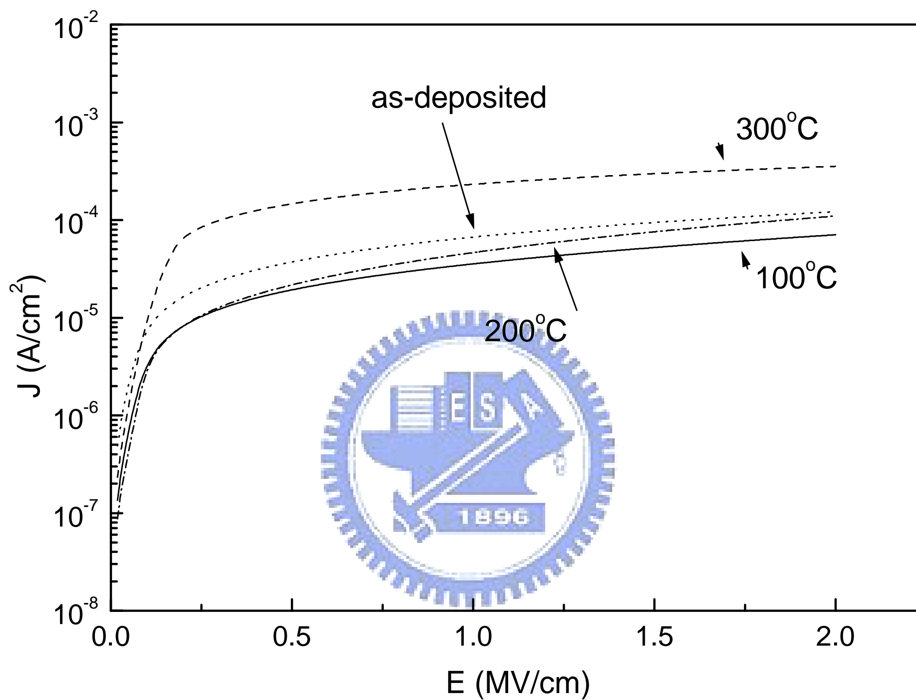

Fig. 3.7 J-E curves of a-C:H films with different vacuum annealing temperatures.

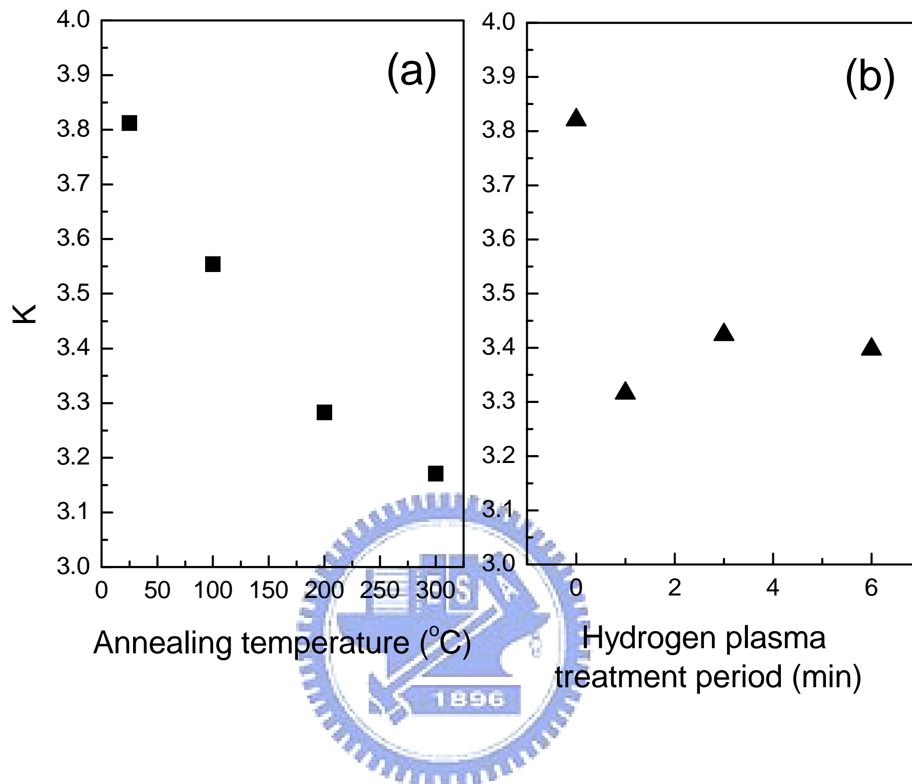

Fig. 3.8 (a) Dielectric constant (K) of a-C:H films with different vacuum annealing temperatures, and (b) Dielectric constant of a-C:H films with different hydrogen plasma treatment periods.

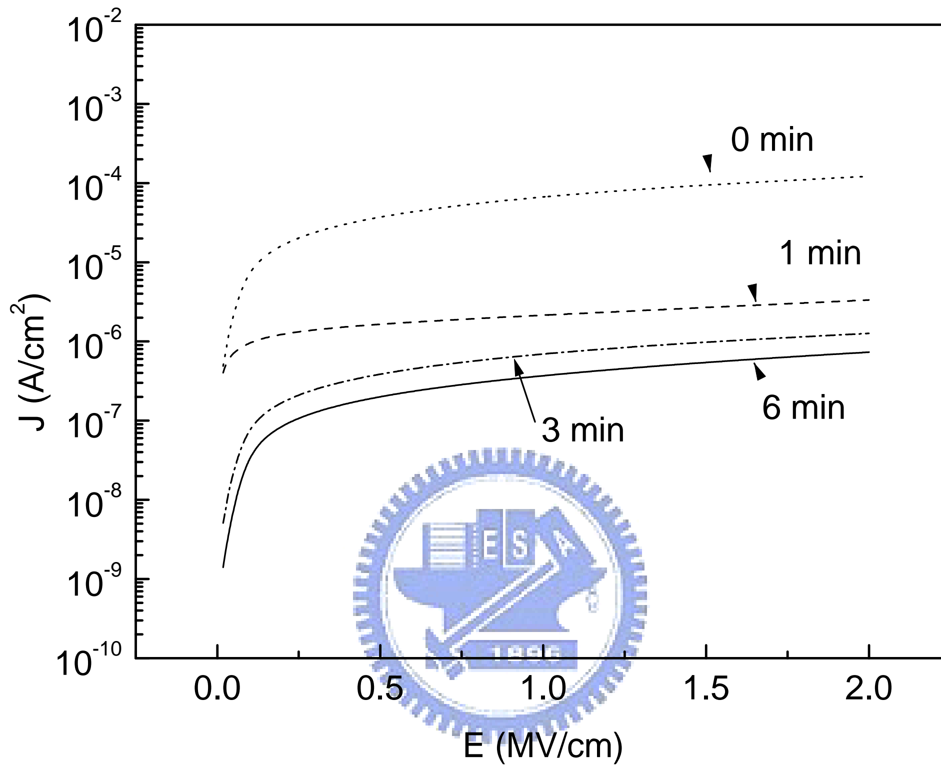

Fig. 3.9 J-E curves of a-C:H films with different hydrogen plasma treatment periods.

Chapter 4

Effects of Hydrogen and Ammonia Plasma Treatment on the Electrical Properties of PECVD a-SiC:H Films

4.1 Introduction

The unique physical and electrical properties of SiC, including its wide band gap, high thermal conductivity, and high melting point, make SiC potentially useful for optoelectronic,[1] high-frequency and high-temperature device applications. Carbon-rich a-SiC:H films with wide band gaps are interesting because of their potential use in optoelectronic devices, such as LEDs, color sensors and so on.[2-4] The incorporation of carbon in the amorphous Si network raises the possibility of tuning the band gap of a-SiC:H alloys in the range between 1.7 and 3.5 eV, although the presence of carbon induces defects in the gap degrading the optoelectronic characteristics of the material.[5] Device-quality films of a-SiC:H, with an energy gap below 2.3 eV, can be deposited by PECVD under suitable plasma conditions, from mixtures of silane and methane.[6] In addition to being used in packaging applications, the a-SiC:H materials are being developed as diffusion barriers, buried hard masks, and etch-stops in copper damascene interconnection technology.[7,8]

Current leakage in conventional SiC contributes to conduction through

silicon. Si has an electronic polarizability 20 times that of carbon. Consequently, substituting the less polarizable carbon atom for silicon in SiC should yield a lower dielectric constant for the pristine SiC. Nevertheless, these low-k materials that contain Si-H groups easily absorb moisture, increasing the leakage current and dielectric constant. The formation of SiC:H films of has limited applicability at present. The hydrogen content in the a-SiC:H film is known to increase with the amount of carbon, and hydrogen is importantly involved in passivating the silicon-dangling bond. Dangling bonds can easily react with water moleculars to form -OH bonds, increasing the dielectric constant and the leakage current. Therefore, hydrogen plasma treatment is often used for providing hydrogen radicals to reduce the density of dangling bonds. Previous report has shown hydrogen or ammonia plasma treatment can significantly improve dielectric properties of many low-K materials. The leakage current of hydrogen silsesquioxane (HSQ) decreases as the hydrogen and ammonia plasma treatment periods are increased.[9,10] Liu et al. have described how the passivation layer effectively reduces the uptake of moisture of HSQ subjected to an ammonia plasma treatment and the diffusion length of copper in the HSQ.[5]

Plasma-enhanced chemical vapor deposition has been extensively utilized to grow hydrogenated amorphous silicon carbide (a-Si_mC_n:H_y) films from

mixtures of silane and methane.[11-13] In earlier reports, grown by low power PECVD a-SiC:H films had a high carbon content (> 0.5), an optical band gap up to 3.7 eV and a high electrical resistivity, suggesting the presence of a diamond-like C-C phase.[14] However, the application of ammonia plasma treatment to the a-SiC:H films has not been extensively reported at this moment. In this work, we investigated properties of carbon-rich a-SiC:H films deposited in a single-wafer PECVD chamber and subsequently treated with the ammonia plasma and hydrogen plasma treatment respectively. The effect of preventing copper diffusion by the a-SiC:H films was examined by taking electrical measurements on MIS (metal-insulator-semiconductor) structures.

4.2 Experimental

One-side-polished, p-type / boron-doped 4-inch silicon wafers with resistivity of 15~25 Ω-cm and (100) orientation, were used as substrates. Before the deposition processes, wafers were cleaned according to the standard RCA procedure and then rinsed in de-ionized water and dried in a nitrogen ambient. The interaction of copper with the dielectrics was studied by electrical measurements using MIS structures. The 1000 Å a-Si_mC_n:H_y films were deposited by PECVD processes in a parallel plate reactor that was operated at 13.56 MHz, as shown in Fig. 4.1. The total pressure inside the chamber was

kept constant by varying the gas flows and the pumping speed. The mixture of silane and methane gases was introduced through the gas line for deposition and then ammonia plasma treatment was performed. In order to analyze the influence of the methane flow rate on the a-Si_mC_n:H_y properties, changing the methane concentration and maintaining the silane flow rate at 5 sccm. The methane flow rate in the mixture of silane and methane gases was varied from 35 to 100 sccm. Table 4.1 specifies the deposition parameters, hydrogen plasma/ammonia plasma treatment parameters and characterizations of the a-Si_mC_n:H_y films. Circular metal insulator silicon structures were formed by sputtering copper through a shadow mask onto dielectric films. Finally, the Al film 1 μm thick was sputtered on the backside of the wafer to ensure a good substrate contact. Al does not drift in SiO_2.[15] The capacitors were all annealed at 200℃ for 30 minutes in a quartz furnace in a pure nitrogen environment.

The thickness, refractive index and optical energy gap of the CVD films were determined by *n&k A*nalyzer 1200. The measurement of water contact angle of a-Si_mC_n:H_y films were carried out in atmospheric conditions at room temperature. A droplet with the volume of 2.5 μl was released onto the surface of sample from a syringe needle. The contour of the liquid drop on the solid

surface was captured by a charge coupled device camera after 15 s, which is to guarantee the liquid drops have reached equilibrium. For each sample, at least three drops were measured. The accuracy of the contact angle is less than 1°. X-ray photoelectron spectroscopy (XPS) and atomic force microscopy (AFM) analyzed the chemical composition and surface morphology of the dielectric films, respectively. The ion bombardment was performed in an ultrahigh vacuum preparation chamber directly attached to the XPS analysis chamber. XPS analysis was performed with an ESCA PHI 1600 instrument using non-monochromatic Mg Kα x-radiation ($h{\cdot}v = 1253.6$ eV). Surface morphology of all samples were studied by DI (Digital Instruments)-AFM D500 system in the tapping mode. The root mean square (Rms) of the height data within the scan area (5×5 μm^2) is used in the following discussion as the roughness value.

The electrical measurements were obtained in the dark at room temperature. The leakage behavior was measured by applying a staircase voltage ramp using an HP 4156B semiconductor parameter analyzer, for which the MIS capacitor biased at accumulation polarity. I-V measurements were made to investigate the leakage properties. The dielectric constants (K) were also measured by determining capacitance-voltage (C-V; Keithley 590A C-V analyzer) characteristics at 1 MHz.

4.3 Results and Discussion

4.3.1 Characteristics of the PECVD a-Si_mC_n:H_y films

The film properties of Si_mC_n:H_y films depend on film deposition conditions. From Table 4.1, the chemical composition of the a-Si_mC_n:H_y films were analyzed by XPS. The atomic ratio of carbon to silicon in the carbon rich a-Si_mC_n:H_y film is 2.32:1. The oxygen content in the a-Si_mC_n:H_y films probably originates from either residual oxygen gas in the deposition chamber or the air to which the film is exposed. Figure 4.2, 4.3, and 4.4 plot the characteristics of a-Si_mC_n:H_y films as a function of x [x=SiH_4/(SiH_4+CH_4)]. From Fig. 4.2, the deposition rate, calculated from the deposited thickness divided by depositing period, changes from 11.3 Å/s to 1.3 Å/s as the SiH_4/(SiH_4+CH_4) flow ratio decreases from 0.41 to 0.048. At low power deposition, the deposition rate of amorphous carbon films using methane as the gas source is very small (< 0.1 μm/h), implying that the decomposition of the methane is insignificant. The relatively large dissociation energy of the C-H bond in methane (104.8 kcal/mol), compared with that of the Si-H bond in silane (~90 kcal/mol). Furthermore, the cross section of dissociation (5×10^{-16} cm^2 for silane and 2.5×10^{-16} cm^2 for methane at an electron energy of 20 eV) [16,17] imply a thermodynamic preference for Si-H bond cleavage over C-H bond cleavage. Although the Si-C

bond on the outmost layer of depositing film, with a dissociation energy of ~88 kcal/mol, is the weakest in the molecule, the gas-phase data reveal that Si-C bond cleavage under plasma conditions has a smaller cross section than does Si-H bond cleavage. Accordingly, silane molecules are more easily decomposed in the plasma, and the concentration of Si or SiH_x radicals in the plasma will increase as the silane flow rate is increased. Furthermore, the sticking coefficient of CH_x radicals may be lower than that of SiH_x radicals [34] such that the deposition rate decreases as the flow rate of silane is reduced. Tong et al. [18] have demonstrated the same trend. According to Fig. 4.3, reducing the silane flow rate decreases the refractive index, while increasing the carbon content and the optical band gap, analyzed by *n&k A*nalyzer 1200. The index of refraction changes from 2.80 to 1.76, the optical band gap changes from 2.17 eV to 3.31 eV, and the dielectric constant changes from 6.2 to 3.6 as the $SiH_4/(SiH_4+CH_4)$ flow ratio decreases from 0.41 to 0.048. Thus as the $SiH_4/(SiH_4+CH_4)$ flow ratio decreases, the deposited film becomes carbon rich, leading to a decrease in the index of refraction and the dielectric constant. C-C single bonds are expected to be generated as the carbon concentration is increased, typically when the original film has more sp^2 bonding character in a graphite-like form, resulting in a bonding structure rich in sp^3 character, and causing a narrowing of the optical

band gap.[19] As the carbon concentration increases, the a-Si_mC_n:H_y films become less dense,[20] which the size and the density of micro-voids increases with increasing carbon content, and the dielectric constant decreases, as shown in Fig. 4.4. The decrease in dielectric constant of the a-Si_mC_n:H_y films may be ascribed to the introduction of voids and the factor of silicon is 20 times the electronic polarizability of carbon.

The interdiffusion of Cu and Si through grain boundaries in a barrier film generates η”–Cu_3Si during post-annealing, resulting in the failure of the diffusion barrier.[21] Amorphous compound barriers are preferable to polycrystalline barriers, because the former barriers do not have grain boundaries, that can act as paths for fast diffusion. In this work, amorphous Si_mC_n:H_y thin films were deposited at 250℃,[22] and the current leakage property of the film were studies in terms of a MIS structure (Cu/a-Si_mC_n:H_y/Si).

Figure 4.5 shows the infrared spectra of the a-Si_mC_n:H_y films deposited with different methane flow rates (35, 50, 70 and 100 sccm). The absorption band at 1000 to 1100 cm^{-1} is associated with CH_n wagging; the peak at 780 cm^{-1} corresponds to Si-C stretching or SiC-CH_3 rocking, and that at 660 cm^{-1} corresponds to SiH_m wagging vibrations. The absorption band at 2140 cm^{-1} is SiH_n stretching and that at ~3000 cm^{-1} corresponds to CH_n stretching vibrations.

Methane is generally incompletely decomposed during the deposition of SiC films in a rf plasma system using a gas source mixture of silane and methane, and the deposited films contains many C-H_3 bonds or $(-CH_2-)_n$ chain-like bonds especially at a high carbon content.[24]

Figure 4.6 and 4.7 show the ESCA spectra and the elemental composition of the near-surface region of the a-Si_mC_n:H_y films is plotted as a function of methane flow rate. It indicates that the carbon concentration decreases from 82.0 at.% to 64.4 at.% with increasing the methane flow rate. Due to that the deposition rate decreases as the methane flow ratio increases, as shown in Fig. 4.2, i.e., increases the period of the reaction between the surface of the a-Si_mC_n:H_y film and plasma species. These results may be explained by the erosion effect [25] of hydrogen radicals, which created in the plasma, as will be discussed latter. The chemical erosion may preferentially consume carbon sp^2 bonding component and thereby generating dangling bonds.[26]

The film surface subjected to plasma treatment degrades with time. Thus it needs to proceed the measurement of contact angle to quantify the degree of surface hydrophobicity. Contact angles are related to the free energy of a surface, where a higher contact angle corresponds to a lower surface energy for the same surface topography. The surface energy of a solid surface can be obtained from

the measurement of the contact angle made with the surface by a reference liquid. Specifically, the contact angle (θ) that a liquid, ℓ, makes with a solid surface, s, is given by Young's equation:

$$(\gamma_{sv}-\gamma_{sl})=\gamma_{lv}\cos\theta_w \qquad (1)$$

where θ_w is a contact angle between a solid surface and water, γ_{sv} and γ_{lv} are the solid and liquid surface energy, respectively; γ_{sl} is the solid/liquid interfacial energy. The contact angle made between the reference liquid and the solid surface can now be rewritten as

$$(\gamma_s-\gamma_{sl})=\gamma_l\cos\theta_w \qquad (2)$$

where the interfacial free energy can be written as $\gamma_{sl}=\gamma_l+\gamma_s-2(\gamma_l\times\gamma_s)^{1/2}$.[27,28] Each of the surface energy terms in equation (2), are conveniently expressed as the sum of two separable components, namely the dispersive, γ^d, and the polar, γ^p, surface energies. The polar component of the surface energy is a measure of the solid surface to participate in specific molecule interactions of the following types: (a) hydrogen-bonding, (b) acid-base neutralization, or (c) chemical bond formation. The dispersive component is simply a measure of the tendency of a material to interact with other substances via van der Waals (VDW) force, or London dispersion force. Since all materials will interact with all other materials via VDW forces, the dispersive surface energy can be determined from

the contact angles made with the surface by saturated hydrocarbons. In this case, the contact angle is given by [29]

$$\cos\theta_w = -1 + 2\,(\gamma_s^{\,d}/\gamma_l^{\,d})^{1/2}. \qquad (3)$$

Figure 4.8 plots the water contact angle and the dispersive component of the free energy of the a-Si_mC_n:H_y films as functions of the methane flow rate. Increasing the methane gas flow rate from 35 sccm to 100 sccm increases the water contact angle from 83.6° to 87.2° and the dispersive component of the free energy from 6.0 mJ/m^2 to 20.4 mJ/m^2. Incorporating silicon into hydrogenated amorphous carbon films (a-C:H) has been reported to reduce the surface energy from 43 to 31 mN/m.[30] Silicon is unable to form double bonds; so it forces carbon into a sp^3 bonding state. The reduction in the surface energy results mainly from the reduction in the polar component of the surface energy, which is believed to be caused by the loss of sp^2 carbon and dangling bonds of the hydrogenated amorphous carbon network.[30] From the result of Fig. 4.2, increasing the methane flow rate, that is, decreases the deposition rate and increases the reacting period between the surface of the a-Si_mC_n:H_y films and plasma. A hydrophilic surface usually has a contact angle less than 70°, and a hydrophobic surface usually has a contact angle of 70° or larger.[31] Therefore, the surface of the a-Si_mC_n:H_y films is more hydrophobic with increasing the methane flow rate.

Figure 4.9(a) ~ (e) show the AFM images and the surface roughness (Rms) of a-Si_mC_n:H_y films against film thickness. The surface becomes rugged as the thickness increases – that is, as the depositing period is increased. It releases hydrogen atoms and the hydrocarbon radicals produced from the plasma, and then erodes the surface of the film while it is being deposited. The following section will discuss the erosion effect of the hydrogen plasma. Figure 4.10 plots the dielectric constant of a-Si_mC_n:H_y films against the thickness of the film. The figure shows that the dielectric constant slightly increases with the thickness of the film. Accordingly, the dielectric constant has negligible increase and the film made more rugged as the film becomes thicker. Meanwhile, a 100 nm silicon nitride film was deposited by PECVD, and the dielectric constant was 6.8, which obvious greater than the dielectric constant of the a-Si_mC_n:H_y films.

4.3.2 The effects of ammonia plasma and hydrogen plasma treatment on the a-$Si_{0.28}C_{0.65}$:H_y films

Robertson has demonstrated that silicon dangling bonds are more likely to be present in silicon-richer films.[24] The leakage current is higher in silicon-richer films since the dangling bands essentially act as traps for carriers hopping from one silicon dangling bond to a nearby one. For nitrogen-rich films, a lower density of silicon dangling bonds may lead to a reduction of the leakage current therein.[18] Thus, from the result of Fig. 4.2, the parameter x

[$=SiH_4/(SiH_4+CH_4)$] = 0.05 was set to deposit carbon-rich a-$Si_mC_n:H_y$ alloys (m=0.28, n=0.65, for films deposited at a methane flow rate at 100 sccm, as shown in Fig. 4.6) with the lowest possible dielectric constant. Sussmann et al.[32] have suggested that the film density of a-$Si_{1-x}C_x$ alloys has a variation between 2.5 g/cm^3 for x=0.2 to about 2.0 g/cm^3 for x=0.8. This decrease in the film density was suggested to be a reflection of a higher hydrogen concentration as the carbon content is increased. However, film deposition at lower temperatures will lead to an increase in the dangling bond defect density in the films.[33,34] The dangling bonds can easily react with moisture in atmosphere to form -OH bonds and thus affect the electrical properties. Thus, hydrogen plasma/ammonia plasma treatment was used to passivate the dielectric films. Figure 4.11(a) ~ (d) present the AFM images and surface roughness of a-$Si_{0.28}C_{0.65}:H_y$ films subjected to the ammonia plasma treatment as a function of the treatment period. The original film has a smooth surface with a roughness of 0.231 nm, but the roughness gradually increases from 0.231 nm to 1.74 nm with the ammonia plasma treatment period. Various ionized species, such as NH^{++}, N_2^+ and H^+, generated in the ammonia plasma, [35] react with the surface of the a-$Si_{0.28}C_{0.65}:H_y$ film and have some important characteristics. First, hydrogen ions may react with CH_x radicals in the film more easily than with SiH_x radicals

because the sticking coefficient of CH_x radicals onto the a-Si_mC_n:H_y film is lower than that of SiH_x radicals;[36,37] therefore less hydrocarbon gas may adsorb on the film surface. Besides, Figure 4.12(a) - (d) present the AFM images and surface roughness of a-$Si_{0.28}C_{0.65}$:H_y films subjected to the hydrogen plasma treatment as a function of the treatment period. Both of ammonia plasma and hydrogen plasma have similar trend on the roughness of a-Si_mC_n:H_y films. Comparing the roughness of the a-Si_mC_n:H_y films by using AFM, ammonia plasma treated film has larger roughness (1.741 nm) than that of by using hydrogen plasma treated films (0.829 nm), may be the ionized species from ammonia plasma are more heavily than that of by using hydrogen plasma. Therefore the surface of a-$Si_{0.28}C_{0.65}$:H_y film becomes rugged because of ion bombardment and erosion effect on the surface of the films by ions and radicals,[38] which are produced in the plasma. Biener et al. [39] and Horn et al. [40] have discussed the chemical erosion of hydrogen-containing carbon films by atomic hydrogen. It has been reported that ion bombarding SiC films with a low impact energy (~ 20 eV) in hydrogen plasma at about 500 K, the erosion yield of carbon is larger than that of silicon.[41] That is, ion bombardment and chemical erosion may preferentially consume carbon sp^2 bonding component and thereby generating dangling bonds.[26] The outmost layer with a higher

silicon content was produced in the a-$Si_mC_n:H_y$ film and the roughness was also increased. In addition, the various ionized nitrogen species could react with Si atom on the film surface, leading to the formation of silicon nitride as shown by the XPS spectra in Fig. 4.13. The oxide species or the surface is thus etched away, and the hydrogen atoms diffuse in the film and passivate the dangling bonds, helping to passivate the surface with respect to oxidation in air. The Si-C bond on the outmost layer of a-$Si_{0.28}C_{0.65}:H_y$ film was vanished in Fig. 4.14 since ion bombardment effect of ammonia plasma or the signal of carbide could not be detected by ESCA since nitride getting growth, and thus carbon content of the outmost layer gradually decrease as the period of plasma treatment increases, as shown in Fig. 4.14. Figure 4.15 shows the infrared spectra of the a-SiC:H films treated with various hydrogen plasma treatment periods (0, 5, 10, 15 and 20 min). The absorption band at 1000 to 1100 cm^{-1} is associated with CH_n wagging; the peak at 780 cm^{-1} corresponds to Si-C stretching or SiC-CH_3 rocking, and the peak at 660 cm^{-1} corresponds to SiH_m wagging vibrations. In all, the absorption bands of the a-SiC:H films with various plasma treatment periods were summarized in Table 4.2. There is no noticeable change in the FTIR spectra as the hydrogen plasma treatment period is increased. Figure 4.16 plots the elemental composition of the outmost layer of hydrogen plasma treated

a-$Si_{0.24}C_{0.68}$:H_y films, which was derived from XPS measurements, against the hydrogen plasma treating period. It indicates the same trend of the reduction in carbon content and increase in silicon content as the plasma treatment period is increased.

As previous described, a silicon nitride layer was formed during the ammonia plasma treatment. Figure 4.14 plots the elemental composition of a-$Si_{0.28}C_{0.65}$:H_y films against the ammonia plasma treating period, as analyzed by XPS. The oxygen content of the ammonia plasma treated a-$Si_{0.28}C_{0.65}$:H_y film is higher than that of the as-deposited a-$Si_{0.28}C_{0.65}$:H_y film. This may be attributed to that dangling bonds are formed on film surface by the ion bombarding effect during the plasma treatment, which can react with moisture in ambient before XPS analysis. Meanwhile, the increase in oxygen content also occurs in hydrogen plasma treated a-$Si_{0.28}C_{0.65}$:H_y films. The nitrogen concentration on the surface of a-$Si_{0.28}C_{0.65}$:H_y films increased as well due to the formation of the silicon nitride thin layer. The reduction in dangling bonds caused by the diffusion of hydrogen and the nitride layer may retard moisture uptake from ambient and Cu diffusion from the Cu electrodes. Consequently, the leakage current density of a-$Si_{0.28}C_{0.65}$:H_y films treated by ammonia plasma treatment is smaller than that of the as-deposited a-$Si_{0.28}C_{0.65}$:H_y films, as shown in Fig. 4.17.

Silicon nitride has been used extensively as a final passivation and coating layer in the integrated circuit fabrication, because of its excellent diffusion barrier characteristics.[42,43] The silicon nitride film was also deposited herein by PECVD, and the dielectric constant was 6.8, which obvious greater than the dielectric constant of the a-$Si_{0.28}C_{0.65}$:H_y films and the leakage characteristics were compared with those of carbon-rich a-$Si_{0.28}C_{0.65}$:H_y films. Figure 4.17 and 4.18 indicate that the retarding effect of a-$Si_{0.28}C_{0.65}$:H_y films treated with the ammonia and hydrogen plasma treatment on Cu diffusion is better than that of as-deposited a-Si_mC_n:H_y films. The leakage current density of a-$Si_{0.28}C_{0.65}$:H_y films after the ammonia plasma treatment at 250ºC for 10 minutes is lower than that of the silicon nitride film before the applied electric field reaches 0.8 MV/cm. Meanwhile, the leakage current density of a-$Si_{0.28}C_{0.65}$:H_y films decreases as hydrogen plasma treatment period is increased. Figure 4.19 presents the dielectric constant of a-$Si_{0.28}C_{0.65}$:H_y films as a function of the ammonia plasma treatment time. After the ammonia plasma treatment, silicon nitride is formed on the film surface, and thereby the dielectric constant increases from 3.6 to 4.4 as the plasma period increases from 0 to 20 minutes. The content increase of the surface silicon nitride with increase the plasma period leads to the increase in the ratio of silicon to carbon, as revealed by XPS.

Besides, Table 4.3 shows the dielectric constant (K) of a-SiC:H films with various hydrogen plasma treatment periods, indicates there is no obvious changes as the plasma treatment period increases. There is no highly dielectric compound formed on the surface after hydrogen plasma treatment, compares with the nitride formed on the surface of a-SiC:H films after ammonia plasma treatment, thus the dielectric constant has no obvious changes.

4.4 Conclusions

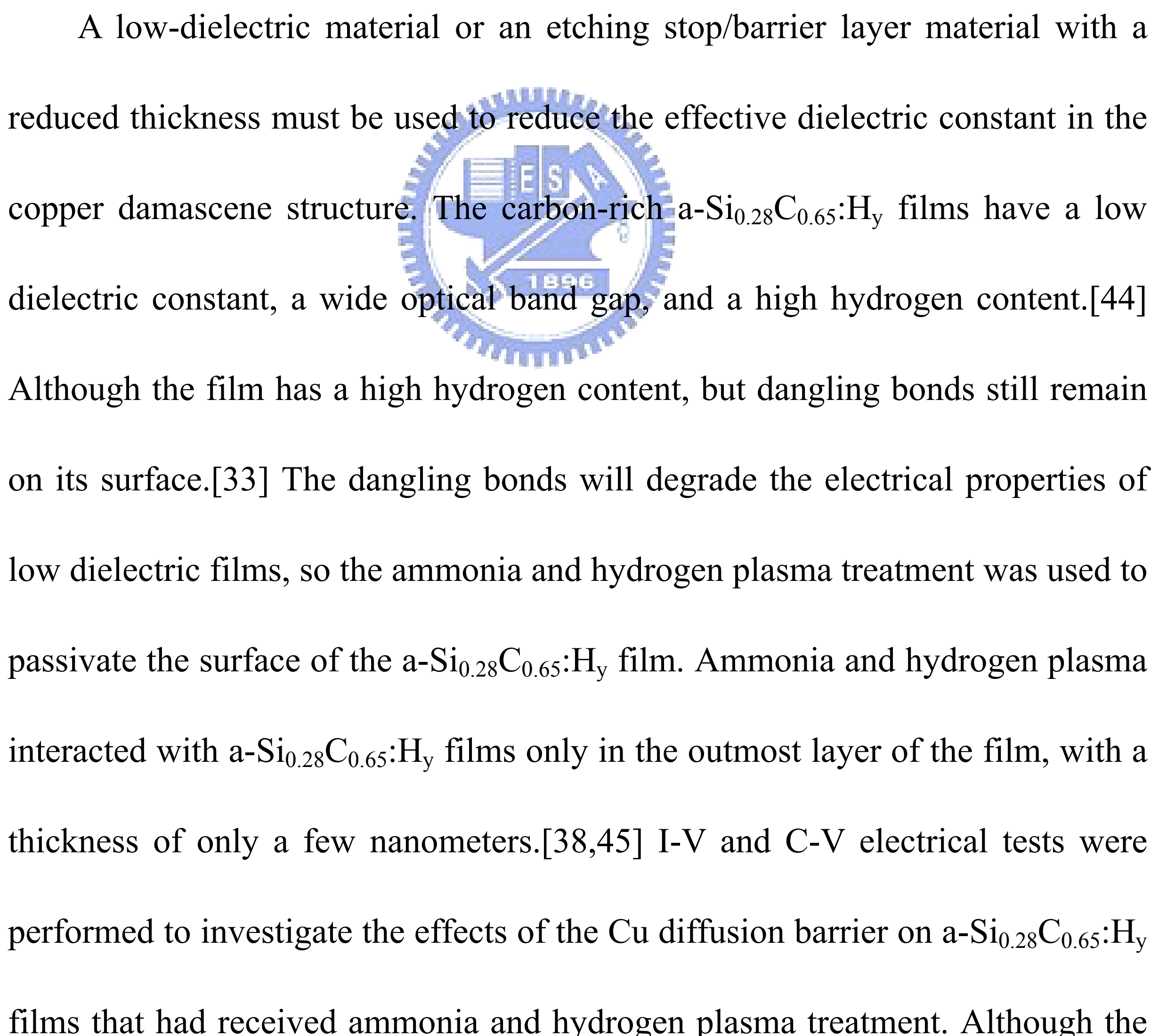

A low-dielectric material or an etching stop/barrier layer material with a reduced thickness must be used to reduce the effective dielectric constant in the copper damascene structure. The carbon-rich a-$Si_{0.28}C_{0.65}$:H_y films have a low dielectric constant, a wide optical band gap, and a high hydrogen content.[44] Although the film has a high hydrogen content, but dangling bonds still remain on its surface.[33] The dangling bonds will degrade the electrical properties of low dielectric films, so the ammonia and hydrogen plasma treatment was used to passivate the surface of the a-$Si_{0.28}C_{0.65}$:H_y film. Ammonia and hydrogen plasma interacted with a-$Si_{0.28}C_{0.65}$:H_y films only in the outmost layer of the film, with a thickness of only a few nanometers.[38,45] I-V and C-V electrical tests were performed to investigate the effects of the Cu diffusion barrier on a-$Si_{0.28}C_{0.65}$:H_y films that had received ammonia and hydrogen plasma treatment. Although the

dielectric constant of the a-$Si_{0.28}C_{0.65}$:H_y films increased with the duration of ammonia plasma treatment, the leakage current density apparently decreased. The leakage current density also apparently decreased as the hydrogen plasma treatment periods increased.

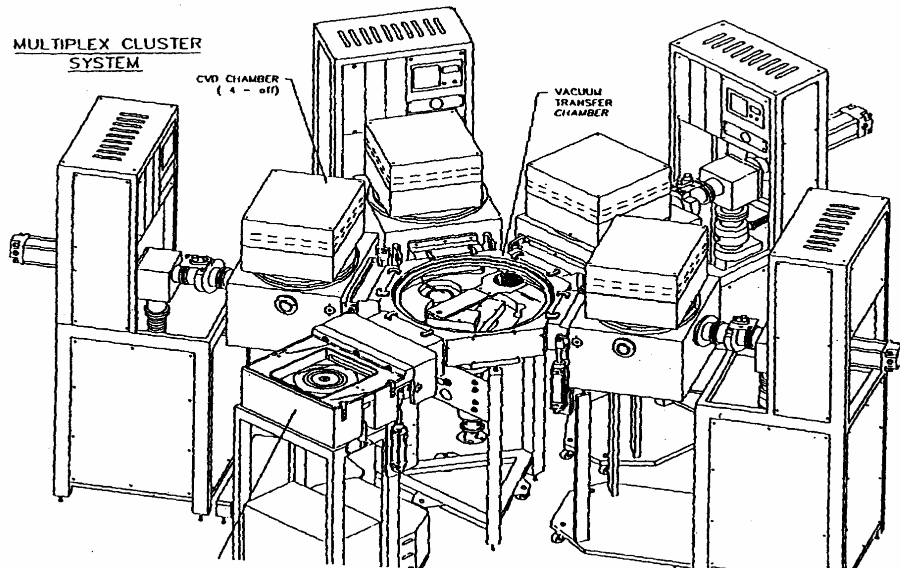

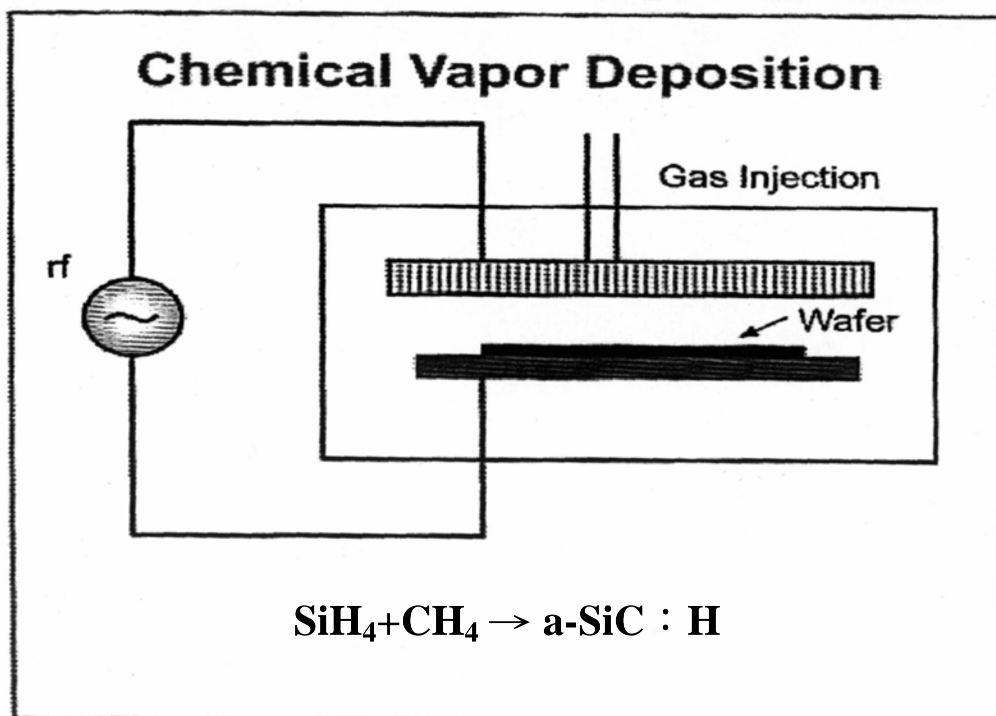

Fig. 4.1 Schematic diagram of the PECVD system.

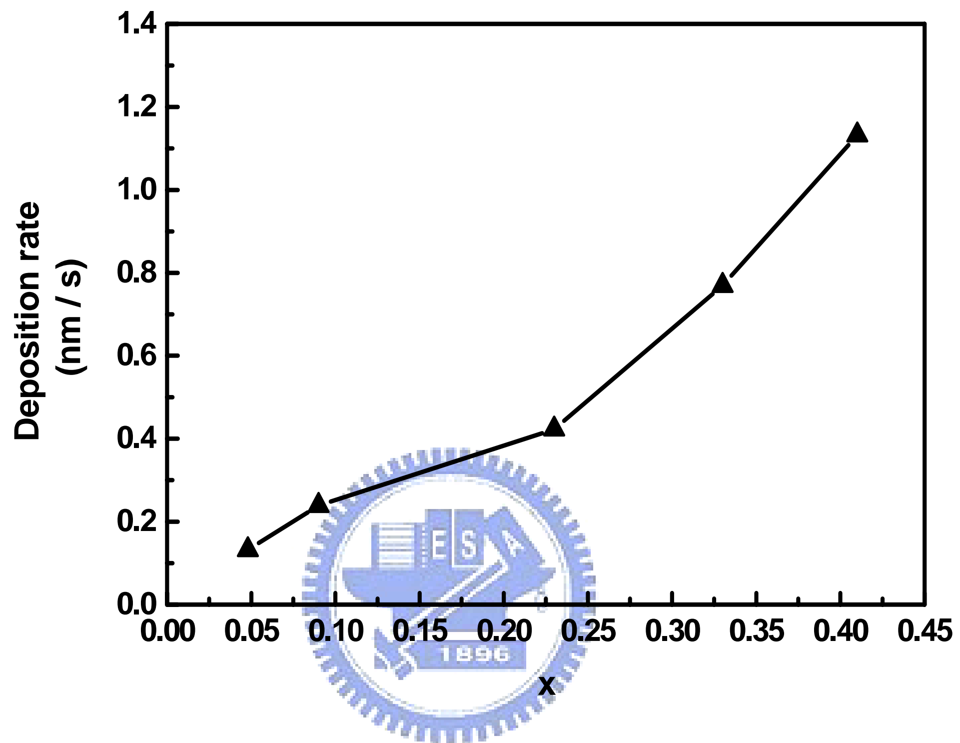

Fig. 4.2 Deposition rate of a-Si_mC_n:H_y films as a function of x value [x = SiH_4/(SiH_4)+(CH_4)].

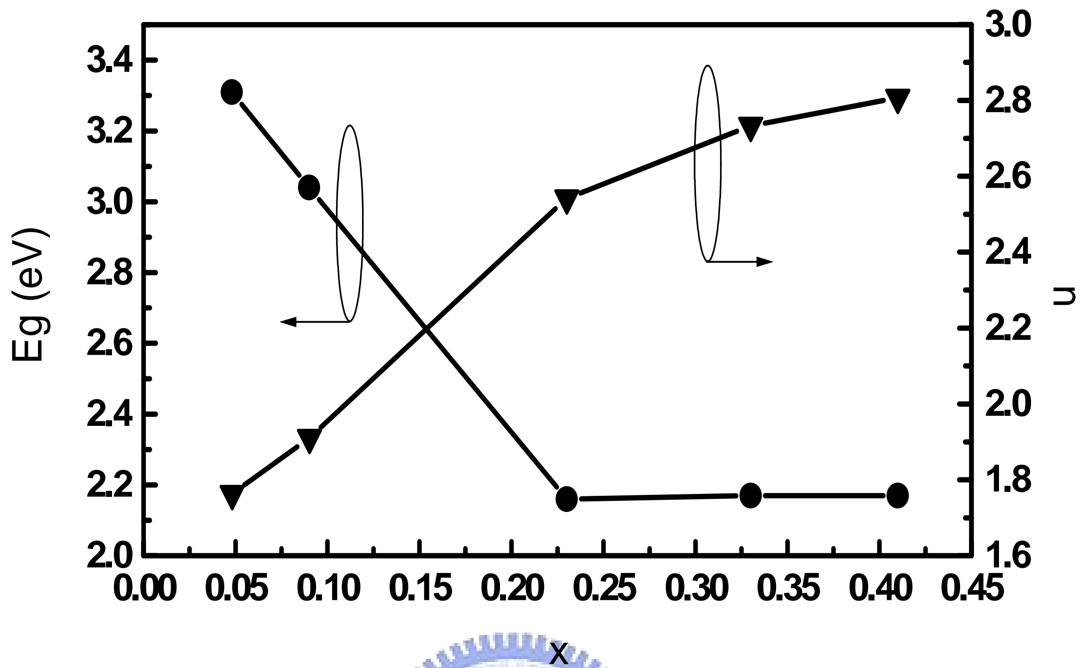

Fig. 4.3 Optical energy gap (Eg), and refraction index (n) of a-Si_mC_n:H_y films as a function of x value [x = SiH_4/(SiH_4)+(CH_4)].

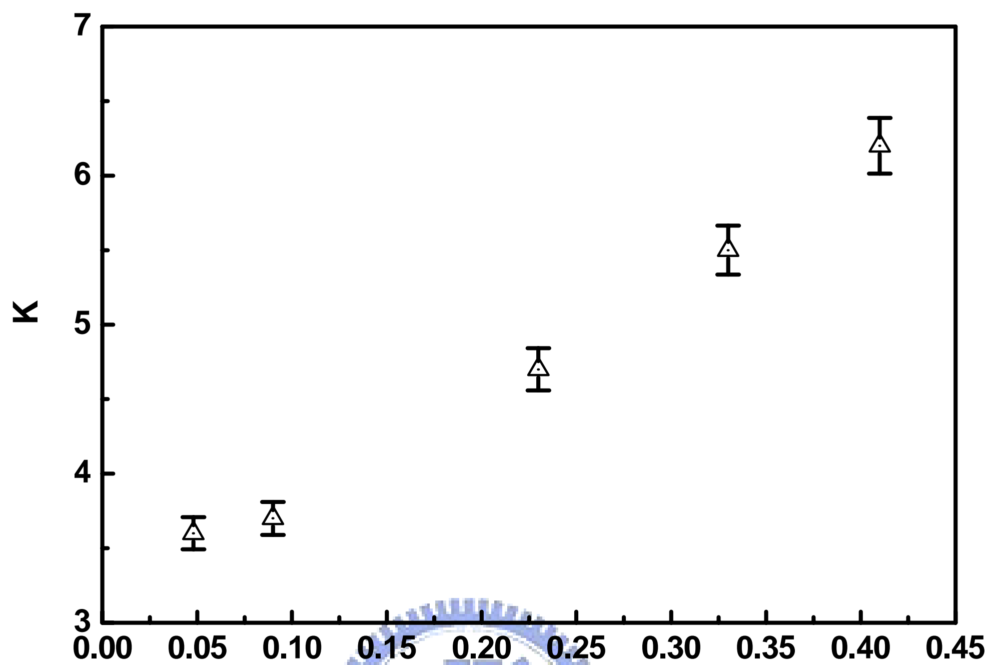

Fig. 4.4 Dielectric constant (K) of a-Si_mC_n:H_y films as a function of x value [x = SiH_4/(SiH_4)+(CH_4)].

1896

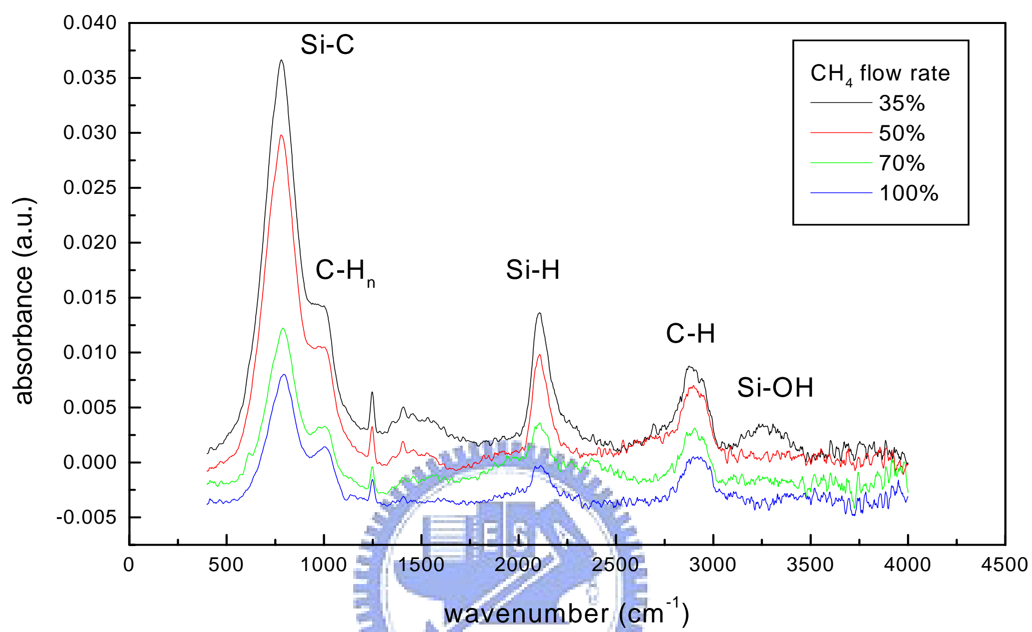

Fig. 4.5 IR spectra of the a-$Si_mC_n:H_y$ films of different methane flow rates.

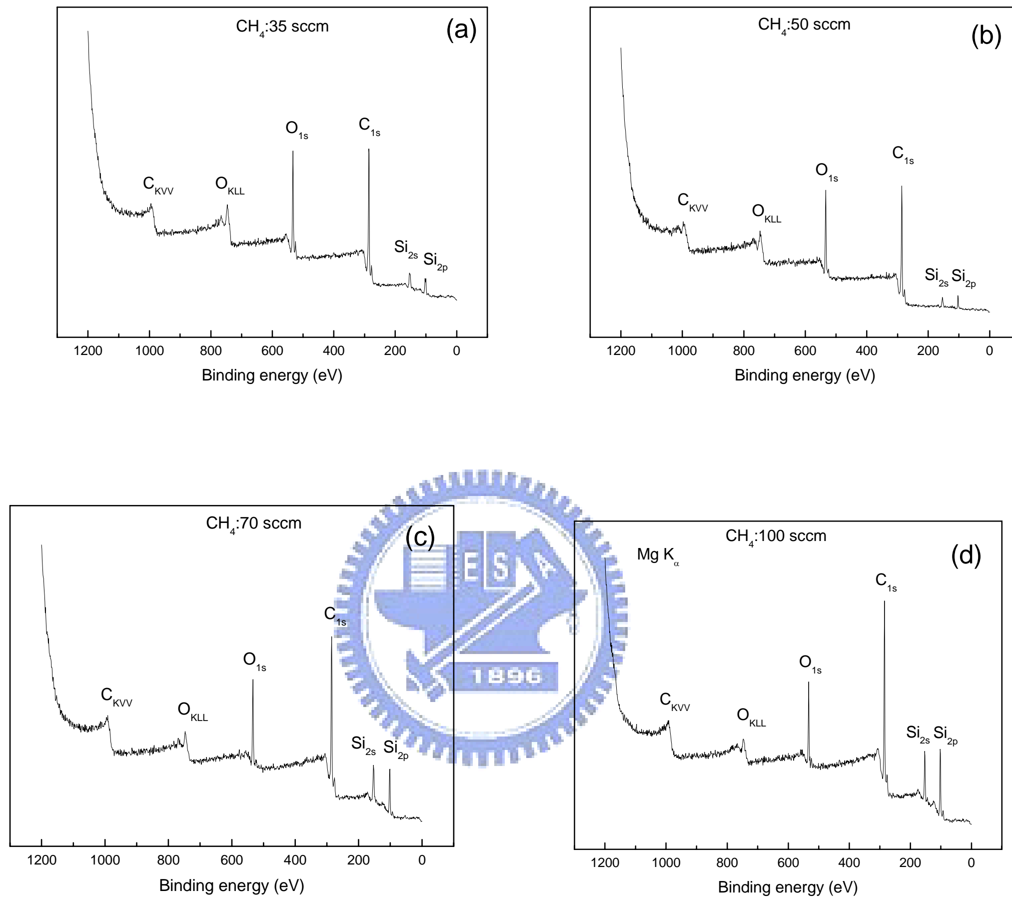

Fig. 4.6 ESCA spectra of the near surface region of a-Si_mC_n:H_y films with various methane flow rate, (a) 35 sccm, (b) 50 sccm, (c) 70 sccm, and (d) 100 sccm.

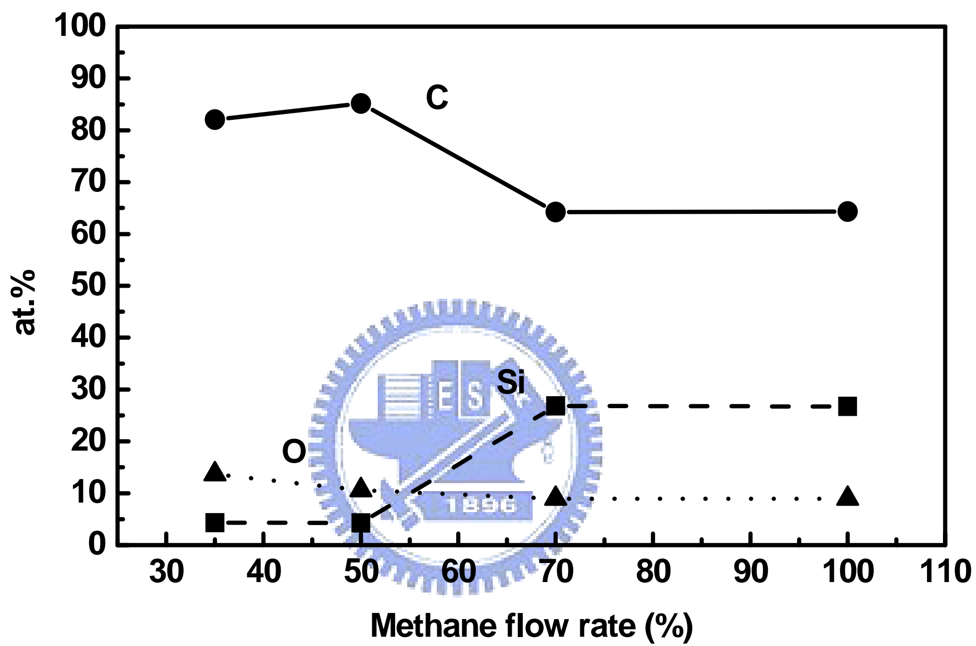

Fig. 4.7 The composition of the near-surface region of the a-Si_mC_n:H_y films with various methane flow rate, analyzed by ESCA.

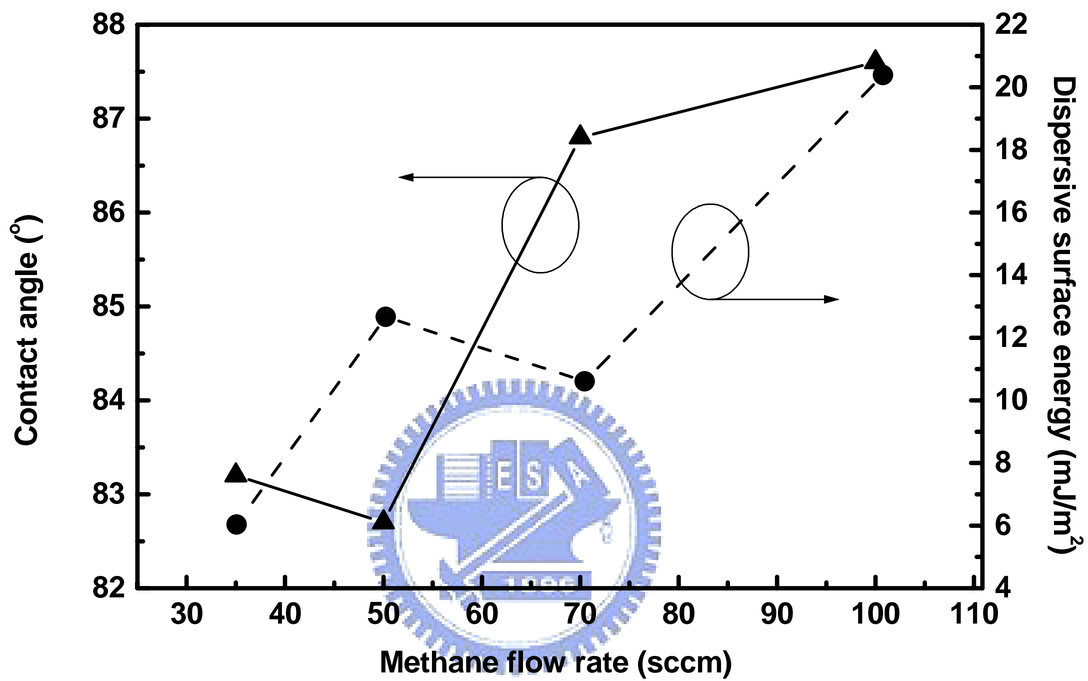

Fig. 4.8 The water contact angle and the dispersive component of the free energy of the a-Si_mC_n:H_y films as a function of methane flow rate.

(a) 10 nm (Rms: 0.084 nm)

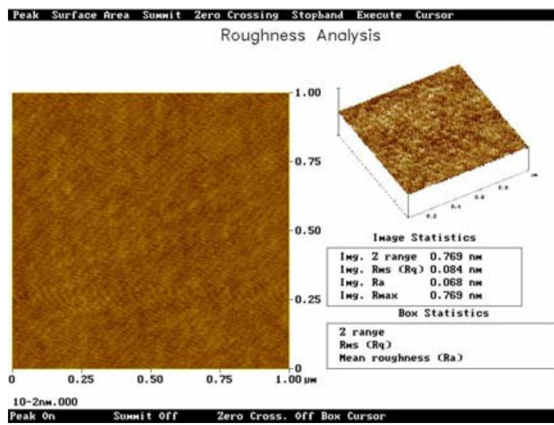

(c) 100 nm (Rms: 0.231 nm)

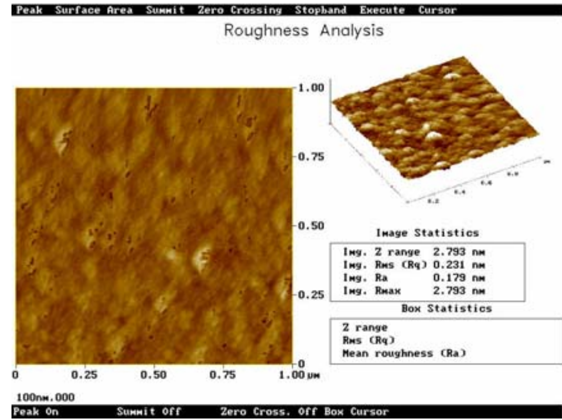

(b) 50 nm (Rms: 0.157 nm)

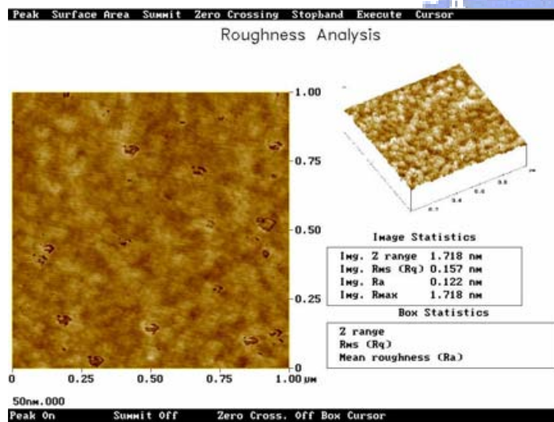

(d) 150 nm (Rms: 0.270 nm)

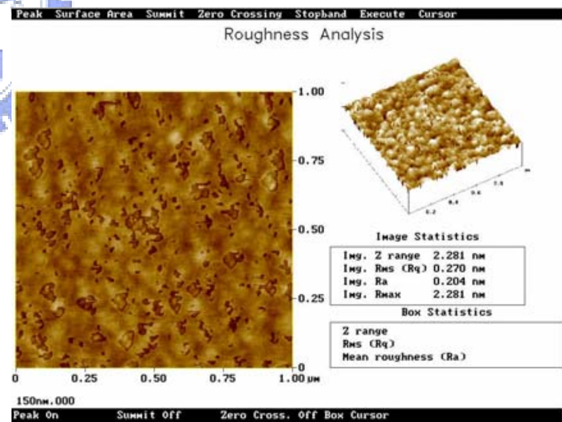

Fig. 4.9 The surface roughness of a-$Si_mC_n:H_y$ films with various films thickness, (a) 10 nm, (b) 50 nm, (c) 100 nm, and (d) 150 nm.

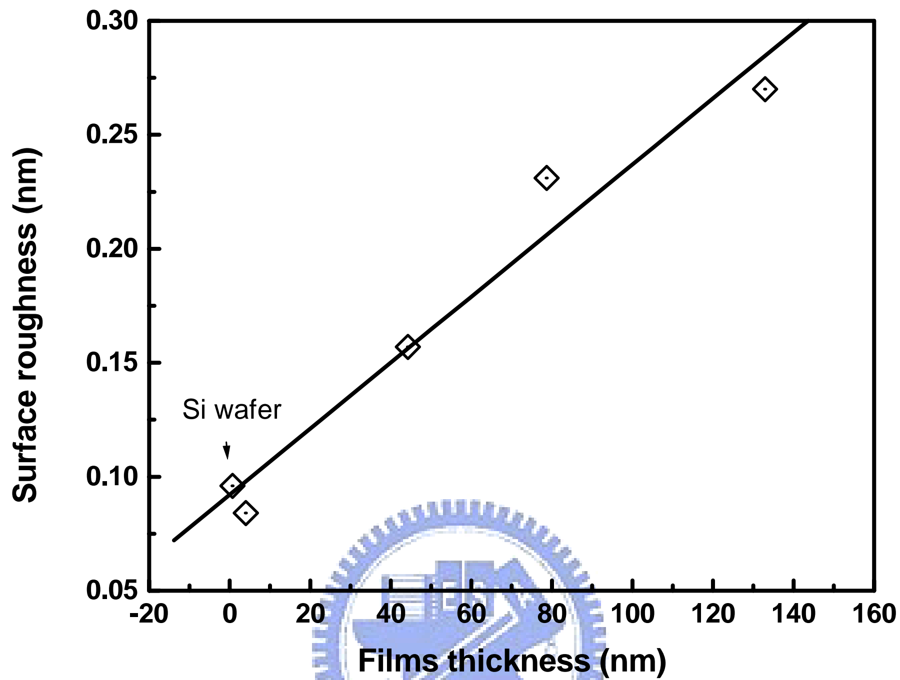

Fig. 4.9(e) The surface roughness of a-Si_mC_n:H_y films with various films thickness.

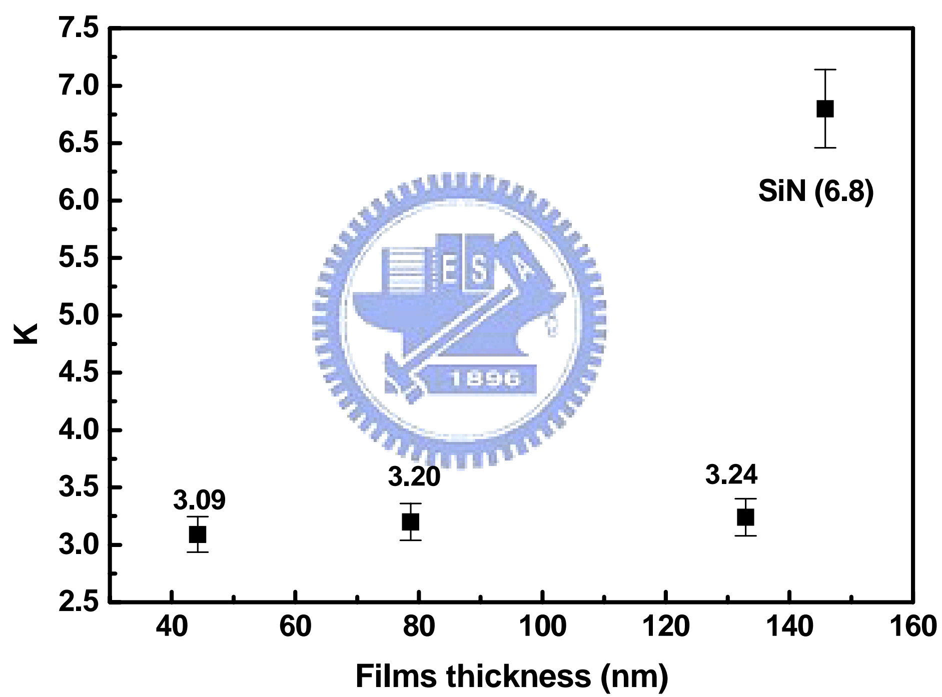

Fig. 4.10 Dielectric constant (K) of a-Si_mC_n:H_y films with various films thickness.

(a) 0 min. (Rms: 0.231 nm)

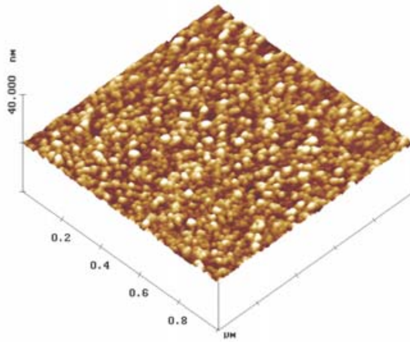

(c) 20 min. (Rms: 1.741 nm)

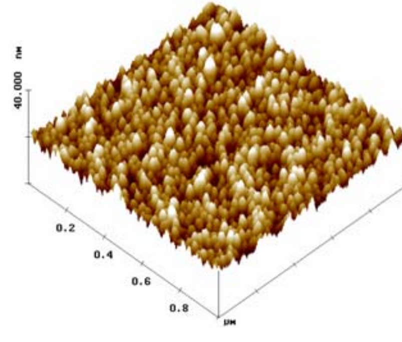

(b) 5 min. (Rms: 0.548 nm)

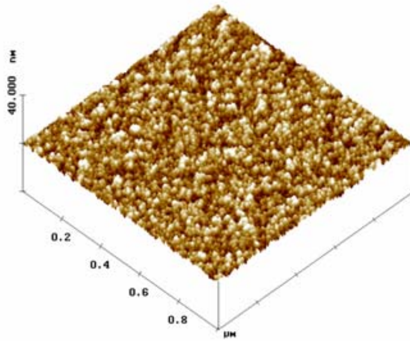

(d) AFM Roughness

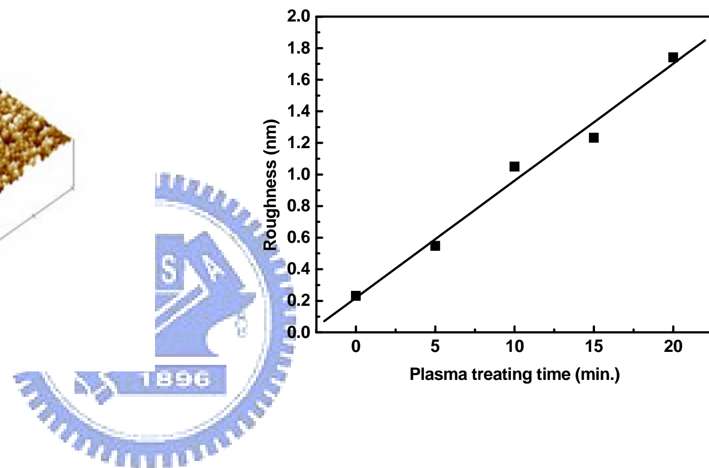

Fig. 4.11 AFM images of a-$Si_{0.28}C_{0.65}$:H_y films with varies ammonia plasma treatment periods, (a) 0 min, (b) 5 min, and (c) 20 min, and (d) AFM roughness of a-SiC:H films with various plasma treating periods.

(a) 5 min (0.461 nm)

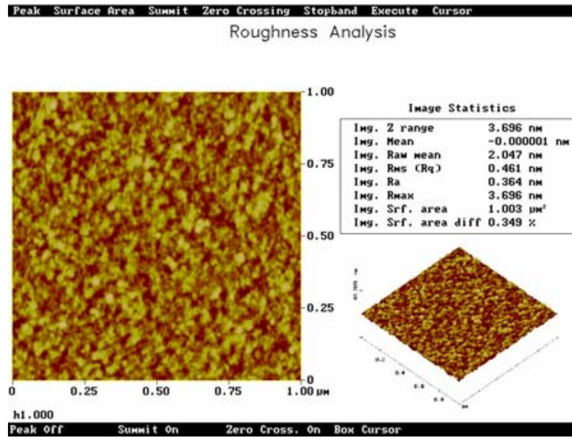

(b) 15 min. (Rms:0.763 nm)

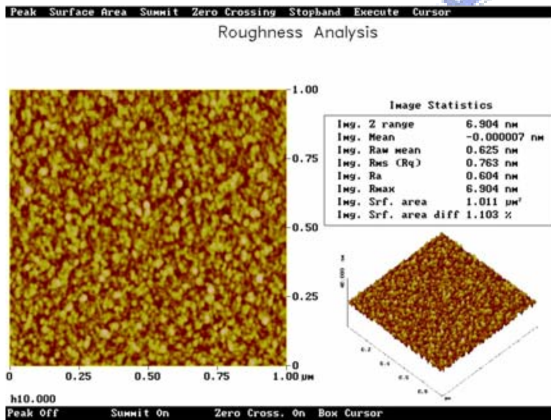

(c) 20 min. (Rms:0.829 nm)

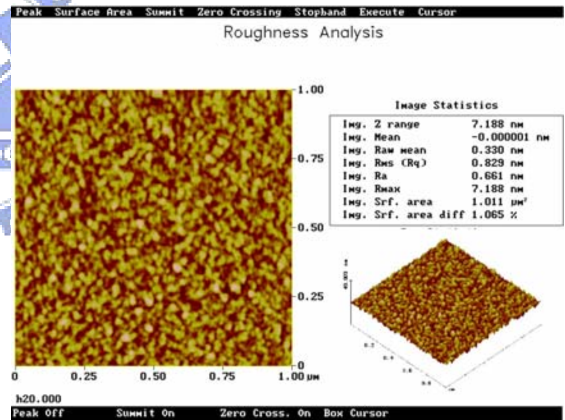

Fig. 4.12 AFM images of hydrogen plasma treated a-SiC:H films with varies hydrogen plasma treatment periods, (a) 5 min, (b) 15 min, and (c) 20 min.

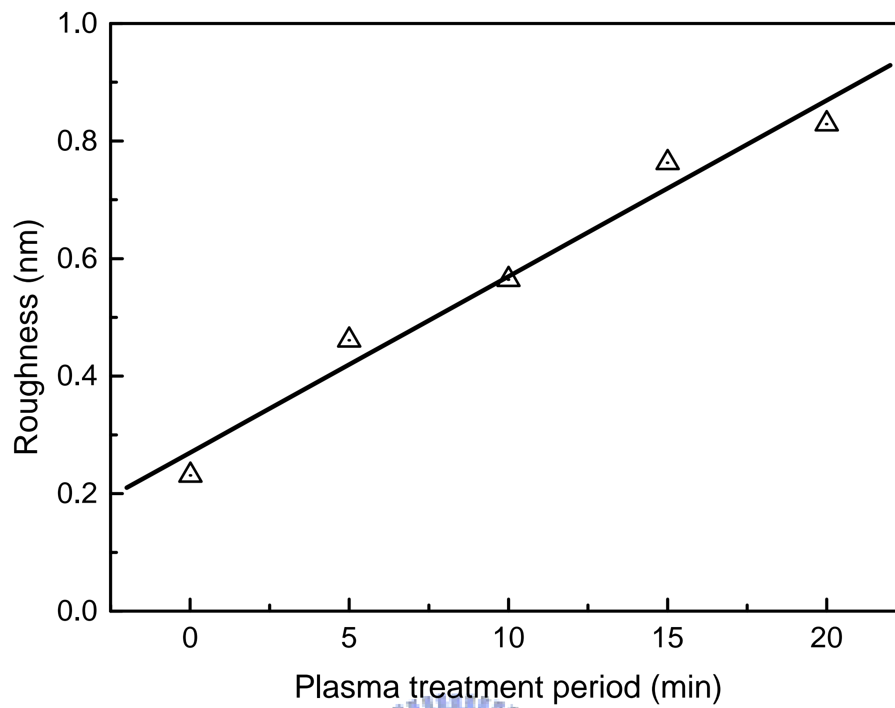

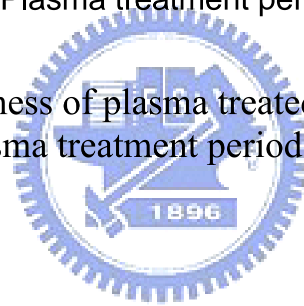

Fig. 4.12 (d) Roughness of plasma treated a-SiC:H films with varies hydrogen plasma treatment periods.

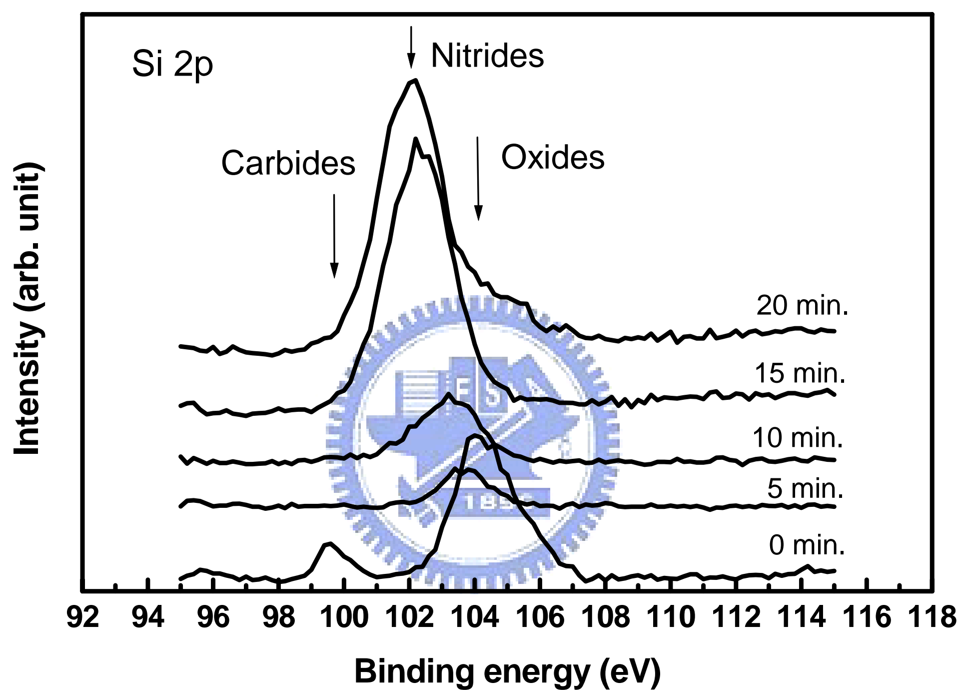

Fig. 4.13 XPS spectra of Si 2p binding peaks for the a-$Si_{0.28}C_{0.65}$:H_y films with various ammonia plasma treatment periods.

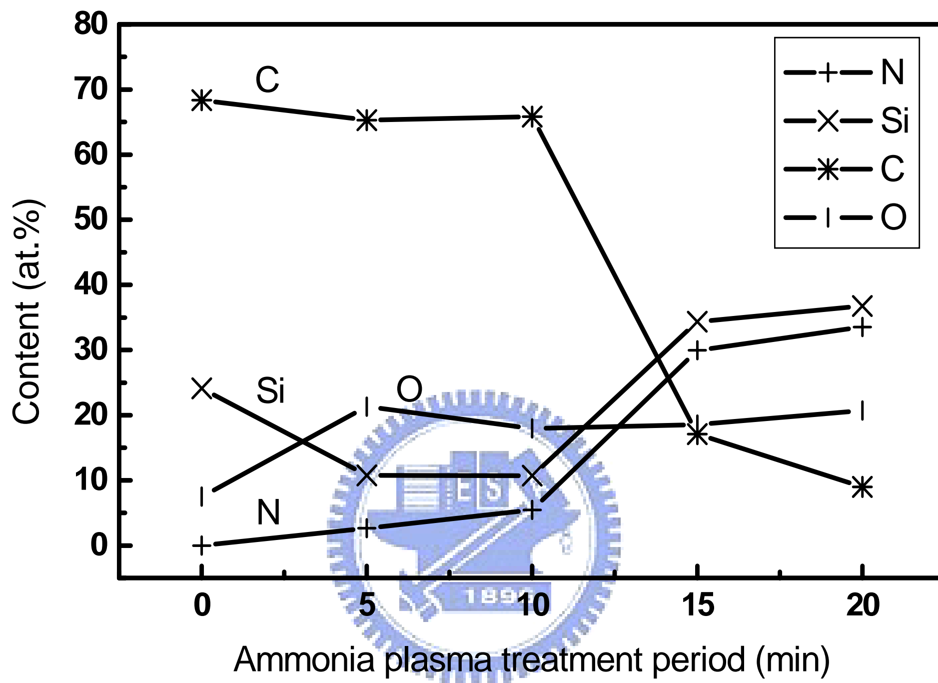

Fig. 4.14 The content of a-$Si_{0.28}C_{0.65}$:H_y films with different ammonia plasma treatment period.

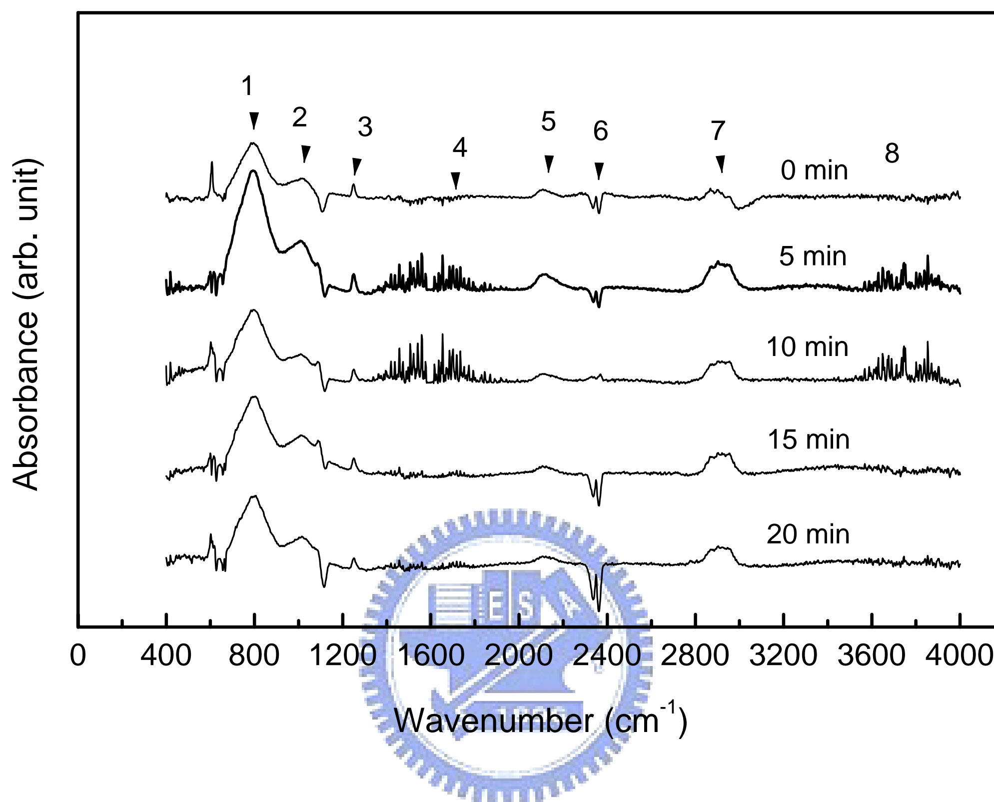

Fig. 4.15 FTIR absorption spectra of a-SiC:H films for various hydrogen plasma treatment periods.

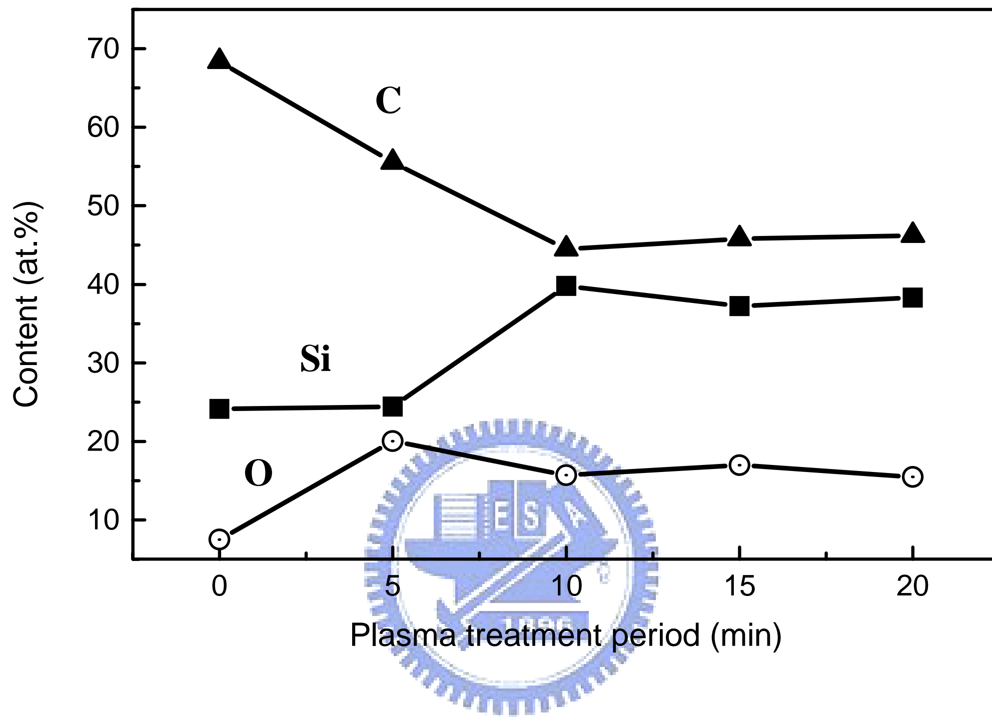

Fig. 4.16 The outmost layer content of a-SiC:H films with various hydrogen plasma treatment periods.

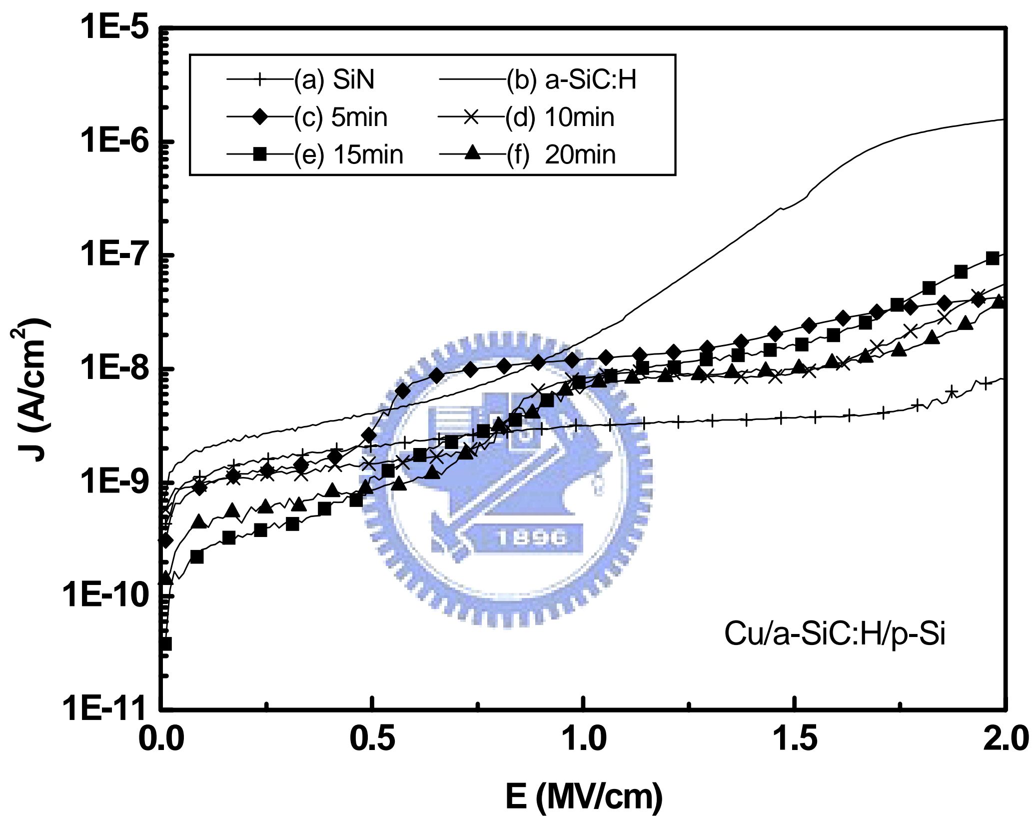

Fig. 4.17 J-E characteristics of a-$Si_{0.28}C_{0.65}$:H_y films before and after ammonia plasma treatment and a-SimNn:Hy films, (a) a-SimNn:Hy, (b) a-$Si_{0.28}C_{0.65}$:H_y, and with various plasma treating periods, (c)5 min, (d)10 min, (e)15 min, and (f) 20 min.

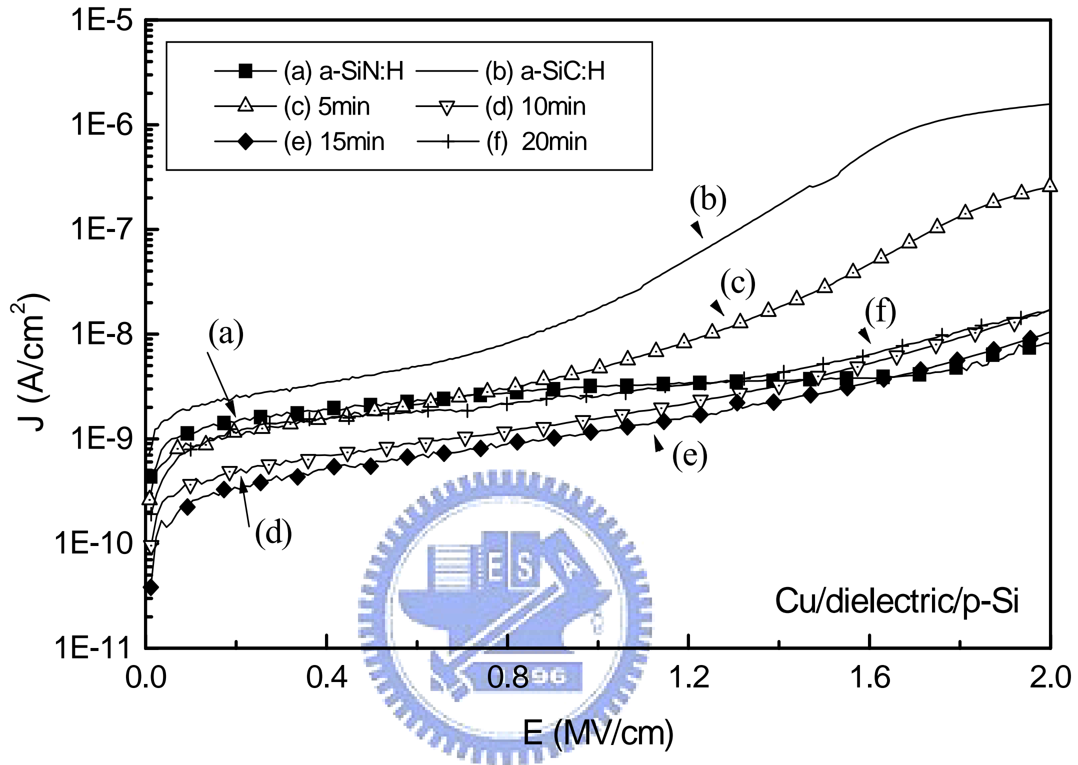

Fig. 4.18 J-E characteristics of a-SiC:H films before and after hydrogen plasma treatment and a-SiN:H films, (a) a-SiN:H, (b) a-SiC:H, and for various plasma treatment periods, (c) 5 min, (d) 10 min, (e) 15 min, and (f) 20 min.

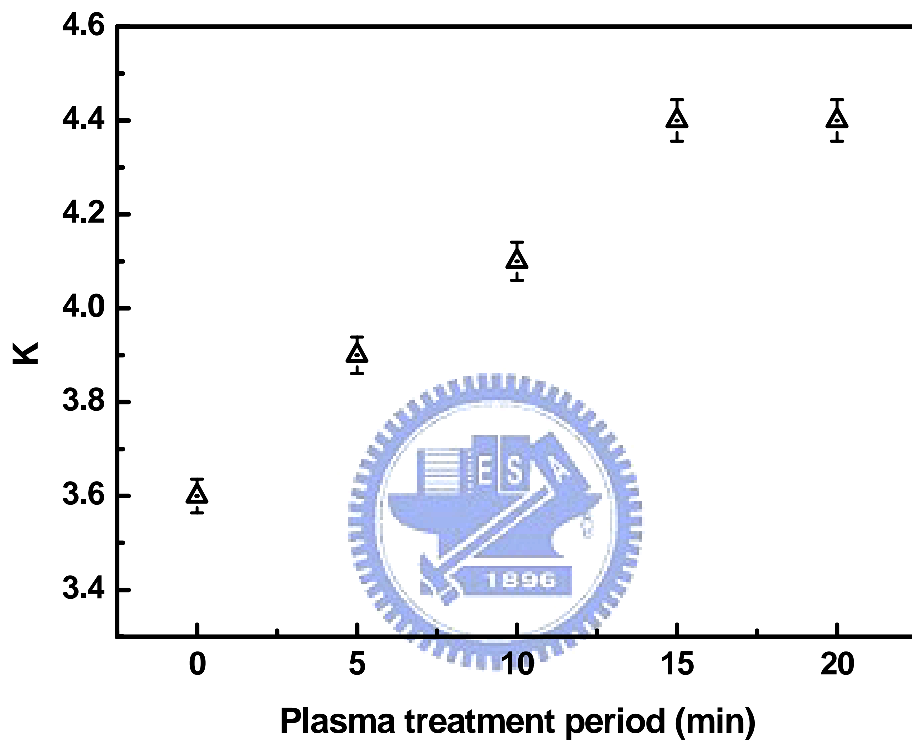

Fig. 4.19 Dielectric constant (K) of a-$Si_{0.28}C_{0.65}$:H_y films with various ammonia plasma treating periods.

Table 4.1 Deposition parameters, hydrogen/ammonia plasma treatment parameters, and characteristics of the a-SiC:H films.

Parameter	a-SiC:H
A. Deposition	
$SiH_4/(SiH_4+CH_4)$	x
Applied rf. power (W)	120
Chamber pressure (mTorr)	600
Substrate temperature (℃)	250
Film thickness (Å)	1000
B. Characteristics (x = 0.05)	
C/Si ratio	2.83
O at.%	7.58
Optical energy gap (eV)	3.31
Refraction index	1.75
C. Hydrogen plasma treatment	
Hydrogen flow rate (sccm)	400
Applied rf. power (W)	100
Chamber pressure (mTorr)	800
Substrate temperature (℃)	250
D. Ammonia plasma treatment	
Ammonia flow rate (sccm)	700
Applied rf. power (W)	200
Chamber pressure (mTorr)	300
Substrate temperature (℃)	250

Table 4.2 Frequencies of IR peaks and assignments.

Identification number	Wavenumber (cm^{-1})	Assignment	Vibrational modes
1	780	$SiCH_n$	wagging
2	1000	sp^3 CH_n	rocking/wagging
3	1250	sp^3 CH_n	bending
4	1609	OH	bending
5	2100	SiH_n	stretching
6	2350	CO_2	gas
7	2800~3000	CH_n	stretching
8	3600	OH	stretching

Table 4.3 The dielectric constant (K) of a-SiC:H films for various plasma treatment periods.

Hydrogen plasma treatment period (min)	0	5	10	15	20
Dielectric constant (K)	3.6	3.6	3.5	3.5	3.4

Chapter 5

Conclusions and future work

5.1 Conclusions

a-C:H films, deposited using a GIBD system, tend more to exhibit diamond-like character as the acetylene gas flow rate increased. When the films are annealed at an elevated temperature, their microstructures gradually change from diamond-like to graphite-like; the film thickness decreases, and the leakage current density increases. The mass density decreases from 3.44 g/cm^3 to 2.89 g/cm^3 as the annealing temperature is increased from 100°C to 300°C, suggesting that the annealed a-C:H film is more graphite-like character and has a higher leakage current than the as-deposited film, but the dielectric constant decreases as the annealing temperature is increased. Hydrogen plasma treatment greatly reduces the leakage current density and the dielectric constant, but roughens the surface. The variation of the properties of these plasma-treated films is hardly noticeable for a-C:H films, whose dielectric properties are greatly enhanced by hydrogen plasma treatment.

a-Si_mC_n:H_y films were deposited from a mixture of silane and methane gases, using plasma-enhanced chemical vapor deposition. Reducing the ratio of the silane flow rate increased the carbon concentration in the a-SiC:H films,

decreasing the refractive index and dielectric constant, but increasing the optical band gap and the hydrophobicity of the surface. The XPS data revealed that the carbon concentration decreased as the methane flow rate increased, but that the silicon concentration increased, perhaps because the hydrogen plasma preferentially eroded the carbon sp^2 sites. A more rugged film with a higher dielectric constant is formed as the a-Si_mC_n:H_y film is thickened. The carbon-rich a-$Si_{0.28}C_{0.65}$:H_y films treated with hydrogen plasma and ammonia plasma for various periods, were converted into films with more silicon content. Both of increasing the ammonia plasma treatment period roughened the surface even though the original film had a smooth surface, with a roughness of 0.231 nm. Ammonia plasma treated film has larger roughness than that of by using hydrogen plasma treated films. The ionized ammonia species reacted with Si to promote the formation of silicon nitride, as measured by XPS. Accordingly, the leakage current density of a-$Si_{0.28}C_{0.65}$:H_y films declined as the duration of the ammonia plasma treatment increased, but the dielectric constant slightly increased. Therefore, the dielectric properties of the hydrogen-plasma-treated and ammonia-plasma-treated a-$Si_{0.28}C_{0.65}$:H_y films are better than those of silicon nitride films when used as the ILD dielectric at low electric field.

5.2 Future works--Kinetics of copper drift in dielectric films deposited by plasma- enhanced chemical vapor deposition

The emergence of new Cu/low-k interconnection requires careful reconsideration of electrical characterization methodology. To reduce the effective dielectric constant in the copper damascene structure, it is important to develop a low-k barrier/etch stop film. Additional requirements for a barrier/etch stop film include good copper diffusion barrier, good insulating properties, high etch selectivity (with respect to ILD), and compatibility with damascene integration. It is required that the film should have good stability under thermal cycles and manufacturability to meet the future ULSI production requirement.

Due to the fundamental material and electronic properties of SiC, which include wide bandgap, high thermal conductivity, and high melting point. These unique physical and electrical properties make SiC a viable material for high power, high frequency and high temperature device applications. In addition to packaging applications, a-SiC:H materials are being developed as a diffusion barriers/buried hard mask/etch-stop in copper damascene interconnection technology [1,2].

Surface and interface reactions have been studied in a large number of metal/Si systems in Si device technology [3]. Initial work by McBayer et al. demonstrate that copper could diffuse easily through the oxide to the silicon/oxide interface where it could give rise to a variety of problems [4]. They also demonstrated that copper transport in the oxide was controlled by both temperature and applied voltage. Copper is a deep level impurity for silicon and

trends to increase junction leakage currents if it is present in devices [5]. Other researchers have also shown that the presence of copper in oxide leads to a degradation of oxide integrity [6]. These observations provide the motivation to study the diffusion mechanism of copper in various dielectric films. To ensure the implementation of the barrier materials in the Cu dual damascene technology, the extent of Cu penetration in these dielectrics must be determined.

Plasma enhanced chemical vapor deposition (PECVD) processes are used extensively in the fabrication of semiconductor integrated circuits. In this work, we used the gas mixture of silane and methane to deposit a-SiC:H films in a single-wafer PECVD chamber. The interaction of copper with the dielectrics was investigated by different electrical measurements using MIS structures. Biased temperature stressing (BTS) and capacitance-voltage (C-V) techniques were applied to determine flatband voltage shifts. While the presence of Cu atoms in the dielectrics is confirmed by secondary ion mass spectroscopy (SIMS), the C-V technique is primarily used to provide more sensitive determination of the Cu concentration.

References

Chapter 1

1. T.M. Hong, S.H. Chen, Y.S. Chiou, C.F. Chen, Appl. Phys. Lett., 67 (1995) 2149.

2. S.H. Chen, S.L. Chen, M.H. Tsai, J.J. Shyu, C.F. Chen, J. Electrochem. Soc., 142 (1995) L 223.

3. T.K. Ku, S.H. Chen, C.P. Wang, N.J. She, C.C. Wang, C.F. Chen, IEEE Electron Device Letter, 17 (1996) 208.

4. H.C. Chen, T.K. Ku, B.B. Hsieh, S.H. Chen, S.Y. Leu, C.C. Wang, C.F. Chen, I.-J. Hsieh, Jammy C.M. Huang, Jpn. J. Appl. Phys., 34 (1995) 6926.

5. Yan-Way Li, Chia-Fu Chen, and Yu-Jen Tseng, Jan. J. Appl. Phys. 40 (2001) 777.

6. Yan-Way Li, Yu-Jen Tseng, and Chia-Fu Chen, Jan. J. Appl. Phys. 40 (2001) 6574.

7. F.Z. Cui and D.J. Li, Surf. Coat. Technol., 131 (2000) 481.

8. E.G. Wang, Physica B 185 (1993) 85.

9. S. Ghosh, P. Battacharyya, and D.N. Bose, Appl. Phys. Lett. 68 (1996) 2979.

10. K. Wu, Y. Fang, J. Ho, W. Hsien, and T. Chen, Appl. Phys. Lett. 72 (1998) 3017.

11. P.K. Bachmann, D. Leers, and H. Lydtin, Diamond Relat. Mater. 1 (1991) 1.

12. C. Sanssand and T. Billon, J. Appl. Phys. 76 (1994) 993.

13. K.K. Chattopadhyay, J. Dutta, S. Chaudhuri, and A.K. Pal, Diamond Relat. Mater. 4 (1995) 122.

14. J. Edgar, J. Mater. Res. 7 (1992) 235.

15. A. Freedman, Diamond Relat. Mater. 4 (1995) 216.

16. J.F. Ying, P.E. Sobol, Z.D. Yang, B.D. Hermsmeier, J. Electron Spectrosc. Relat. Phenom., 98-99 (1999) 209.

17. Hans-Joachim Scheibe, Bernd Schultrich, Holger Ziegele, and Peter Siemroth, IEEE Trans. Plasma Sci., 25 (1997) 685.

18. D.R. McKenzie, D. Muller, and B.A. Pailthorpe, Phys. Rev. Lett. 67 (1991)

773.

19. B. S. Satyanarayana, A. Hart, W. I. Milne, and J. Robertson, Appl. Phys. Lett. **7**1 (1997) 1430.
20. L. K. Cheah, X. Shi, B. K. Tay, S. R. P. Silva, and Z. Sun, Diamond Relat. Mater. 7 (1998) 640.
21. M. Kühn, P. Meja, and F. Richter, Diamond Relat. Mater., 2 (1993) 1350.
22. S.R.P. Silva, Shi Xu, B.K. Tay, H.S. Tan, H.-J. Scheibe, M. Chhowalla, and W.I. Milne, Thin Solid Films, 290-291 (1996) 317.
23. Dihu Chen, Aixiang Wei, S.P. Wong, Shaoqi Peng, J.B. Xu, and I.H. Wilson, J. Non-Cryst. Solids, 254 (1999) 161.
24. Simone Anders, André Anders, and Ian Brown, J. Appl. Phys., 74(6) (1993) 4239.
25. S. Anders, A. Anders, M.R. Dickinson, R.A. MacGrill, and I.G. Brown, IEEE Trans. Plasma Sci., 25(4) (1997) 670.
26. H.-C. Tsai and D.B. Bogy: J. Vac. Sci. & Technol. A **5** (1987) 3287.
27. M. Kamo, Y. Sato, S. Matsumoto, and N. Setaka, J. of Crystal Growth, 62 (1983) 642.
28. H. Kawarada, K.S. Mar, and A. Hiraki, Jpn. J. Appl. Phys. 26(6) (1987) L1032.
29. K.M. Krishna, H. Ebisu, K. Hagimoto, Y. Hayashi, T. Soga, T. Jimbo, and M. Umeno, Appl. Phys. Lett. **78** (2001) 294.
30. Y. Ushiki, H. Kushibe, H. Ono, and A. Nishiyama, Proc. of the VLSI Multilevel Interconnection Conf., (1990) pp. 413.
31. Y. Igarashi and T. Ito, J. Vac. Sci. Technol., B 16 (1998) 2745.
32. S. Takeishi, H. Kudo, R. Shinohara, M. Hoshino, S. Fukuyama, J. Yamaguchi, M. Yamada, J. Electrochem. Soc., 144(5) (1997) 1797.
33. A. Grill, Diamond Relat. Mater., 10 (2001) 234.
34. V.L. Shannon and M.Z. Karim, Thin Solid Films, 270 (1995) 498.
35. J.P. Reynard , C. Verove, E. Sabouret, P. Motte, B. Descouts, C. Chaton, J. Michailos, and K. Barla, Microelectronic Engineering, 60 (2002) 113.
36. Mohan K. Bhan, Judy Huang, and David Cheung, Thin Solid Films, 308–309 (1997) 507.

37. Tetsuya Homma, J. Non-Cryst. Solids, 187 (1995) 49.

38. Sang-Soo Han, Hun Rae Kim, and Byeong-Soo Bae, J. Electrochem. Soc., 146(9) (1999) 3383.

39. S.E. Kim and C. Steinbruchel, The interaction of metals and barrier layer with fluorinated silicon oxides, Solid-State Electronics, 43 (1999) 1019.

40. M. Morita, T. Kubo, T. Ishihara, and M. Hirose, Appl. Phys. Lett., 45(12) (1984) 1312.

41. C. Cytermann, R. Brener, E. Sacher, B. Pratt, and R. Weil, Appl. Phys. Lett., 52(3) (1988) 191.

42. T.L. Chu, J. Vac. Sci. Technol., 6 (1970) 25.

43. A.K. Sinha, H.J. Levinstein, T.E. Smith, G. Quintana, and S.E. Haszko, J. Electrochem. Soc., 125 (1978) 601.

44. M. Ino, N. Inoue, and M. Yoshimaru, IEEE Trans. Electron Dev., 41 (1994) 703.

45. A.K. Sinha and T.E. Smith, J. Appl. Phys., 49(5) (1978) 2756.

46. L. Tong, M. Mehregany and L.G. Matus, *Silicon Carbide as A New Micromechanics Material*, in Technical Digest, IEEE Solid-State Sensor and Actuator Workshop, Hilton-Head, SC, June 25-27, 1992, pp. 198.

47. Ping Xu, Kegang Huang, Anjana Patel, and et al., IEEE IITC, (1999) 109.

48. Hichem M'Saad, Seon-Mee Cho, Manoj Vellaikal, and Zhuang Li, Mater. Res. Soc. Symp. Proc. vol. 612 (2000) D9.14.1.

49. M.N.P. Carreno, L. Pereyra, M.C.A. Fantini, H. Takabashi, and R. Landers, J. Appl. Phys., 75 (1) (1994) 538.

50. K. Nakazava, S. Ueda, M. Kumeda, A. Morimoto and T. Shimizu: Jpn. J. Appl. Phys. 21 (1982) 176.

51. M.P. Schmidt, J. Solomon, H. Tran-Quoc and J. Bullot: J. Non-Cryst. Solids 77-78 (1985) 849.

52. B. Ruttensperger, G. Krots, G. Miller, G. Derst and S. Kalbitzer: J. Non-Cryst. Solids 137-138 (1991) 635.

53. S.Z. Han, H.M. Lee and H.S. Kwon, J. Non-cryst. Solids, 170 (1994) 199.

54. F. Demichelis, G. Crovini, F. Giorgis, C.F. Pirri and E. Tresso, Diamond Relat. Mater., 4 (1995) 473.

55. I. Solomon, M.P. Schmidt, and H. Tran-quoc, Phys. Rev. B, 38 (14) (1988)

9895.

56. I. Pereyra, M.N.P. Carreño, M.H. Tabacniks, R.J. Prado, and M.C.A. Fantini, J. Appl. Phys., 84 (5) (1998) 2371.

57. P.T. Liu, T.C. Chang, S.M. Sze, F.M. Pan, Y.J. Mei, W.F. Wu, M.S. Tsai, B.T. Dai, C.Y. Chang, F.Y. Shih, and H.D. Huang, Thin Solid Films, 332 (1998) 345.

58. Y.S. Kim, D. Jung, D.J. Kim, and S. Min, Jpn. J. Appl. Phys. Part 2 37 (1998) L991.

59. Po-Tsun Liu, Ting-Chang Chang, Ya-Liang Yang, Yi-Fang Cheng, and Simon M. Sze, IEEE Trans. Electron Devices, 47 (9) (2000) 1733.

Chapter 2

1. A.G. Engelhardt and A.G. Phelps, Phys. Rev. 131 (1963) 2115.

2. L. Peters, Semicond. Int., (Sept. 1998) 64.

3. R.H. Havemann, M.K. Jain, R.S. List, A.R. Ralston, W.-Y. Shih, C. Jin, M.C. Chang, E.M. Zielinski, G.A. Dixit, A. Singh, S.W. Russell, J.F. Gaynor, A.J. McKerrow, and W.W. Lee, Mater. Res. Soc. Symp. Proc., 511 (1998) 3.

4. The National Technology Roadmap for Semiconductors. San Jose, CA: Semicond. Indust. Assoc., 1997.

5. R.G. Wu, Physical and Electrical Characteristics of Low Dielectric Constant Spin-on-Polymer X418 for Intermetal Dielectric Applications, Master Thesis, National Chiao-Tung University, Hsinchu, Taiwan, 1998.

6. Z.W. Shiung, Electrical Reliability Analyses of Integrating Low-K cvd Dielectrics with Cu Metallization, Master Thesis, National Chiao-Tung University, Hsinchu, Taiwan, 2000.

7. T. Takewaki, R. Kaihara, T. Ohmi, and T. Nitta, Int. Electron Device Meet. Tech. Dig., 1995, 253.

8. P. Singer, Semicond. Int., (Nov. 1994) 52.

9. J. Torres, IEEE Int. Interconnect Tech. Conf., 1999, 253.

10. T. Ritzdorf, L. Graham, S. Jin, C. Mu, and D. Fraser, IEEE Int. Interconnect Tech. Conf., 1998, pp. 166.

11. C.H. Lee, K.H. Shen, T.K. Ku, C.H. Luo, C.C. Tso, H.W. Chou, and C.

Hsia, IEEE Int. Interconnect Tech. Conf., 2000, pp. 242.

12. J. Zhang, D. Denning, G. Braeckelmann, R. Venkatraman, R. Fiordalice, and E. Weitzman, IEEE Int. Interconnect Tech. Conf., 1998, pp. 163.

13. R.P. Vinci, E.M. Zielinski, and J.C. Bravman, Thin Solid Films 262 (1995) 142.

14. D.R. Lide, Editor-in-Chief, CRC Handbook of Chemical and Physics, 73rd ed. Boca Raton, FL: CRC, 1992, Section 12: Properties of Solids.

15. T.B. Massalski, Editor-in-Chief, Binary Alloy Phase Diagrams, 2nd ed. Materials Park, OH: ASM Int., 1990.

16. K.P. Rodbell, E.G. Colgan, and C.K. Hu, Mater. Res. Soc. Symp. Proc., 337 (1994) 59.

17. S. Shingubara, K. Fujiki, A. Sano, H. Sakaue, and Y. Horiike, Mater. Res. Soc. Symp. Proc., 338 (1994) 441.

18. T.H. Lee, Nitridation Effect on the Barrier Property of Mo and Cr Layer in Cu/Barrier/SiO2/Si MOS Structure, Master Thesis, National Chiao-Tung University, Hsinchu, Taiwan, 1997.

19. Y.C. Lin, Barrier Property of W-Silicide and Ta-Nitride for Cu Metallization, Master Thesis, National Chiao-Tung University, Hsinchu, Taiwan, 1997.

20. J.D. Mcbrayer, R.M. Swanson, and T.W. Sigmon, J. Electrochem. Soc., 133 (6) (1986) 1242.

21. Y.S. Diamand, A. Dedhia, D. Hoffstetter, and W.G. Oldham, J. Electrochem. Soc., 140 (8) (1993) 2427.

22. A.L.S. Loke, C. Ryu, C.P. Yue, J.S.H. Cho, and S.S. Wong, IEEE Electron Device Lett., EDL-17 (1996) 549.

23. D. Gupta. Mater. Res. Soc. Symp. Proc., 337 (1994) 209.

24. G. Raghavan, C. Chiang, P.B. Anders, S.M. Tzeng, R. Villasol, G. Bai, M. Bohr, and D.B. Fraser, Thin Solid Films, 262 (1995) 168.

25. S.M. Sze, Physics of Semiconductor Devices, 2nd ed. New York: John Wiley & Sons, 1981, Chap. 6-8.

26. A. Cros, M.O. Aboelfotoh, and K.N. Tu, J. Appl. Phys., 67 (7) (1990)

3328.

27. L. Stolt and F. D'heurle, Thin Solid Films, 189 (1990) 269.

28. J. Echigiya, H. Enoki, T. Satoh, T. Waki, M.Otsuki, and T. Shibata, Appl. Surf. Sci., 56-58 (1992) 463.

29. M.T. Bohr, Int. Electron Device Meet. Tech. Dig., (1995) 241.

30. C.N. Wang, Thermal Stability of Cu/SiOF/Si MOS Structure, National Chiao-Tung University, Hsinchu, Taiwan, 1999.

31. A.L.S. Loke, J.T. Wetzel, P.H. Townsend, T. Tanabe, R.N. Vrtis, M.P. Zussman, D. Kumar, C. Ryu, and S.S. Wong, IEEE Trans. Electron Devices, ED-46 (1999) 2178.

32. D. Edelstein, J. Heidenreich, R. Goldblatt, W. Cote, C. Uzoh, N. Lustig, P. Roper, T. McDevitt, W. Motsiff, A. Simon, J. Dukovic, R. Wachnik, H. Rathore, R. Schulz, L. Su, S. Luce, and J. Slattery, Int. Electron Device Meet. Tech. Dig., (1997) 773.

33. X.W. Lin and D. Pramanik, Solid State Technol., (Oct. 1998), 63.

34. L. Peters, Semicond. Int., (Jan. 2000) 52.

35. R.A. Donaton, B. Coenegrachts, K. Maex, H. Struyf, S. Vanhaelemeersch, G. Beyer, E. Richard, I. Vervoort, W. Fyen, J. Grillaert, S.V. Groen, M. Stucchi, and D.D. Roest, IEEE Int. Interconnect Tech. Conf., 1999, pp. 262.

36. C.H. Ting and T.E. Seidel, Mater. Res. Soc. Symp. Proc., 381 (1995) 3.

37. D. Pramanik, Solid State Technol., (Sept. 1995), 69.

38. S.P. Muraka, Solid State Technol., (March 1996), 83.

39. B. Zhao and M. Brongo, Mater. Res. Soc. Symp. Proc., 565 (1999) 137.

40. R.K. Laxman, N.H. Hendricks, B. Arkles, and T.A. Tabler, Semicond. Int., (Nov. 2000) 95.

41. R.P. Mandal, V. Rana, M. Naik, D. Yost, D. Cheung, and W.F. Yau, 1999 Int. VLSI Multilevel Interconnection Conf. Proc., Sept. 1999, Santa Clara, CA, pp. 585.

42. B.K. Hwang, M.J. Loboda, G.A. Cerny, R.F. Schneider, J.A. Seifferly, and

T. Washer, IEEE Int. Interconnect Tech. Conf., 2000, pp. 52.

43. A. Grill and V. Patel, J. Appl. Phys., 85 (6) (1999) 3314.

44. L. Peters, Semicond. Int., (June 2000) 108.

45. L. Peters, Semicond. Int., (Nov. 1999) 56.

46. M.-A. Nicolet, Thin Solid Films, 52 (1978) 415.

47. M. Wittmer, J. Vac. Sci. Technol. A, 2 (2) (1984) 273.

48. H. Ono, T. Nakano, and T. Ohta, Appl. Phys. Lett., 64 (12) (1994) 1511.

49. C. Ryu, H. Lee, K.W. Kwon, A.L.S. Loke, and S.S. Wong, Solid State Technol., (Apr. 1999) 53.

50. M. Tanaka, S. Saida, and Y. Tsunashima, J. Electrochem. Soc. 147 (6) (2000) 2284.

51. P. Xu, K. Huang, A. Patel, S. Rathi, B. Tang, J. Ferguson, J. Huang, C. Ngai, and M. Loboda, IEEE Int. Interconnect Tech. Conf., 1999, pp. 109.

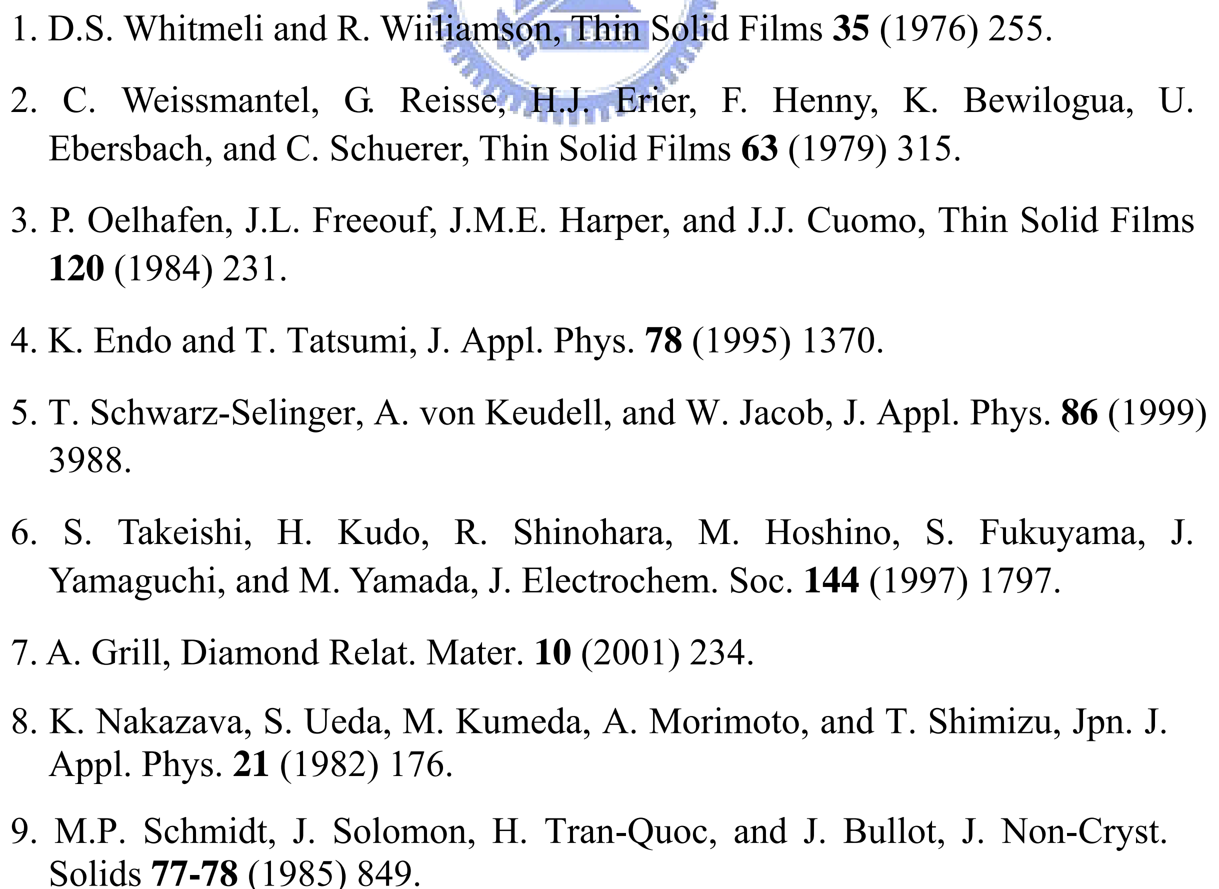

Chapter 3

1. D.S. Whitmeli and R. Wiiliamson, Thin Solid Films **35** (1976) 255.

2. C. Weissmantel, G. Reisse, H.J. Erier, F. Henny, K. Bewilogua, U. Ebersbach, and C. Schuerer, Thin Solid Films **63** (1979) 315.

3. P. Oelhafen, J.L. Freeouf, J.M.E. Harper, and J.J. Cuomo, Thin Solid Films **120** (1984) 231.

4. K. Endo and T. Tatsumi, J. Appl. Phys. **78** (1995) 1370.

5. T. Schwarz-Selinger, A. von Keudell, and W. Jacob, J. Appl. Phys. **86** (1999) 3988.

6. S. Takeishi, H. Kudo, R. Shinohara, M. Hoshino, S. Fukuyama, J. Yamaguchi, and M. Yamada, J. Electrochem. Soc. **144** (1997) 1797.

7. A. Grill, Diamond Relat. Mater. **10** (2001) 234.

8. K. Nakazava, S. Ueda, M. Kumeda, A. Morimoto, and T. Shimizu, Jpn. J. Appl. Phys. **21** (1982) 176.

9. M.P. Schmidt, J. Solomon, H. Tran-Quoc, and J. Bullot, J. Non-Cryst. Solids **77-78** (1985) 849.

10. A. Ishii, S. Amadatsu, S. Minomo, M. Taniguchi, M. Sugiyo, and T. Kobayashi, J. Vac. Sci. & Technol. A **12** (1994) 1068.

11. J. Theil, F. Mertz, M. Yairi, K. Seaward, and G. Ray, Mater. Res. Soc. Symp. Proc. **476** (1997) 31.

12. T. Mōri and Y. Namba, J. Vac. Sci. & Technol. A **1** (1983) 23.

13. A. Grill, V. Patel, S.A. Cohen, D.C. Edelstein, J.R. Paraszczak, and C. Jahnes, *Advanced Metallization and Interconnect Systems for ULSI Applications in 1996*, eds.: R. Haveman, J. Schmitz, H. Komiyama and K. Tsubouchi (Materials Research Society, Pittsburg, PA,1997) p.417.

14. W.K. Choi, T.Y. Ong, L.S. Tan, F.C. Loh, and K.L. Tan, J. Appl. Phys. **83** (1998) 4968.

15. P.T. Liu, T.C. Chang, S.M. Sze, F.M. Pan, Y.J. Mei, W.F. Wu, M.S. Tsai, B.T. Dai, C.Y. Chang, F.Y. Shih, and H.D. Huang, Thin Solid Films **332** (1998) 345.

16. H.-C. Tsai and D.B. Bogy, J. Vac. Sci. & Technol. A **5** (1987) 3287.

17. Yan-Way Li, Chia-Fu Chen, Yew-Bin Shue, Teng-Chien Yu, and Jack Jyh-Kau Chang, Jan. J. Appl. Phys. 40 (2001) 6574.

18. H.R. Kaufman, R.S. Robinson, and R.I. Seddon, J. Vac. Sci. & Technol. A **5** (1987) 2081.

19. J.W. Zou, K. Schmidt, K. Reichelt, and B. Dischler, J. Appl. Phys. 67 (1990) 487.

20. B. Marchon, P.N. Vo, M.R. Khan, and J.W. Ager III, IEEE Trans. Magn. **27** (1991) 5160.

21. R.O. Dillon, J.A. Woollam, and V. Katkanant, Phys. Rev. B **29** (1984) 3482.

22. J. Robertson, Prog. Solid St. Chem. 21 (1991) 199.

23. F. Tuinstra and J.L. Koenig, J. Chem. Phys. 53 (1970) 1126.

24. D. Beeman, J. Silverman, R. Lynds, M.R. Anderson, Phys. Rev. B 30 (1984) 870.

25. Z.Y. Chen, Y.H. Yu, J.P. Zhao, S.Q. Yang, T.S. Shi, X.H. Liu, E.Z. Luo, J.B. Xu, and I.H. Wilson, Thin Solid Films **339** (1999) 74.

26. N. Savvides, J. Appl. Phys. **59** (1986) 4133.

27. C.-C. Hung, G.J. Valco, S.M. Aithal, and V.V. Subramaniam, J. Appt. Phys.

78 (1995) 7109.

28. E. Vainonen, J. Likonen, T. Ahlgren, P. Haussalo, J. Keinonen, and C. H. Wu, J. Appl. Phys. **82** (1997) 3791.

29. A. Grill, V. Patel, and B.S. Meyerson, J. Mater. Res. **5** (1990) 2531.

30. T. Friessnegg, M. Boudreau, J. Brown, P. Maschera, P.J. Simpson, and W. Puff, J. Appl. Phys. **80** (1996) 2216.

31. H.L. Bai, E.Y. Jiang, C.D. Wang, R.Y. Tian, J. Appl. Phys. 82 (5) (1997) 2270.

32. Z.L. Akkerman, H. Efstathiadis, and F.W. Smith, J. Appl. Phys. **80** (1996) 3086.

33. Ch. Wild and P. Koidl, Appl. Phys. Lett. **51** (1987) 1506.

34. H. Yang, D.J. Tweet, Y. Ma, and T. Nguyen, Appl. Phys. Lett. 73 (1998) 1514.

35. A. Horn, A. Schenk, J. Biener, B. Winter, C. Lutterloh, M. Wittmann, and J. Küppers, Chem. Phys. Lett. **231 (1994)** 193.

36. M. M. Waite and S. I. Shah, Appt. Phys. Lett. 60 (1992) 2344.

37. A. von Keudell and W. Jacob, J. Appl. Phys. **79** (1996) 1092.

38. A. von Keudell, W. Jacob, and W. Fukarek, Appl. Phys. Lett. **66** (1995) 1322.

Chapter 4

1. S. Ghosh, P. Bhattacharya and D.N. Bose, Appl. Phys. Lett. 68 (21) (1996) 2979.

2. Y. Tawada, K. Kondo, H. Okamoto and Y. Hamakawa, J. Appl. Phys. 53 (1982) 5273.

3. J. Kanicki, in *Amorphous and Microcrystalline Semiconductor Devices*, Vol. 1, Artech House, Boston, MA, 1991.

4. K.C. Chang, K.Y. Chang, J.K. Fang and S.C. Jwo, IEEE Electron Devices Lett. 8 (1987) 64.

5. F. Demichelis, C.F. Pirri, E. Tresso, G.J. Adriaenssens, W. Grevendonk, H. Herremans, G. Amato and U. Coscia, Appl. Surf. Sci. 70-71 (1993) 664.

6. G. Crovini, C.F. Pirri, E. Tresso, R. Galloni, R. Rizzoli, C. Summonte, F.

Zignani, P. Rava and A. Madan, Philos. Mag. B 69 (1994) 377.

7. Y. Matsubara, K. Kishimoto, K. Endo and et al., IEDM, (1998) 841.

8. P. Xu, K. Huang, A. Patel, S. Rathi, B. Tang, J. Ferguson, J. Huang, C. Ngai and M. Loboda, IITC (1999) 109.

9. P.T. Liu, T.C. Chang, S.M. Sze, F.M. Pan, Y.J. Mei, W.F. Wu, M.S. Tsai, B.T. Dai, C.Y. Chang, F.Y. Shih and H.D. Huang, Thin Solid Films 332 (1998) 345.

10. Po-Tsun Liu, Ting-Chang Chang, Ya-Liang Yang, Yi-Fang Cheng and Simon M. Sz*e*, IEEE Trans. Electron Devices vol. 47, 9 (2000) 1733.

11. K. Nakazava, S. Ueda, M. Kumeda, A. Morimoto and T. Shimizu, Jpn. J. Appl. Phys. 21 (1982) 176.

12. M.P. Schmidt, J. Solomon, H. Tran-Quoc and J. Bullot, J. Non-Cryst. Solids 77-78 (1985) 849.

13. B. Ruttensperger, G. Krots, G. Miller, G. Derst and S. Kalbitzer, J. Non-Cryst. Solids 137-138 (1991) 635.

14. R.K. Onmori, I. Pereyra, C. Sassaki and M.N.P. Carreño, *Proceedings of the 9th European Photov. Solar Energy Conference*, (Kluwer, Dordrecht, 1989), pp.33.

15. R. Nandan, S.P. Murarka, A. Pant, C. Shepard and W.A. Lanford, *Mater. Res. Soc. Symp. Proc.*, **260**, 1999 p. 929.

16. R. Walsh, Acc. Chem. Res. 14 (1981) 246.

17. J.P.M. Schmitt, J. Non-Cryst. Solids 59-60 (1983) 649.

18. Lijun Tong, Mehran Mehregany and W.C. Tang, *MEMS '93, Proceedings An Investigation of Micro Structures, Sensors, Actuators, Machines and Systems,* IEEE. (1993), pp. 242.

19. M.N.P. Carreño, I. Pereyra, M.C.A. Fantini, H. Takahashi and R. Landers, J. Appl. Phys. 75 (1) (1994) 538.

20. A.H. Mahan, B.P. Nelson, R.S. Crandll, and D.L. Williamson, IEEE Trans. Electron Devices vol. 36 (1989) 2859.

21. Dong-Soo Yoon, Hong Koo Baik and Sung-Man Lee, J. Appl. Phys. **83** (3) (1998) 1333.

22. D.K. Basa and F.W. Smith, Thin Solid Films 192 (1990) 121.

23. M. Yoshimoto, T. Fuyuki and H. Matsunami, Proc. 8th Int. Symp. Plasma Chem., Tokyo, (1987), pp. 1455.

24. J. Robertson, Philos. Mag. B 69 (1994) 307.

25. J. Küppers, Surf. Sci. Rep. **2**2 (1995) 249.

26. A. von Keudell, T. Schwarz-Selinger, and W. Jacob, J. Appl. Phys. 89 (2001) 2979.

27. A.W. Adamson, Physical Chemistry of Surfaces, 4th Ed. (Wiley, New York, 1982) pp. 357-359.

28. M.E. Schrader, Langmuir 12 (1996) 3728.

29. G.W. Tyndall, P.B. Leezenber, R.J. Waltman, and J. Castenada, Tribology Letters 4 (1998) 103.

30. M. Grischke, K. Bewilogua, K. Trojan, and H. Dimigen, Surf. Coat. Technol. 74–75 (1995) 739.

31. S. Adachi, T. Arai, and K. Kobayashi, J. Appl. Phys. 80 (1996) 5422.

32. R.S. Sussman and R. Ogden, Philos. Mag. B 44 (1981) 117.

33. A. Morimoto, T. Miura, M. Kumeda, and T. Shimizu: J. Appl. Phys. 53 (1982) 7299.

34. V.I. Kuznetsov, M. Zeman, L.L. A. Vosteen, B.S. Girwar, and J.W. Metselaar: J. Appl. Phys. 80 (1996) 6496.

35. Y.S. Kim, D. Jung, D.J. Kim and S. Min, Jpn. J. Appl. Phys. Part 2 37 (1998) L991.

36. C.-C. Liu, C. Lee, K.-L. Cheng, H.-C. Cheng and T.-R. Yew, Appl. Phys. Lett. **66** (2) (1995) 168.

37. G.M. Petrov and J.L. Giuliani, J. Appl. Phys. 90 (2001) 619.

38. A. von Keudell and W. Jacob, J. Appl. Phys. 79 (1996) 1092.

39. J. Biener, A. Schenk, B. Winter and J. Küppers, J. Electron. Spectrosc. Relat. Phenom. 64/65 (1993) 331.

40. A. Horn, A. Schenk, J. Biener and et al., Chem. Phys. Lett. 231 (1994) 193.

41. M. Balden, S. Picarle, and J. Roth, J. Nucl. Mater. 290-293 (2001) 47.

42. M. Vogt, M. Kachel, M. Plötner and K. Drescher, Microelectronic Engineering 37/38 (1997) 181.

43. H. Miyazaki, H. Kojima and K. Hinode, J. Appl. Phys. **81** (12) (1997) 7746.

44. M.L. Oliveira and S.S. Camargo, J. Appl. Phys. 71 (1992) 1531.

45. A. von Keudell, W. Jacob and W. Fukarek, Appl. Phys. Lett. **66** (1995) 1322.

Chapter 5

1. Y. Matsubara, K. Kishimoto, K. Endo, and et al., IEDM, (1998) 841.

2. P. Xu, K. Huang, A. Patel, S. Rathi, B. Tang, J. Ferguson, J. Huang, C. Ngai, and M. Loboda, IITC (1999) 109.

3. L.J. Brillson, Surf. Sci. Rep. 2 (1982) 123.

4. J.D. McBayer, R.M. Swanson, and T.W. Sigmon, J. Electrochem. Soc. 133 (1986) 1242.

5. Y Shacham-Diamand, A. Dedhia, D.Hofstetter, and W.G. Oldham, J. Electrochem. Soc. 140 (1993) 2427.

6. M. Vogt, and K. Drescher, Appl. Surf. Sci. 91 (1995) 303.

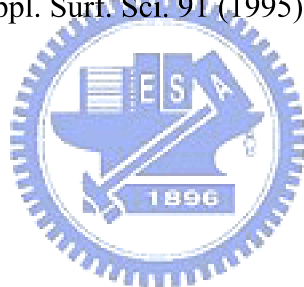

Publications List

A. Journal Papers:

1. "Yan-Way Li", Chia-Fu Chen, and Yu-Jen Tseng, ***Electrical properties of diamond-like carbon films deposited using a filtered cathodic arc system***, Jan. J. Appl. Phys., 40 (2001) 777.

2. "Yan-Way Li", Chia-Fu Chen, Yew-Bin Shue, Teng-Chien Yu, and Jack Jyh-Kau Chang, ***Substrate Bias Effect on Amorphous Hydrogenated Carbon Films Deposited by Filtered Cathodic Arc Deposition***, Jan. J. Appl. Phys. 40 (2001) 6574.

3. "Yan-Way Li", Yew-Bin Shue, Chia-Fu Chen, Teng-Chien Yu, and Jack Jyh-Kau Chang**,** ***Substrate Bias Effect on Amorphous Nitrogenated Carbon Films Deposited by Filtered Arc Deposition***, Diamond and Related Materials 11 (2002) 1227.

4. "Yan-Way Li" and Chia-Fu Chen, ***Effects of Ammonia Plasma Treatment on the Electrical Properties of Plasma-Enhanced Chemical Vapor Deposition amorphous hydrogenated silicon carbide Films***, Jan. J. Appl. Phys. 41 (2002) 5734.

5. Chia-Fu Chen, "Yan-Way Li", and Hsiu-Ling Huang, ***Effect of Post-treatment on Electrical Properties of Amorphous Hydrogenated Carbon Films Deposited by Gridless Ion Beam Deposition***, Jan. J. Appl. Phys. 42 (2003) 1.

6. Chia-Fu Chen and "Yan-Way Li", ***The Effects of Hydrogen Plasma Treatment on the PECVD a-SiC:H Films*****,** Accepted by Jan. J. Appl. Phys.

B. International Conferences Papers:

1. C.-F. Chen, "Y.-W. Li", and Y.-B. Shue, ***Substrate bias effect on amorphous hydrogenated carbon films deposited by filtered cathodic arc deposition***, International Conference on Metallurgical Coatings and Thin Films, (2000) DP-1-39.

2. "Yan-Way Li", Yew-Bin Shue, Chia-Fu Chen, Teng-Chien Yu, and Jack Jyh-Kau Chang**,** *Substrate Bias Effect on Amorphous Nitrogenated Carbon Films Deposited by Filtered Arc Deposition*, Diamond 2001 - the 12th European Conference on Diamond-Like Materials, (2001) DIAMAT 15.11.27.